UNIVERSITI TEKNOLOGI MARA

THE EFFECTS OF BISMUTH SUBSTITUTION ON STRUCTURAL, ELASTIC, DC CONDUCTIVITY AND RADIATION SHIELDING PROPERTIES OF $98[20Li_2O\text{-}xBi_2O_3\text{-}(80\text{-}x)B_2O_3]\text{-}2Ag$ MIXED IONIC-ELECTRONIC GLASS SYSTEM

NURUL ATIKA BINTI MOHD KHALID

MSc

June 2026

UNIVERSITI TEKNOLOGI MARA

THE EFFECTS OF BISMUTH SUBSTITUTION ON STRUCTURAL, ELASTIC, DC CONDUCTIVITY AND RADIATION SHIELDING PROPERTIES OF 98[20Li_2O-xBi_2O_3-(80-x)B_2O_3]-2Ag MIXED IONIC-ELECTRONIC GLASS SYSTEM

NURUL ATIKA BINTI MOHD KHALID

Thesis submitted in fulfilment
of the requirements for the degree of
Master of Science
(Physics)

Faculty of Applied Science

June 2026

CONFIRMATION BY PANEL OF EXAMINERS

I certify that a Panel of Examiners has met on 18th December 2025 to conduct the final examination of Nurul Atika binti Mohd Khalid on her Masters of Science thesis entitled "The Effects Of Bismuth Substitution on Structural, Elastic, DC Conductivity And Radiation Shielding Properties Of $98[20Li_2O\text{-}xBi_2O_3\text{-}(80\text{-}x)B_2O_3]\text{-}2Ag$ Mixed Ionic-Electronic Glass System" in accordance with Universiti Teknologi MARA Act 1976 (Akta 173). The Panel of Examiner recommends that the student be awarded the relevant degree. The Panel of Examiners was as follows:

Muhamad Kamil Yaakob
Associate Professor
Faculty of Applied Sciences
Universiti Teknologi MARA
(Chairman)

Zakiah Mohamed
Associate Professor
Faculty of Applied Sciences
Universiti Teknologi MARA
(Internal Examiner)

Muhamad Noorazlan Abd Azis
Associate Professor
Faculty of Science and Mathematics
University Pendidikan Sultan Idris
(External Examiner)

PROFESSOR DR HJH ZURAEDA IBRAHIM
Dean
Institute of Postgraduates Studies
Universiti Teknologi MARA

Date: 13 June 2026

AUTHOR'S DECLARATION

I declare that the work in this thesis was carried out in accordance with the regulations of Universiti Teknologi MARA. It is original and is the results of my own work, unless otherwise indicated or acknowledged as referenced work. This thesis has not been submitted to any other academic institution or non-academic institution for any degree or qualification.

I, hereby, acknowledge that I have been supplied with the Academic Rules and Regulations for Postgraduate, Universiti Teknologi MARA, regulating the conduct of my study and research.

Name of Student	:	Nurul Atika binti Mohd Khalid
Student ID. No.	:	2019604372
Programme	:	Master of Science (Physics) – AS759
Faculty	:	Applied Sciences
Thesis Title	:	The Effects Of Bismuth Substitution on Structural, Elastic, DC Conductivity and Radiation Shielding Properties 98[20Li_2O-$x$$Bi_2O_3$-(80-$x$)$B_2O_3$]-2Ag
Signature of Student	:	……..
Date	:	June 2026

ABSTRACT

This study highlights the transformative effect of bismuth substitution on the structural, elastic, electrical and radiation shielding properties of the 98[20Li_2O-$x$$Bi_2O_3$-(80-$x$)$B_2O_3$]-2Ag glass system ($x$ ranging from 3 to 11 mol%). Bismuth's role as a network modifier introduces significant changes to the glass matrix, influencing its overall performance and suitability for advanced applications. The need for effective radiation shielding arises from the increasing use of ionizing radiation in various fields, including medicine, industry, and scientific research. Ionizing radiation, which includes x-rays, gamma rays, and high-energy particles which poses significant risks to human health and materials due to its ability to ionize atoms, damaging biological tissues, and degrade structural integrity. In medical applications, for instance, radiation is widely used in diagnostic imaging and cancer treatment, necessitating materials that can protect patients and medical personnel. Consequently, the development of advanced radiation shielding materials with high attenuation efficiency, low thickness requirements, and durability has become a critical area of research. Structurally, bismuth plays a critical role in altering the glass network. FTIR spectroscopy reveals that Bi_2O_3 introduces both non-bridging oxygens (NBOs) and bridging oxygens (BOs), with the presence of BiO_6 and BO_3 groups indicating higher NBO content, while BiO_3 and BO_4 groups signify increased BOs. This shift in the NBO/BO ratio reflects significant changes in network connectivity. The molar volume and density increase notably between x = 7 and x = 9 mol%, attributed to the formation of additional NBOs, which expand the glass matrix and modify its structural integrity. In terms of elastic properties, bismuth substitution reduces structural rigidity. Longitudinal and bulk moduli decrease at x = 7 mol%, indicating a softer glass network due to the increased prevalence of NBOs. Furthermore, the maximum K_{bc}/K_e ratio and the highest ring parameter observed at x = 7 mol% suggest that bismuth significantly alters the glass's ring structure, highlighting its impact on the elastic response of the material. Bismuth also influences the electrical conductivity of the glass. DC conductivity reaches its lowest value at x = 9 mol%, which corresponds to a critical concentration where the structural changes induced by bismuth disrupt ion mobility. This suggests that bismuth affects the pathways available for ionic conduction, leading to reduced conductivity at higher concentrations. Radiation shielding properties of the glass improve substantially with higher bismuth content. Phy-X/PSD simulations reveal that bismuth enhances shielding performance across a wide photon energy range (15 keV to 15 MeV). The mass attenuation coefficient (MAC) increases with bismuth concentration, while the half-value layer (HVL) and mean free path (MFP) decrease, indicating more effective radiation attenuation. Additionally, the effective atomic number Z_{eff} peaks at x = 11 mol%, confirming bismuth's ability to enhance photon interaction probability and improve the protective performance of the glass. In conclusion, bismuth substitution exerts a profound impact on the structural organization, elastic properties, electrical conductivity, and radiation shielding capabilities of the glass system. These findings underscore bismuth's potential as a key dopant for designing advanced materials with tailored properties for applications in radiation protection, optoelectronics, and other high-performance technologies. By addressing the pressing need for efficient radiation shielding materials, this research contributes to the safety and sustainability of radiation-intensive environments.

ACKNOWLEDGEMENT

Firstly, I wish to thank merciful Allah S.W.T for giving me the opportunity to embark on my MSc and for completing this long and challenging journey successfully. My gratitude and sincere thanks go to my supportive supervisor Assoc. Prof. Ts. Dr Rosdiyana Hasham @ Hisam.

My special appreciation goes to my lovely parents, Mr Mohd Khalid bin Ismail and Ms for their endless support. Lovely appreciation also goes to my beloved husband, Mr Mohamed Rajaie bin Abd Halim for his infinite understanding and encouragement. To my firstborn son, Budi Rajaie bin Mohamed Rajaie, you are my truly inspiration in my long journey to complete this MSc.

Finally, this thesis is dedicated to my fellow lab mates for their assistance and guidance during the time this research was conducted. Alhamdulillah.

TABLE OF CONTENTS

LIST OF TABLES

LIST OF FIGURES

LIST OF SYMBOLS

Symbols

C_L	Longitudinal Modulus
d	Thickness
F	Stretching Force Constant
$\bar{F}$	Average Stretching Force
H	Hardness
$\hbar$	Plank's Constant
$\hbar v$	Incident Photon Energy
k_b	Boltzmann's Constant
K_{bc}	Calculated Value For Bulk Modulus
K_e	Bulk Modulus
l	Network Bond Length
ℓ	Average Ring Size
N_4	Fraction Of Four Coordinated Boron Atoms
n_b	Number Of Network Bonds Per Unit Volume
n_c	Crosslink Density Per Cation
n_f	Coordination Number
$n_{f_{ave}}$	Average Coordination Number
$\bar{n}_c$	Average Crosslink Density

μ	Shear Modulus
ρ	Density
t	Transit Time
V_a	Molar Volume
v_L	Longitudinal Velocity
v_s	Shear Velocity
v_m	Mean Sound Velocity
σ	Poisson's Ratio
Θ_D	Debye's Temperature
Y	Young's Modulus

LIST OF ABBREVIATIONS

Abbreviations

BO	Bridging Oxygen
DSC	Differential Scanning Calorimetry
FTIR	Fourier Transform Infrared
IR	Infrared
LAC	Linear Attenuation Coefficient
MAC	Mass Attenuation Coefficient
MIE	Mixed Ionic-Electronic
NBO	Non-Bridging Oxygen
UV-Vis	Ultra-Violet Spectroscopy
XRD	X-ray Diffraction
Z_{eff}	Effective Atomic Number

CHAPTER 1
INTRODUCTION

1.1 Research Background

Glasses are non-crystalline solid materials that have gained considerable importance due to their ease of fabrication and versatile physicochemical properties. Compared with crystalline materials, glasses offer greater compositional flexibility, enabling their properties to be tailored for specific applications. As a result, glass materials are extensively used in industrial and high-technology sectors such as electro-optical systems, electronic components, energy storage devices, and electrochemical applications. Oxide glasses are generally categorized as network formers, modifiers, or intermediates based on their single bond strength, which influences their ability to form stable glass networks and determines the overall structural connectivity of the material (Kaur et al., 2021). Oxides with higher single bond strength typically exhibit a stronger tendency to act as glass formers, contributing to improved rigidity and thermal stability (Singh et al., 2020).

Among various oxide glass systems, boron oxide-based glasses have attracted significant attention due to their distinctive structural and physical characteristics. These glasses are known for their high chemical durability, low coefficient of thermal expansion, good thermal stability, low refractive index, and relatively high phonon energy, making them suitable for optical and electronic applications (Wang et al., 2022; Elbashir et al., 2023). In addition to these properties, borate glasses are advantageous because they can be produced through cost-effective melting techniques, further enhancing their appeal for advanced technological applications. Structurally, vitreous B_2O_3 forms a covalently bonded network in which boron atoms are coordinated either in trigonal BO_3 or tetrahedral BO_4 configurations. These structural units can link together to form complex groups such as diborate, tetraborate, pentaborate, and boroxol ring structures. The introduction of alkali oxides into the borate glass network modifies this structure by breaking boroxol rings, leading to the formation of non-bridging oxygen atoms and an increase in BO_4 units. Such structural transformations significantly influence the physical, elastic, and electrical properties of the glass system (Doweidar et al., 2021).

Mixed ionic–electronic conducting glasses represent a class of materials capable of simultaneously transporting ionic and electronic charge carriers. The coexistence of these two conduction mechanisms results in complex electrical behaviour and notable changes in structural and thermal characteristics. Ionic conduction in these systems is primarily controlled by the concentration and mobility of alkali ions within the glass network, while electronic conduction is commonly described by the small polaron hopping mechanism. Although an increase in alkali content is often expected to enhance overall electrical conductivity, experimental studies on transition metal oxide and silver-containing glasses have demonstrated non-linear and sometimes anomalous conductivity behaviour. Recent investigations indicate that adjusting the ratio of alkali or silver oxide relative to transition metal oxides allows the dominant conduction mechanism to be tuned from ionic to electronic conduction, providing greater control over the electrical performance of mixed conducting glasses (Sharma et al., 2021; Ahmed et al., 2022).

The incorporation of modifier oxides into glass networks also affects their mechanical and elastic properties. In glass systems such as tellurite, phosphate, and silicate, the addition of alkali or alkaline earth oxides leads to the formation of non-bridging oxygen atoms, resulting in network depolymerization. This structural weakening generally causes a reduction in elastic moduli and acoustic velocities due to decreased network rigidity (El-Mallawany et al., 2020). However, borate glasses often display anomalous elastic behaviour when modified with alkaline earth oxides. In such cases, elastic parameters may vary non-linearly with modifier concentration as a consequence of competing structural effects, including changes in BO_3–BO_4 conversion and network packing density (Hassan et al., 2023).

In addition to their structural, elastic, and electrical properties, glasses have emerged as promising materials for radiation shielding applications. Radiation shielding plays a crucial role in medical diagnostics, radiotherapy facilities, nuclear laboratories, scintillation detectors, and x-ray imaging rooms. Transparent shielding materials, particularly glass, are highly desirable in medical and industrial environments where both radiation protection and visibility are required (Sayyed et al., 2020). Traditional lead-based glasses have been widely used for radiation shielding; however, concerns regarding lead toxicity have driven the search for safer and environmentally friendly alternatives.

Bismuth-based glasses have gained increasing attention as effective substitutes for lead-containing materials due to the high atomic number of bismuth, which enhances photon attenuation while posing lower environmental and health risks. The incorporation of Bi_2O_3 into borate and silicate glass systems has been shown to increase glass density and improve gamma-ray shielding efficiency, as reflected by higher mass attenuation coefficients (Zaid et al., 2021; Al-Buriahi et al., 2022). Furthermore, recent studies have demonstrated that increasing Bi_2O_3 content in zinc–borate and silver-containing glass systems further enhances radiation shielding performance (Tekin et al., 2021; Rammah et al., 2023).

Recent research has also highlighted the beneficial role of silver and silver nanoparticles in glass matrices for radiation shielding applications. The presence of silver improves particle dispersion and increases the effective interaction surface area within the glass, leading to enhanced photon attenuation. These combined effects suggest that glass systems containing both heavy metal oxides and mixed ionic–electronic components offer significant potential for advanced radiation shielding applications (Sutrisno et al., 2022; El-Sharkawy et al., 2024).

1.2 Problem Statement

The problem statements for this research are:

1. Oxide glasses containing both transition metal ions and alkali metals are well known for exhibiting mixed ionic–electronic (MIE) conduction, in which charge transport arises from the combined contribution of mobile ions and electronic charge carriers. In these glass systems, transition metal ions undergo reversible changes in oxidation state, enabling electronic transport through small polaron hopping mechanisms. Such redox activity significantly influences the structural arrangement, electrical behaviour, and physicochemical stability of the glass network, making MIE glasses an important subject of contemporary research (Sharma et al., 2021; Ahmed et al., 2022). Recent studies have shown that MIE behaviour is often associated with anomalous or non-linear trends in DC conductivity, particularly within specific compositional ranges where a transition from ionic to electronic charge transport occurs. Investigations on lithium-, silver-, and transition metal–containing borate and tellurite glass systems have reported conductivity minima or weak composition dependence that cannot be adequately explained by conventional ion mobility models

alone (Hassan et al., 2021; Tekin et al., 2022). These anomalies are commonly attributed to structural rearrangements within the glass network, especially changes in the distribution of bridging oxygen (BO) and non-bridging oxygen (NBO), which directly affect charge transport pathways. Beyond electrical properties, recent research has demonstrated that MIE-related anomalies are closely coupled with elastic behaviour, including variations in elastic moduli, sound velocities, and Debye temperature. Several studies have reported correlated anomalies in DC conductivity and elastic parameters, indicating a strong relationship between mechanical rigidity and charge transport mechanisms in mixed conducting glasses (Elbashir et al., 2023; Rammah et al., 2023). These findings highlight the sensitivity of elastic properties to subtle structural modifications induced by compositional changes. Borate-based glass systems exhibit particularly complex behaviour due to the ability of boron atoms to exist in both trigonal BO_3 and tetrahedral BO_4 coordination states. The incorporation of modifier oxides can induce BO_3–BO_4 conversion and generate non-bridging oxygen sites, leading to non-linear changes in both elastic and electrical properties (Kaur et al., 2021; Hassan et al., 2024). In particular, bismuth oxide (Bi_2O_3) has attracted attention as a heavy metal oxide modifier due to its large ionic radius and strong influence on glass network structure. Although recent studies have shown that Bi_2O_3 significantly alters glass structure and physical properties, most investigations primarily focus on optical and thermal characteristics, with limited emphasis on its role in MIE-related elastic and electrical behaviour (Doweidar et al., 2021; El-Mallawany et al., 2022). Furthermore, the incorporation of silver (Ag) introduces additional complexity by contributing both ionic and electronic charge carriers, potentially enhancing MIE effects (Sutrisno et al., 2022; El-Sharkawy et al., 2024). However, systematic studies examining the combined effects of Bi_2O_3 substitution and silver incorporation on the structural, elastic, and DC conductivity properties of lithium–borate glass systems remain scarce. Therefore, there is a clear need for a comprehensive investigation into the influence of bismuth substitution on $98[20Li_2O\text{-}xBi_2O_3\text{–}(80–x)B_2O_3]$–2Ag glasses to elucidate the relationship between structural modifications, elastic behaviour, DC conductivity, and mixed ionic–electronic conduction across varying bismuth concentrations.

2. Conventional radiation shielding materials such as lead and concrete have been widely used due to their effectiveness in attenuating ionizing radiation; however, they suffer from several inherent limitations. Concrete-based shielding materials are opaque,

bulky, non-portable, and susceptible to mechanical degradation over long-term radiation exposure. Their shielding performance may also deteriorate due to dehydration and microstructural changes induced by radiation-related heating, resulting in inconsistent attenuation efficiency (Sayyed et al., 2020; Tekin et al., 2021). Similarly, although lead provides excellent radiation shielding due to its high density and atomic number, its application is increasingly restricted because of serious drawbacks such as high toxicity, environmental hazards, opacity, low melting point, and stringent disposal requirements (Al-Buriahi et al., 2021; Rammah et al., 2022). These limitations have motivated extensive research into lead-free, transparent, and environmentally friendly radiation shielding materials, particularly glass-based systems. Among various alternatives, bismuth oxide (Bi_2O_3) has emerged as a promising heavy metal oxide due to its high atomic number, good glass-forming ability, and relatively low toxicity compared to lead-based compounds. Recent studies have demonstrated that Bi_2O_3-containing glasses exhibit enhanced gamma-ray attenuation while maintaining optical transparency, making them suitable for medical and industrial shielding applications (Zaid et al., 2021; Sayyed et al., 2022). Borate-based glass systems are especially attractive for radiation shielding due to their low melting temperature, structural flexibility, and ability to accommodate high concentrations of heavy metal oxides. Recent investigations have shown that incorporating Bi_2O_3 into borate glass matrices significantly increases glass density and mass attenuation coefficients, thereby improving shielding effectiveness (Tekin et al., 2021; Al-Hadeethi et al., 2022). Furthermore, systematic variation of Bi_2O_3 concentration has been reported to enable fine control of key shielding parameters such as half-value layer and mean free path (Rammah et al., 2024). Despite these advances, most existing studies on Bi_2O_3-containing borate glasses primarily emphasize radiation shielding and optical properties, with limited attention given to the influence of structural and transport characteristics on shielding performance. In particular, the role of mixed ionic–electronic (MIE) conduction and its correlation with structural modifications in radiation attenuation remains insufficiently explored. Moreover, although silver (Ag) incorporation has been shown to modify glass structure and electronic environments, comprehensive studies combining bismuth substitution and silver incorporation in lithium–borate glass systems are still scarce. This limitation resulted in fragmented and largely empirical findings, restricting the establishment of reliable structural relationships and hindering the rational design and optimization of lead-free shielding

glass materials.

1.3 Research Objectives

The objectives of this study are:

1. To investigate the effects of bismuth (Bi_2O_3) substitution on the elastic properties of the 98[20Li_2O-$x$$Bi_2O_3$-(80-$x$)$B_2O_3$]–2Ag glass system within the mixed ionic–electronic (MIE) transition region, with supporting structural characterisation using x-ray diffraction (XRD) and Fourier transform infrared (FTIR) spectroscopy, Raman spectroscopy and correlation with DC conductivity behaviour obtained from impedance spectroscopy respectively.

2. To determine the influence of bismuth (Bi_2O_3) substitution on the radiation shielding properties of 98[20Li_2O-$x$$Bi_2O_3$-(80-$x$)$B_2O_3$]–2Ag glass samples using the Phy-X/PSD simulation program over a photon energy range of 15 keV to 15 MeV, representing low-to high-energy radiation relevant to practical shielding applications.

1.4 Significance of Study

The structural, elastic, DC conductivity and radiation shielding properties of the investigated glass system are systematically analysed using FTIR spectroscopy, ultrasonic velocity measurements, impedance spectroscopy and Phy-X/PSD simulation techniques respectively. A detailed examination of the structural evolution of the glass network provides insight into the role of bismuth substitution in modifying bonding configurations, particularly the formation of bridging oxygen (BO) and non-bridging oxygen (NBO) units which are known to strongly influence glass properties.

Changes in elastic behaviour such as stiffness and rigidity are interpreted through ultrasonic velocity measurements which reflect variations in glass compactness and network connectivity. These structural modifications are closely linked to variations in DC conductivity as ion mobility and charge transport mechanisms are affected by network openness and the mixed ionic–electronic (MIE) nature of the glass system.

Mixed ionic–electronic behaviour arises when both ionic and electronic charge carriers coexist within the glass matrix at different molar concentrations often resulting

in anomalous or non-linear trends in physical properties. While previous studies have demonstrated that mixed ionic–electronic (MIE) effects significantly influence the electrical and elastic behaviour of oxide glasses, radiation shielding performance has often been evaluated independently using parameters such as the mass attenuation coefficient (MAC), linear attenuation coefficient (LAC), half-value layer (HVL), mean free path (MFP), and effective atomic number (Z_{eff}). However, limited attention has been given to how variations in charge transport mechanisms and glass network rigidity influence photon attenuation behaviour, particularly within the MIE transition region.

The novelty of this research lies in its comprehensive and correlated investigation of structural, elastic, DC conductivity, and radiation shielding properties within a single mixed ionic-electronic glass system. Unlike previous studies that focus on radiation attenuation or electrical behaviour separately, this work systematically links MIE-induced structural modifications, elastic anomalies, and charge transport behaviour to radiation shielding efficiency. In addition, the incorporation of Bi_2O_3 into a Li_2O–B_2O_3–Ag glass matrix provides new insight into the dual role of bismuth as both a network modifier influencing MIE behaviour and a high-Z element enhancing photon attenuation. This integrated approach contributes new understanding of the structural and shielding relationship while supporting the development of transparent, environmentally friendly alternatives to conventional lead-based radiation shielding materials.

1.5 Thesis Scope

The structural, elastic, DC conductivity and radiation shielding characteristics of the mixed ionic-electronic 98[20Li_2O-$x$$Bi_2O_3$-(80-$x$)$B_2O_3$]-2Ag glass system are the main areas of this proposed study. Using the melt-quenching approach, this glass system will be produced by combining silver nanoparticles, bismuth oxide, boron oxide, and lithium oxide in the appropriate proportions. The X'Pert Pro Panalytical diffractometer will be used to measure x-ray diffraction in order to confirm the amorphous nature of glass samples. The Perkin Elmer model Spectrum One FTIR spectrometer will next be used to obtain IR absorption spectra in order to determine any structural alterations of the glasses' basic units. The elastic velocities and elastic moduli are investigated by using ultrasonic measurement. Furthermore, impedance spectroscopy measurement will be used to measure the DC conductivity of the glass sample. Meanwhile, for radiation

shielding properties of the glasses will be obtained by using Phy-X/PSD simulation program at 15 keV to 15 MeV photon energy range. The selected energy range enables a comprehensive assessment of photon–matter interaction mechanisms which covers photoelectric absorption, Compton scattering, and pair production ensuring relevance to medical, industrial, and nuclear applications.

CHAPTER 2
LITERATURE REVIEW

2.1 Introduction

This chapter provides insights into the attributes of borate glasses and imparts fundamental knowledge concerning the MIE phenomena. The discussion encompasses structural investigations, including infrared absorption, density, and molar volume of borate glasses. Additionally, the chapter also explores into elastic modulus, semi-empirical models, DC conductivity and radiation shielding studies, drawing upon findings from previous research on glasses based on borate compositions.

2.2 Introduction to Glass

Glass is widely recognized as a non-crystalline or amorphous solid characterized by a short-range order and a random arrangement of atoms resulting from fusion, which after cooling below its solidification point, assumes a rigid shape without undergoing crystallization. In contrast, crystalline solids exhibit a high content of long-range order, with atoms arranged in a periodic manner, as illustrated in Figure 2.1

Glass represents a distinctive material that is generated under controlled conditions. These conditions encompass diverse techniques employed in the process of glass formation, including the melt-quenching technique, vapor deposition, and sol-gel processing of solutions. Despite the methodological variations, glasses exhibit consistent characteristics and behaviours. Conventional inorganic glasses, such as borate, phosphate, silicate, germanate, and tellurite, are typically synthesized through the melt-quenching method. This involves the rapid cooling of a pre-heated liquid, resulting in the formation of a solid glass material. The transition from liquid to solid phase is predominantly observed at the glass transition temperature (T_g), where the material behaves in a rubbery state above T_g and solidifies below T_g.

Each oxide-based glass exhibits a distinctive glass transition temperature. In contrast, crystals are characterized by their melting temperature (T_m), where gradual cooling of the molten sample below T_m can lead to crystal formation. When the melt is cooled at a temperature below the crystal's T_m, there is a rapid decrease in enthalpy and

volume, resulting in the material transitioning to a crystalline state. Conversely, as the temperature decreases, molecular motion slows down, and with a sufficiently rapid cooling rate, molecules do not attain their lattice points. Eventually, the material undergoes dynamic arrest, forming a disordered glass at a specific temperature known as T_g. Figure 2.2 illustrates the volume or enthalpy plotted against temperature for glass development, where the change in gradient indicates the glass transformation region and temperature.

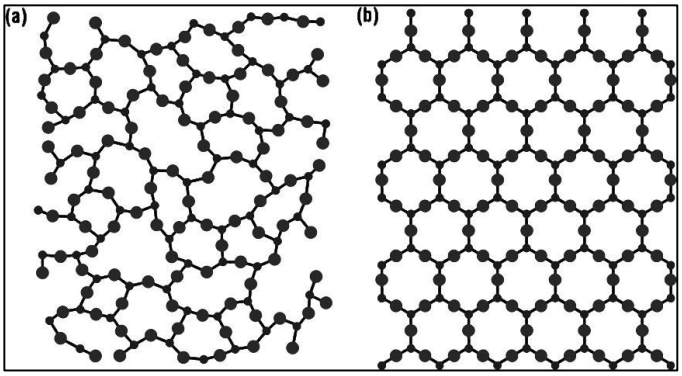

Figure 2.1 Atomic Arrangement in (a) Glass and (b) Crystal

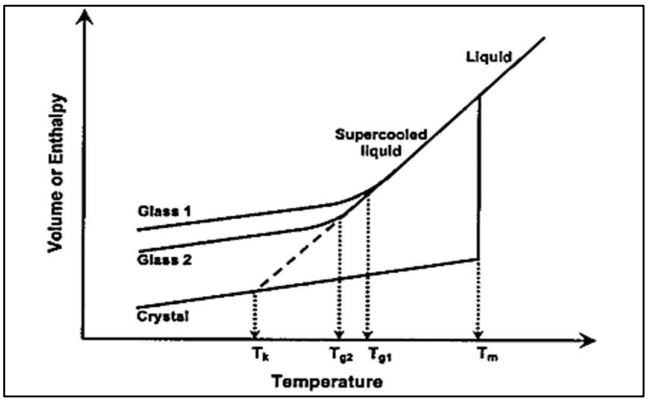

Figure 2.2 Volume or Enthalpy Against Temperature for Amorphous and Crystal Formation

2.3 Classification of Oxide Glasses

Zachariasen elucidated that certain polyhedra can give rise to expansive three-dimensional networking structures characterized by a high degree of random atomic arrangement and energy content comparable to that of corresponding crystal networks. His findings contribute valuable insights into the development of glass. It was

confirmed that the mechanical properties of glass closely resemble those of crystals, indicating the similarity in atomic forces within both crystalline and amorphous solids. Moreover, it is noteworthy that not all oxides readily undergo glass formation.

Zachariasen's criteria for the formation of amorphous structures, focusing on experimental observations for oxides, are outlined as follows:

I. Oxygen atoms should not be bonded to more than two cations.

II. Small cation coordination numbers are preferred, specifically 3 or 4.

III. Oxygen polyhedra should share corners, rather than edges or faces.

IV. In the context of three-dimensional networks, a minimum of three corners must be shared.

In summary, adherence to each of the four principles is imperative for the creation of amorphous solids, a criterion met by oxides like B_2O_3, SiO_2, GeO_2, and P_2O_5 (Karmakar, 2016). Notably, oxides capable of forming glasses can be categorized into three types: glass former, modifier, and intermediate.

Network-forming oxides, including borate (B_2O_3), silicate (SiO_2), germanate (GeO_2), arsenate (As_2O_3), and phosphate (P_2O_5), establish a densely interconnected three-dimensional array of chemical bonds, forming a polyhedral network of covalent bonds that constitutes a glass. Notably, glass formers have the intrinsic capacity to independently construct a glass network. Moreover, oxide glass formers exhibit high unit field strength and covalency, exemplified by elements such as Si^{4+}, Te^{4+}, and B^{3+}. This characteristic gives network formers with the role of acting as a bridge between structural units within the glass. Consequently, glass formers are frequently associated with bridging oxygen.

Conversely, the introduction of network modifiers, such as alkali and alkaline earth metal oxides (Li_2O, Na_2O, K_2O, MgO, CaO, SrO, and BaO), into the glass networks leads to the disruption of the covalently bonded glass structure. This disruption manifests in an open-ended glass structure, facilitated by the formation of non-bridging oxygen ions. The inclusion of these modifiers results in a reduction in the relative number of strong bonds within the material, consequently lowering the viscosity of the melt and the glass transition temperature. Notably, modifier oxides do not directly participate in the glass network structure; instead, they play a facilitating role in glass formation and occupy interstitial sites.

In contrast, intermediate oxides, including Al_2O_3, TiO2, ZrO_2, and Ga_2O_3, exhibit dual functionalities as network formers and or modifiers under specific

compositions. In instances where intermediate oxides function as glass modifiers, their involvement does not actively contribute to the formation of the glass structure; rather, they occupy interstitial sites and aid in the glass-forming process. Conversely, when intermediate oxides assume the role of glass formers, they integrate into the structure, forming bonds that enhance the connectivity of the glass network. Figure 2.3 provides a visual representation of the roles of glass formers, modifiers, and intermediates in the glass structure.

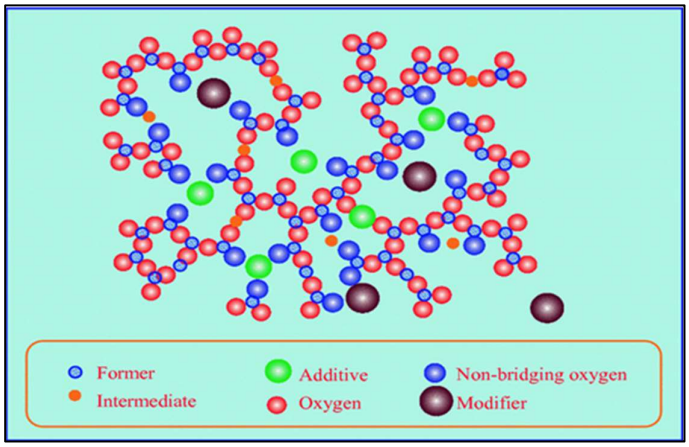

Figure 2.3 Role of glass former, modifier and intermediate

2.4 Bismuth Borate Glasses

Bismuth borate glasses have attracted considerable research interest over the past decade due to their unique combination of high density, optical transparency, structural flexibility, and enhanced radiation shielding capability. The incorporation of bismuth oxide (Bi_2O_3) into borate glass matrices is particularly advantageous because Bi_2O_3 possesses a high atomic number (Z = 83), high density, and strong photon interaction cross-sections, while still maintaining good glass-forming ability. These characteristics make bismuth borate glasses promising candidates for multifunctional applications such as optical devices, solid-state electrolytes, and lead-free radiation shielding materials.

Borate glasses are known for their structural versatility, which arises from the dual coordination states of boron in the form of trigonal BO_3 and tetrahedral BO_4 units. The relative distribution of these units governs the degree of network connectivity, rigidity, and openness of the glass structure. Several studies have shown that the

addition of modifier oxides leads to the conversion of BO_3 units into BO_4 units at low concentrations, followed by the formation of non-bridging oxygens (NBOs) at higher modifier contents. This structural adaptability allows borate glasses to accommodate a wide range of dopants, including heavy metal oxides such as Bi_2O_3 (El-Mallawany et al., 2020; D'Souza et al., 2021).

When Bi_2O_3 is introduced into the borate glass network, it can act either as a network modifier or an intermediate oxide, depending on its concentration and the presence of other constituents. At lower Bi_2O_3 contents, bismuth ions tend to disrupt the B–O–B network, resulting in the formation of NBOs and a reduction in network connectivity. At higher concentrations, Bi_2O_3 participates in the glass network through the formation of BiO_6 octahedral units, which contribute to increased glass density and altered bonding configurations. FTIR and Raman spectroscopy studies conducted between 2020 and 2024 have consistently reported the emergence of Bi–O vibrational bands corresponding to BiO_6 structural units, alongside changes in BO_3 and BO_4 band intensities (Al-Buriahi et al., 2021; Lakshminarayana et al., 2022).

Recent investigations have further demonstrated that the formation of BiO_6 units introduces structural heterogeneity and increases the average bond length within the glass network. Sayyed et al. (2022) and Kaur et al. (2023) reported that increasing Bi_2O_3 content results in a heavier yet more open glass structure, which significantly affects both mechanical and functional properties. This dual effect of increased density and reduced network rigidity highlights the complex role of Bi_2O_3 in determining glass behaviour.

From a mechanical perspective, numerous studies have reported that the elastic properties of bismuth borate glasses exhibit non-linear trends with increasing Bi_2O_3 concentration. Sabri et al. (2021) observed that elastic moduli and ultrasonic velocities initially decrease with Bi_2O_3 addition due to increased NBO formation, followed by partial recovery at higher concentrations as BiO_6 units enhance network rigidity. Similar anomalous behaviour was reported by El-Mallawany et al. (2022), who linked elastic anomalies to structural transitions within the glass matrix. These findings suggest that elastic behaviour in bismuth borate glasses is governed by a balance between network disruption and reinforcement effects.

In addition to elastic behaviour, the electrical properties of bismuth borate glasses have been widely studied, particularly in systems containing alkali or noble metal ions. The presence of Bi^{3+} ions modifies the local potential landscape, influencing

ion migration pathways and electronic hopping mechanisms. Recent impedance spectroscopy studies in years 2020 to 2024 have shown that bismuth-containing borate glasses often exhibit mixed ionic-electronic conduction behaviour, especially when doped with Li^+ or Ag^+ ions (Hisam et al., 2021; Singh et al., 2023). In such systems, ionic conduction is facilitated by NBO-rich pathways, while electronic conduction arises from localized states associated with heavy metal or noble metal species. This coexistence of conduction mechanisms frequently leads to anomalous DC conductivity behaviour within specific compositional ranges.

More recently, bismuth borate glasses have been extensively investigated for radiation shielding applications. The high atomic number and density of bismuth significantly enhance photon interaction probabilities, particularly via the photoelectric absorption mechanism at low photon energies. Studies by Kaur et al. (2021), Al-Hadeethi and Sayyed (2022), and Lakshminarayana et al. (2024) demonstrated that increasing Bi_2O_3 content leads to higher mass attenuation coefficients (MAC), lower half-value layers (HVL), and reduced mean free paths (MFP) compared to conventional borate, silicate, and phosphate glasses. These improvements are particularly significant in the low-energy photon region, which is relevant to medical diagnostic imaging and radiation protection.

Despite the growing body of literature on radiation shielding performance, most existing studies focus primarily on numerical attenuation parameters without considering the influence of structural evolution, elastic properties, or charge transport mechanisms. In particular, the role of mixed ionic–electronic (MIE) behaviour in governing radiation attenuation efficiency has received limited attention. Only a few recent studies have suggested that changes in glass density, network rigidity, and elastic response may indirectly influence photon interaction behaviour, but systematic correlations remain scarce.

Although bismuth borate glasses have been widely studied for their structural, elastic, electrical, and radiation shielding properties individually, there remains a lack of comprehensive understanding of how these properties are interrelated within a single glass system. This gap is especially evident in mixed ionic-electronic borate glasses containing both alkali and noble metal species.

2.5 Mixed Ionic-Electronic Glasses

Mixed ionic-electronic (MIE) glasses are characterised by the simultaneous presence of both ionic and electronic charge carriers within a single glass matrix, resulting in complex charge transport behaviour. In such systems, alkali ions such as Li^+ act as mobile ionic charge carriers that migrate through the glass network via thermally activated hopping between non-bridging oxygen (NBO) sites. Recent studies on lithium-based borate and tellurite glasses have confirmed that ionic conduction is strongly governed by network depolymerisation, NBO concentration, and glass structural openness (Singh et al., 2022; El-Mallawany et al., 2023). In contrast, electronic conduction arises from multivalent metal ions or noble metal species, where charge transport occurs through localized electron hopping between neighbouring sites or oxidation states associated with metal-oxygen polyhedral units (Hisam et al., 2021; Lakshminarayana et al., 2022).

The coexistence of ionic and electronic conduction mechanisms leads to competition between these two transport processes, which defines mixed ionic–electronic (MIE) behaviour. At low concentrations of electronic contributors, ionic conduction dominates due to continuous Li^+ migration pathways. However, with increasing concentrations of multivalent or heavy metal oxides, electronic hopping becomes increasingly significant and disrupts ionic pathways by modifying the potential landscape for ion migration. This competition produces non-linear and anomalous trends in physical properties, particularly DC conductivity, where a minimum or maximum is commonly observed within a specific compositional range known as the MIE transition region (Hisam et al., 2021; Singh et al., 2023).

Beyond electrical transport, MIE behaviour has been shown to strongly influence the mechanical and elastic properties of glass systems. Structural modifications associated with MIE, such as increased NBO formation and the incorporation of rigid metal-oxygen polyhedral units such as BiO_6 or MoO_6, directly affect network rigidity and bonding strength. Sabri et al. (2021) reported that elastic moduli, ultrasonic velocities, and Debye temperature exhibit anomalous variations at compositions corresponding to DC conductivity anomalies. Similar correlations between elastic softening and MIE transition regions were observed by El-Mallawany et al. (2023), confirming strong coupling between charge transport mechanisms and glass network structure.

Furthermore, the dielectric response of MIE glasses is also affected by dual conduction behaviour. The simultaneous presence of ionic and electronic carriers enhances polarization mechanisms, leading to frequency- and temperature-dependent dielectric anomalies. Recent impedance and dielectric studies (2020–2024) have emphasized that these coupled electrical and elastic anomalies are intrinsic features of MIE glass systems and arise from the interdependence of structure, charge transport, and mechanical response (Singh et al., 2022; Lakshminarayana et al., 2024). Consequently, MIE glasses represent an important class of functional materials in which electrical, elastic, and structural properties must be analysed in a correlated manner rather than independently.

Recent studies have shown that the emergence of MIE behaviour is strongly dependent on glass composition and network structure. Hisam et al. (2021) investigated lithium-based oxide glasses containing multivalent oxides and reported that the simultaneous presence of Li^+ ions and electronic hopping centres leads to a non-linear variation in DC conductivity with composition. In their study, a distinct minimum in DC conductivity was observed within a specific compositional range, which was attributed to competition between ionic mobility and electronic transport mechanisms. Similar observations were reported by Singh et al. (2022), who demonstrated that MIE behaviour arises when the concentration of electronic carriers becomes comparable to that of ionic carriers, resulting in a disruption of continuous ionic conduction pathways.

The structural origin of MIE behaviour has been extensively discussed in recent literature. El-Mallawany et al. (2023) reported that the incorporation of heavy metal oxides into borate-based glass systems increases the concentration of non-bridging oxygens (NBOs), which initially enhances ionic conduction. However, at higher dopant concentrations, the formation of rigid metal–oxygen polyhedral units alter network connectivity and hinders ion migration. This structural competition plays a crucial role in governing the balance between ionic and electronic conduction in MIE glasses.

Elastic anomalies are a common feature of MIE glass systems and are closely linked to changes in network rigidity and bonding configuration. Sabri et al. (2021) observed that elastic moduli and Debye temperature exhibit minima in lithium-based MIE glasses at compositions corresponding to DC conductivity anomalies. These findings suggest that elastic softening occurs when network depolymerisation caused by NBO formation dominates, whereas elastic recovery is associated with the formation of rigid polyhedral units that reinforce the glass network. Hisam et al. (2021) further

demonstrated that similar compositional regions exhibited concurrent anomalies in mean sound velocity and DC conductivity, providing strong evidence of coupling between mechanical and electrical behaviour under MIE conditions.

In recent years, the role of heavy metal oxides in inducing MIE behaviour has gained increasing attention. Bismuth oxide (Bi_2O_3), in particular, has been shown to play a dual role as both a network modifier and an intermediate oxide. Lakshminarayana et al. (2022) reported that Bi_2O_3 incorporation into borate glasses leads to the formation of BiO_6 octahedral units, which contribute to electronic conduction while simultaneously increasing glass density. Singh et al. (2023) demonstrated that heavy Bi^{3+} ions modify the potential landscape for Li^+ migration, resulting in reduced ionic mobility at higher Bi_2O_3 concentrations. This transition from ionic-dominated to electronic-dominated conduction is a key characteristic of MIE behaviour.

The presence of noble metal species, such as silver, further enhances MIE effects in glass systems. Al-Buriahi et al. (2021) reported that Ag-containing glasses exhibit enhanced electronic conduction due to the availability of Ag-related localized states, which facilitate electron hopping. In combination with alkali ions, silver contributes to mixed conduction behaviour and intensifies electrical and elastic anomalies. Singh et al. (2023) further noted that the inclusion of silver species increases charge carrier density and alters conduction pathways, particularly in borate-based glass systems.

Despite extensive investigations into MIE behaviour in oxide glasses, most recent studies have focused primarily on electrical and elastic properties. Limited attention has been given to how MIE-induced structural and mechanical changes influence radiation shielding behaviour. While some authors have suggested that increased density and network rigidity may indirectly affect photon attenuation, systematic correlations between MIE behaviour, elastic anomalies, DC conductivity, and radiation shielding performance remain scarce.

2.6 Ag Nanoparticles Doped Glasses

Silver (Ag) nanoparticle-doped glasses have attracted significant research attention due to the active role of silver in modifying the electronic structure, local bonding environment, and photon–matter interaction mechanisms of oxide glass systems. Unlike conventional dopants, silver does not behave as a passive component;

instead, it actively participates in charge transport and structural modification depending on its oxidation state and distribution within the glass network.

In oxide glasses, silver may exist as Ag^+ ions, neutral Ag atoms, or silver nanoparticles (AgNPs), with the relative population governed by glass composition, melting temperature, redox conditions, and cooling rate during glass preparation. Ag^+ ions typically occupy modifier or interstitial sites and interact strongly with non-bridging oxygens (NBOs). This interaction lowers the potential barrier for electron transport and promotes localized electronic hopping, causing silver to contribute primarily to electronic conduction rather than ionic conduction. Singh et al. (2022) reported that Ag-containing borate glasses exhibit enhanced electronic conductivity due to Ag-related localized states, while El-Mallawany et al. (2023) showed that silver incorporation reduces the activation energy for charge transport by introducing additional electronic conduction pathways.

Partial reduction of Ag^+ ions during melt quenching or subsequent thermal treatment can lead to the formation of Ag nanoparticles. Al-Buriahi et al. (2021) demonstrated that Ag nanoparticles readily form under suitable thermal conditions and significantly enhance dielectric and electrical responses by increasing the effective surface area for charge carrier interaction. From a theoretical perspective, Ag nanoparticles introduce localized metallic clusters within the insulating glass matrix, creating discrete electronic energy states near the Fermi level. These localized states act as intermediate hopping sites, enhancing electronic conductivity through hopping and percolation mechanisms.

In mixed ionic–electronic (MIE) glass systems, silver plays a particularly important role by strengthening the electronic contribution to charge transport. When Ag species are incorporated alongside alkali ions such as Li^+, competition occurs between Li^+ ionic migration through NBO sites and Ag-related electronic hopping processes. Singh et al. (2023) reported non-linear DC conductivity behaviour, including conductivity minima within specific compositional ranges in Ag-doped lithium borate glasses, which is a characteristic feature of MIE systems.

Silver incorporation also influences the glass structure. FTIR studies by Lakshminarayana et al. (2022) showed that silver addition promotes NBO formation in borate glasses, enhancing ionic mobility but simultaneously weakening network rigidity. This structural modification can lead to elastic softening, particularly when combined with heavy metal oxides such as Bi_2O_3. Furthermore, Ag nanoparticles

introduce localized rigid regions due to metallic bonding, resulting in structural heterogeneity. The coexistence of flexible NBO-rich regions and rigid Ag-rich regions contributes to elastic anomalies commonly observed in Ag-doped MIE glass systems.

In addition to electrical and structural effects, silver nanoparticles enhance radiation shielding performance. The relatively high atomic number of silver ($Z = 47$) increases photon interaction probability, particularly through photoelectric absorption at low photon energies. Al-Hadeethi and Sayyed (2022) demonstrated that noble metal-doped glasses exhibit higher mass attenuation coefficients than undoped systems. More recently, Lakshminarayana et al. (2024) confirmed that Ag-containing heavy metal oxide glasses show improved photon attenuation parameters when evaluated using the Phy-X/PSD simulation program.

When incorporated into bismuth borate glass systems, silver produces a synergistic effect. While Bi_2O_3 contributes to radiation shielding primarily through its high atomic number and density, silver enhances electronic conduction and photon interaction at the microscopic level. This synergy improves overall shielding efficiency while simultaneously influencing elastic and electrical properties. Consequently, Ag-doped bismuth borate glasses provide an ideal platform for investigating the coupled effects of structure, elasticity, DC conductivity, and radiation shielding performance in mixed ionic-electronic glass systems.

2.7 Structural Properties of the Glass System

2.7.1 Structural Properties of Borate Glass

Borate glasses are widely studied due to their excellent glass-forming ability and remarkable structural flexibility. The glass network is primarily composed of trigonal BO_3 units and tetrahedral BO_4 units, which coexist within the structure. The relative proportion of these units governs the degree of network connectivity, rigidity, and openness of the glass. Pure borate glass is predominantly composed of BO_3 units arranged in planar triangular configurations, resulting in a relatively open and less rigid network structure.

The addition of modifier oxides, such as alkali or alkaline earth oxides, significantly alters the borate glass network. At low modifier concentrations, modifier cations promote the conversion of BO_3 units into BO_4 units to maintain charge

neutrality. This transformation enhances network polymerisation, increases cross-link density, and improves glass rigidity. FTIR studies by Lakshminarayana et al. (2022) confirmed this structural modification through increased intensity of BO_4-related vibrational bands.

At higher modifier concentrations, the glass network undergoes depolymerisation due to the formation of non-bridging oxygens (NBOs). NBOs are created when B–O–B linkages are broken, resulting in oxygen atoms bonded to only one boron atom. The presence of NBOs increases structural disorder and reduces network rigidity, leading to lower elastic moduli and enhanced ionic mobility. Recent studies by Sabri et al. (2021) and El-Mallawany et al. (2023) demonstrated that increasing NBO concentration weakens the borate network and facilitates alkali ion migration, thereby directly influencing DC conductivity behaviour.

X-ray diffraction (XRD) patterns of borate glasses typically exhibit a broad diffuse halo without sharp diffraction peaks, confirming their amorphous nature. The position and width of this halo provide information on average interatomic spacing and medium-range order. Fourier transform infrared (FTIR) spectroscopy further enables identification of short-range structural units and evaluation of bonding changes induced by compositional variation. FTIR spectra of borate glasses are characterised by absorption bands associated with BO_3 and BO_4 structural units. The asymmetric stretching vibrations of BO_3 units are generally observed in the range of 1200–1600 cm^{-1}, corresponding to B–O stretching in trigonal borate groups, including boroxol rings and non-ring BO_3 units. Lakshminarayana et al. (2022) and Sabri et al. (2021) reported that increased intensity in this region indicates a higher concentration of BO_3 units and NBOs, reflecting network depolymerisation.

In contrast, the stretching vibrations of BO_4 units typically appear in the 800–1200 cm^{-1} range, which corresponds to B–O stretching in tetrahedral borate groups. El-Mallawany et al. (2023) reported that increased BO_4-related band intensity signifies enhanced network polymerisation and increased cross-link density. The relative intensity ratio of BO_4 to BO_3 bands is therefore commonly used to evaluate structural transformations in borate glasses induced by modifier addition. At low modifier contents, the BO_3-to-BO_4 conversion results in increased network rigidity, whereas at higher modifier concentrations, increased NBO formation leads to higher BO_3-related vibrations and reduced network connectivity. These structural trends are consistent with

FTIR analyses of lithium- and alkali-modified borate glasses reported by Singh et al. (2022).

Overall, the structural adaptability of borate glasses allows them to accommodate a wide range of modifiers and dopants. However, their relatively low density and low effective atomic number limit their suitability for radiation shielding applications, which motivates the incorporation of heavy metal oxides such as Bi_2O_3 to enhance functional performance.

2.7.2 Strucutral Properties of Bismuth Borate Glass

The incorporation of bismuth oxide (Bi_2O_3) into borate glass systems induces significant structural modifications due to the dual role of Bi_2O_3 as both a network modifier and an intermediate oxide. The structural behaviour of Bi_2O_3 within the glass network is strongly dependent on its concentration and the presence of other constituents such as alkali or noble metal ions.

At lower Bi_2O_3 concentrations, bismuth ions predominantly act as network modifiers. They disrupt B–O–B linkages within the borate network, leading to the formation of non-bridging oxygens (NBOs) and increased structural disorder. This process results in a more open and depolymerised glass network. FTIR studies by Al-Buriahi et al. (2021) and Lakshminarayana et al. (2022) reported an increase in the intensity of NBO-related B–O vibrational bands with increasing Bi_2O_3 content, confirming the depolymerisation of the borate network.

With further increase in Bi_2O_3 concentration, Bi_2O_3 begins to participate more actively in the glass network through the formation of BiO_6 octahedral structural units. These BiO_6 units are associated with Bi–O–Bi and Bi–O–B linkages and contribute to increased glass density and altered bonding configurations. The presence of BiO_6 units have been consistently confirmed by FTIR absorption bands corresponding to Bi–O stretching vibrations appearing in the low-wavenumber region of 400–600 cm^{-1}. Al-Buriahi et al. (2021) and Lakshminarayana et al. (2022) identified bands within this region and attributed them to BiO_6 octahedra incorporated into the borate glass network.

In addition to introducing BiO_6 units, Bi_2O_3 substitution influences the relative distribution of BO_3 and BO_4 structural units. Several recent FTIR investigations (Sabri et al., 2021; El-Mallawany et al., 2023) have shown that increasing Bi_2O_3 content enhances NBO formation, leading to increased BO_3-related vibrational bands in the

1200–1600 cm^{-1} region and a corresponding reduction in BO_4-related bands in the 800–1200 cm^{-1} region. This behaviour indicates gradual network depolymerisation when Bi_2O_3 acts primarily as a modifier at lower concentrations.

At higher Bi_2O_3 concentrations, the increasing contribution of rigid BiO_6 octahedral units partially compensates for network depolymerisation by reinforcing the glass structure. As a result, the glass network exhibits structural heterogeneity characterised by the coexistence of NBO-rich regions and rigid BiO_6-based polyhedral units. This structural competition plays a crucial role in governing the elastic and electrical behaviour of bismuth borate glasses. Sabri et al. (2021) and El-Mallawany et al. (2023) reported non-linear variations in elastic moduli and ultrasonic velocities in bismuth borate glass systems, which were attributed to structural transitions associated with changes in NBO concentration and BiO_6 formation. Similar structural features have also been linked to mixed ionic–electronic conduction behaviour (Hisam et al., 2021).

X-ray diffraction (XRD) patterns of bismuth borate glasses typically exhibit a broad amorphous halo without sharp diffraction peaks, indicating that the incorporation of Bi_2O_3 does not induce crystallisation within the investigated compositional range. However, shifts in the position of the amorphous halo suggest changes in average interatomic spacing and medium-range order caused by the presence of heavy bismuth ions. The high atomic mass and polarizability of bismuth further enhance photon–matter interaction probability, contributing to improved radiation attenuation properties.

In summary, the structural characteristics of bismuth borate glasses are governed by a balance between network depolymerisation through NBO formation and network reinforcement through the incorporation of BiO_6 octahedral units. These structural modifications strongly influence elastic properties, DC conductivity, and radiation shielding performance. A comprehensive understanding of these structure–property relationships is therefore essential for optimising bismuth borate glass systems for multifunctional applications, particularly in mixed ionic–electronic and radiation shielding contexts.

2.8 Elastic Properties of the Glass System

Elastic properties provide essential information on the mechanical stability, rigidity, and interatomic bonding strength of glass systems. These properties are directly

related to the atomic arrangement and connectivity of the glass network and are highly sensitive to compositional and structural variations. In oxide glasses, elastic parameters such as Young's modulus, shear modulus, bulk modulus, Poisson's ratio, Debye temperature, and mean sound velocity are commonly evaluated using ultrasonic velocity measurements.

Ultrasonic analysis is a reliable and non-destructive technique widely employed to investigate the elastic behaviour and structural characteristics of glass networks. The elastic properties derived from ultrasonic measurements are closely related to glass density and sound wave velocities, providing insight into network compactness, bond strength, and rigidity. The mechanical response of glass under applied stress is commonly described using three fundamental elastic moduli: Young's modulus (Y), shear modulus (μ), and bulk modulus (K).

Young's modulus (Y) represents the stiffness of a material and is defined as the ratio of uniaxial stress to the corresponding longitudinal strain, as illustrated in Figure 2.10. It describes the resistance of a material to elastic deformation under tensile or compressive loading. Mathematically, Young's modulus is expressed as:

$$\mathrm{Y} = \frac{Stress}{Strain} = \frac{Fl}{A\Delta l} \tag{2.1}$$

where F is external force, l is original length, Δl is change in length and A is cross-sectional area.

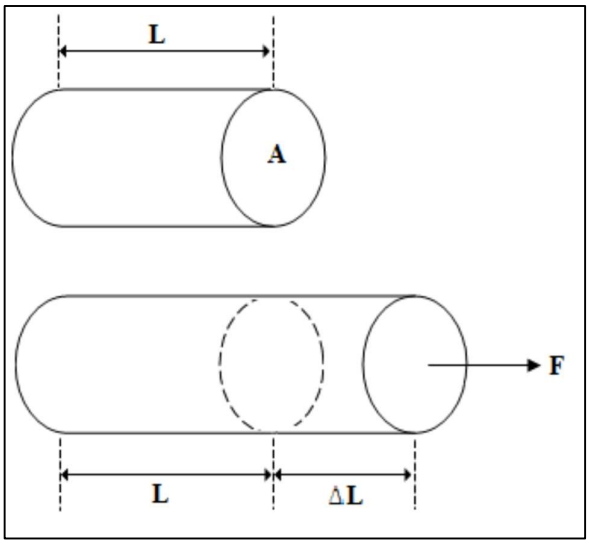

Figure 2.4 Definition of Young's Modulus
(Samsudin et al., 2021)

The shear modulus (μ) quantifies the resistance of a material to shape deformation under shear stress, where the applied force acts parallel to the surface of the material. This modulus is defined as the ratio of shear stress to shear strain, as shown in Figure 2.11, and is given by:

$$\mu = \frac{Shear\ stress}{Shear\ Strain} = \frac{Fh}{A\Delta x} \tag{2.2}$$

where h is initial height and Δx is the transverse displacement.

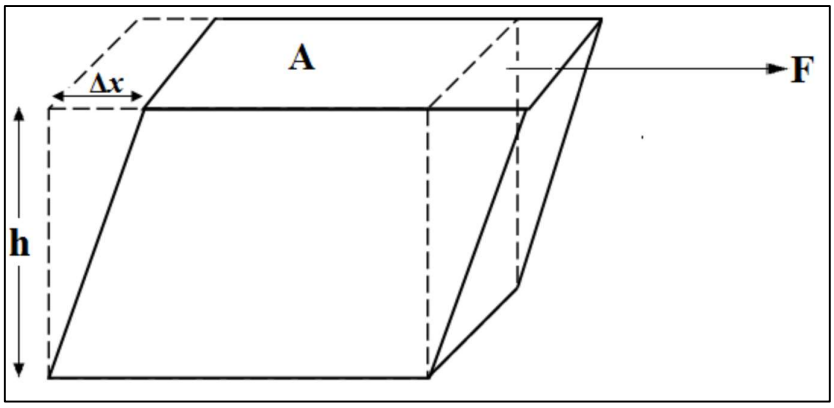

Figure 2.5 Definition of Shear Modulus
(Samsudin et al., 2021)

The bulk modulus (K) measures a material's resistance to uniform volume change when subjected to hydrostatic pressure, while maintaining its shape. It describes the compressibility of the material and is defined as the ratio of applied pressure to volumetric strain, as illustrated in Figure 2.12. The bulk modulus is expressed as:

$$\mu = \frac{Stress}{Volumetric\ Strain} = \frac{F/A}{-V/V} \tag{2.3}$$

where V is the original volume and ΔV is change in volume.

These elastic moduli are strongly influenced by the rigidity of the glass network and the nature of interatomic bonds. Variations in ultrasonic velocities and elastic parameters therefore provide valuable insight into structural modifications, such as network depolymerisation, NBO formation, and the incorporation of heavy metal oxide units. As a result, elastic properties serve as an important tool for correlating structural evolution with mechanical, electrical, and radiation shielding behaviour in glass systems.

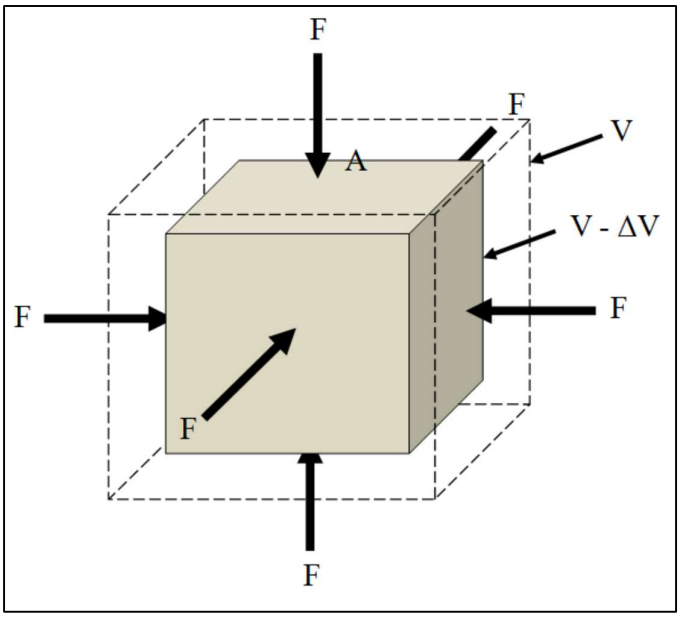

Figure 2.6 Definition of Bulk Modulus
(Samsudin et al., 2021)

2.8.1 Elastic Properties of Borate Glass

The elastic properties of oxide glasses are fundamentally governed by interatomic forces, bond strength, coordination number, and the potential energy distribution within the disordered glass network. Unlike crystalline materials, glasses lack long-range order; therefore, their elastic response depends primarily on short-range structural units and the connectivity between them. In borate-based systems, the elastic behaviour is strongly influenced by the relative distribution of trigonal BO_3 and tetrahedral BO_4 structural units, as well as the formation of non-bridging oxygens (NBOs). These structural entities determine the degree of network polymerisation and cross-link density, which directly control stiffness, rigidity, and resistance to deformation.

Recent investigations between 2020 and 2026 have confirmed that the addition of modifier oxides significantly alters ultrasonic velocities and elastic moduli by restructuring the borate network (Sabri et al., 2021; Singh et al., 2022; El-Mallawany et al., 2023). Ultrasonic measurements, including longitudinal velocity (V_L) and shear velocity (V_S) provide insight into the mechanical integrity of the glass system. Since

elastic moduli such as longitudinal modulus (C_L), shear modulus (μ), Young's modulus (Y), and bulk modulus (K) are directly proportional to density and ultrasonic velocity, any structural rearrangement within the glass network manifests clearly in these parameters.

Studies on heavy-metal-oxide-doped borate glasses during 2020–2026 consistently report non-linear variations in V_L and V_S with increasing modifier concentration. At lower concentrations of modifier oxides, a partial conversion of BO_3 units into BO_4 units often occurs to maintain charge neutrality. This transformation enhances cross-link density and increases network dimensionality, leading to improved rigidity and higher elastic moduli. Such behaviour reflects enhanced network polymerisation and stronger B–O bonding interactions (Lakshminarayana et al., 2022).

However, as modifier content increases further, the borate network undergoes depolymerisation due to the generation of NBOs. The breaking of B–O–B linkages weakens interatomic bonding and reduces structural compactness, resulting in elastic softening. This softening is reflected by reductions in ultrasonic velocities, Young's modulus, bulk modulus, and Debye temperature (Al-Hadeethi et al., 2023; Rahman et al., 2024). The presence of NBOs increases free volume within the glass network and enhances structural disorder, thereby decreasing resistance to mechanical deformation.

In bismuth-containing borate glasses specifically, Bi_2O_3 exhibits a dual structural role. At lower concentrations, Bi^{3+} ions act predominantly as network modifiers, disrupting B–O–B bonds and generating NBOs. This results in reduced stiffness and lower elastic moduli. At higher concentrations, however, BiO_6 octahedral units may form and contribute to local structural reinforcement due to their higher coordination number and relatively rigid geometry (El-Mallawany et al., 2023; Kumar et al., 2024). The competition between network depolymerisation via NBO formation and local reinforcement via BiO_6 formation often produces non-linear elastic behaviour across composition ranges.

These recent ultrasonic studies further highlight that elastic moduli are closely associated with oxygen molar volume and bond stretching force constants. An increase in oxygen molar volume indicates network expansion and weaker bonding interactions, which reduce stiffness. Conversely, higher bond stretching force constants (F) enhance Young's modulus and bulk modulus, indicating stronger resistance to bond stretching and compression. Therefore, elastic behaviour can be interpreted through microscopic

parameters such as bond length, bond strength, and coordination environment (Singh et al., 2022; Rahman et al., 2024).

Additionally, contemporary research has linked elastic anomalies to mixed ionic–electronic (MIE) transitions in glass systems containing both alkali and heavy metal oxides. In such systems, charge transport involves competition between ionic migration such as Li^+ hopping and electronic conduction mechanisms. Recent reports show that minima in DC conductivity often coincide with anomalies in elastic moduli and ultrasonic velocities (Hisam et al., 2021; El-Mallawany et al., 2023). This correlation suggests that structural rearrangements affecting mechanical rigidity simultaneously influence charge transport pathways. Consequently, elastic softening may not only arise from NBO formation but also from modifications in electronic density states and ionic mobility within the glass matrix.

Poisson's ratio (σ) remains a crucial parameter for evaluating network connectivity and cross-link density. Lower σ values generally indicate higher resistance to lateral expansion under compression, reflecting stronger covalent bonding and higher cross-link density. Recent studies (2020–2025) confirm that σ decreases with increasing BO_4 formation and increases with higher NBO concentration, supporting its inverse relationship with network connectivity (Lakshminarayana et al., 2022; Al-Hadeethi et al., 2023).

Furthermore, the field strength of modifier cations plays an essential role in determining elastic response. High-field-strength cations tend to strengthen local bonding environments and enhance rigidity, whereas low-field-strength, large-radius cations such as Bi^{3+} may promote structural expansion and network depolymerisation. The overall elastic behaviour therefore reflects a balance between structural reinforcement and weakening mechanisms (Kumar et al., 2024).

These recent studies published between 2020 and 2026 indicate that the elastic behaviour of borate-based glasses is controlled by the combined effects of structural transformations and compositional modifications. The interconversion between BO_3 and BO_4 units, the generation of non-bridging oxygens (NBOs), the incorporation of heavy metal oxides, variations in cross-link density, and the presence of mixed ionic–electronic interactions collectively influence the mechanical response of the glass network. These structural and electronic factors directly affect key elastic parameters, including longitudinal modulus, shear modulus, Young's modulus, bulk modulus, Debye temperature, and ultrasonic wave velocities. A comprehensive understanding of

these interdependent mechanisms is therefore crucial for explaining the elastic anomalies observed in bismuth-substituted mixed ionic-electronic borate glass systems.

2.8.2 Elastic Properties of Bismuth Borate Glass

The incorporation of bismuth oxide (Bi_2O_3) into borate glass systems produces distinct elastic behaviour compared to conventional modifier-doped borate glasses. Unlike simple alkali modifiers, Bi_2O_3 exhibits dual structural functionality, acting both as a network modifier and as an intermediate oxide depending on concentration. This duality significantly influences interatomic bonding, network connectivity, and consequently, the elastic response of the glass system.

Recent studies (2020–2026) have demonstrated that the addition of Bi_2O_3 leads to non-monotonic variations in ultrasonic velocities and elastic moduli in borate-based glasses. At lower Bi_2O_3 concentrations, Bi^{3+} ions tend to break B–O–B linkages and generate non-bridging oxygens (NBOs), resulting in reduced network connectivity and decreased stiffness. This structural depolymerisation weakens the glass network, which is reflected by reductions in longitudinal modulus (C_L), shear modulus (μ), Young's modulus (Y), and bulk modulus (K). The decrease in ultrasonic wave velocities at this stage indicates reduced resistance to both compressional and shear deformation.

However, as the Bi_2O_3 concentration increases, the structural role of bismuth evolves. The formation of BiO_6 octahedral units introduce locally rigid polyhedral structures within the glass network. These units possess higher coordination numbers compared to boron structural groups and contribute to increased density and enhanced short-range ordering. Contemporary investigations (El-Mallawany et al., 2023; Kumar et al., 2024) report that this structural rearrangement may temporarily increase elastic moduli due to improved local packing density and stronger Bi–O interactions. Consequently, a compositional region may exist where elastic moduli increase before declining again at higher concentrations.

This non-linear elastic behaviour is strongly associated with the competition between network depolymerisation via NBO formation and local reinforcement via BiO_6 formation. When NBO formation dominates, the glass network becomes more flexible and exhibits elastic softening. When BiO_6 structural units contribute significantly to the network framework, local rigidity increases, leading to higher elastic parameters. Therefore, the elastic response of bismuth borate glass is governed by a

delicate structural balance rather than a simple modifier effect.

Furthermore, recent literature highlights that the large ionic radius and high polarizability of Bi^{3+} ions influence bond force constants and lattice potential energy. The relatively lower Bi–O bond strength compared to B–O bonding can contribute to reduced overall stiffness when B–O–B linkages are replaced by Bi–O bonds. At the same time, the increased atomic mass of bismuth enhances density, which directly affects elastic moduli through the density–velocity relationship. This explains why elastic parameters in bismuth borate glasses often show complex trends rather than linear dependence on composition.

Another important aspect reported in recent years is the correlation between elastic anomalies and mixed ionic–electronic (MIE) behaviour in heavy-metal-doped borate systems. In glasses containing both alkali ions such as Li^+ and heavy metal oxides such as Bi_2O_3, changes in elastic parameters frequently coincide with minima in DC conductivity. This suggests that structural modifications affecting mechanical rigidity simultaneously influence charge transport mechanisms. Elastic softening in certain compositional ranges may therefore indicate increased structural disorder and enhanced NBO concentration, which also alter ionic mobility and electronic hopping processes.

Debye temperature (θ_D) and mean sound velocity (V_m) further support this interpretation. Higher θ_D values correspond to stronger interatomic bonding and greater lattice stiffness, whereas reductions in θ_D indicate weakened bonding and structural relaxation. In bismuth borate glasses, compositional regions exhibiting elastic softening typically coincide with lower Debye temperature values, reinforcing the link between structural depolymerisation and mechanical response.

Poisson's ratio (σ) also provides insight into the cross-link density of the bismuth borate network. Lower σ values suggest higher resistance to transverse deformation and stronger covalent bonding, while higher σ values reflect reduced network connectivity and increased structural flexibility. Recent investigations confirm that increasing Bi_2O_3 content can initially decrease σ due to structural rearrangement but may increase σ at higher concentrations when NBO formation becomes dominant.

Based on these recent studies, elastic properties of bismuth borate glasses differ fundamentally from those of simple modifier-doped borate systems due to the dual structural role of Bi_2O_3, the formation of BiO_6 units, the generation of NBOs, and the coupling between structural rigidity and mixed ionic–electronic conduction. The elastic behaviour is therefore controlled by a complex interplay between density enhancement,

bond strength modification, coordination number changes, and structural heterogeneity. Understanding these mechanisms is essential for interpreting elastic anomalies and optimising bismuth borate glasses for multifunctional applications, including mechanical stability and radiation shielding performance.

2.8.3 Structural Bonding of Elastic Behaviour of Bismuth Borate Glass

Previous studies have reported that the ratio between the theoretical bulk modulus predicted by the bond compression framework and the experimentally determined bulk modulus is often greater than unity in borate-based glass systems. This observation suggests that isotropic deformation of the glass network is not governed solely by bond compression but also involves bond bending and ring deformation mechanisms within the glass structure (El-Mallawany et al., 2023; Kumar et al., 2024). Larger values of this ratio are commonly associated with increased structural flexibility and reduced resistance to volumetric compression.

The ring deformation framework further describes this behaviour using the average ring size parameter (ℓ), which represents the effective size of structural rings within the borate network. Studies have shown that larger ℓ values correspond to expanded ring structures and a more open network configuration, whereas smaller values indicate a more compact and rigid structure. The expansion of borate rings is frequently attributed to the formation of non-bridging oxygens (NBOs), which occur when modifier oxides disrupt B–O–B linkages in the glass network (Lakshminarayana et al., 2022).

In heavy-metal-modified borate glasses, the incorporation of oxides such as Bi_2O_3 significantly alters the network structure by modifying the distribution of BO_3 and BO_4 structural units and promoting the formation of BiO_6 polyhedral groups (Kumar et al., 2024). These structural modifications introduce heterogeneity within the glass network and may enhance ring distortion during compression. As a result, borate glasses containing heavy metal oxides often exhibit increased structural openness and reduced network rigidity.

Recent investigations on heavy-metal-oxide and borate-based glass systems continue to employ the bond compression framework to interpret the compositional dependence of elastic moduli. Although initially developed for single-component oxide glasses, this structural bonding approach remains applicable to multicomponent

systems, including bismuth-containing borate glasses (Lakshminarayana et al., 2022; El-Mallawany et al., 2023). Recent applications of this model show that the theoretical bulk modulus generally increases with higher bond density and stronger interatomic interactions, particularly when rigid structural units such as BO_4 or polyhedral groups are present (Kumar et al., 2024).

However, several contemporary studies have reported that the theoretical bulk modulus (K_{bc}) is typically higher than the experimentally determined bulk modulus (K_e) (El-Mallawany et al., 2023; Rahman et al., 2024). This discrepancy indicates that the actual deformation of oxide glass networks involves additional mechanisms beyond pure bond stretching. In particular, angular deformation, bond bending, and ring distortion contribute significantly to the isotropic compression behaviour of disordered glass structures.

The ratio K_{bc}/K_e has therefore been widely used in recent literature as an indicator of the relative contribution of bending mechanisms in elastic deformation. When this ratio approaches unity, the glass network exhibits stronger structural connectivity and deformation is mainly governed by bond stretching. In contrast, higher values of the ratio indicate increased structural openness, greater network flexibility, and the dominance of bond bending processes (Singh et al., 2022).

Several recent studies on alkali- and heavy-metal-modified borate glasses have also reported non-linear variations in the K_{bc}/K_e ratio with composition (El-Mallawany et al., 2023; Kumar et al., 2024). These compositional anomalies are commonly associated with structural transitions involving the formation of non-bridging oxygens and changes in coordination environment. In bismuth-containing borate glasses, the addition of Bi_2O_3 modifies bond density and local structural geometry, thereby influencing both theoretical and experimentally measured bulk modulus values.

Within this framework, the K_{bc} is expressed as:

$$K_{bc} = \frac{n_b r^2 F}{9} \tag{2.4}$$

where r is the bond length and F is the stretching force constant. This computed modulus is directly proportional to the number of network bonds per unit volume, n_b which is given by:

$$n_b = \frac{n_f N_A}{V_A} \tag{2.5}$$

where n_f is the number of network bonds per glass formula unit, N_A is Avogadro's number, ρ is density and V_a is the molar volume of the glass. Recent studies confirm that K_{bc} is directly proportional to bond density and bond strength, implying that glasses with higher cross-link density and shorter bond lengths exhibit greater resistance to volumetric compression (Singh et al., 2022; Rahman et al., 2024).

For multicomponent oxide glasses such as bismuth borate systems, the model has been extended to account for ontributions from different structural units The generalized expression can be written as in Equation 2.6:

$$K_{bc} = \frac{N_A}{9V_a}\sum_i (xn_f F r^2)_i \tag{2.6}$$

where x is the mole fraction of each oxide component. The F is the stretching force constant and is commonly approximated as:

$$F = \frac{1.7}{r^3} \tag{2.7}$$

The average ring size (ℓ), which represents the effective size of borate structural rings within the glass network. The average ring size is defined in terms of the bond perimeter and is estimated from the relationship between the average bond stretching force constant and the experimentally determined bulk modulus. The expression for ℓ is given by:

$$\ell = [0.0106\frac{\overline{F}}{K_{exp}}]^{0.26} \tag{2.8}$$

where K_{exp} is the experimental bulk modulus and $\bar{F}$ is the average stretching force constant. The average force constant is calculated as:

$$\bar{F} = \frac{\sum(xn_f F)_i}{\sum(xn_f)_i} \tag{2.9}$$

where x is the mole fraction, n_f is the number of network bonds per structural unit, and F is the bond stretching force constant. These parameters reflect the atomic-scale bonding characteristics previously defined in the bond compression framework.

These recent literatures imply that the combined application of bond compression and ring deformation analyses provides a comprehensive structural interpretation of elastic properties in heavy-metal-doped borate glasses. By linking microscopic ring topology with macroscopic mechanical response, these frameworks offer critical insight into how compositional variation influences network rigidity and deformation mechanisms.

2.9 DC Conductivity Properties

DC conductivity is an important electrical parameter used to understand charge transport behaviour in glass systems. In oxide glasses, electrical conduction typically occurs through the movement of charge carriers such as mobile ions or electrons within the disordered glass network. The conductivity behaviour is strongly influenced by the structural arrangement of the glass network, including network connectivity, the presence of non-bridging oxygens (NBOs), and the type and concentration of modifier oxides incorporated into the glass matrix (Singh et al., 2022; El-Mallawany et al., 2023).

Recent studies have shown that the electrical properties of glass systems are closely related to their structural features. The introduction of modifier oxides breaks the bridging oxygen bonds within the glass network, leading to the formation of NBOs that create pathways for charge carrier movement. This structural modification increases the free volume of the glass network and enhances the mobility of charge carriers, which contributes to higher electrical conductivity (Lakshminarayana et al., 2022).

The DC conductivity behaviour of oxide glasses is commonly described by thermally activated hopping mechanisms, where charge carriers migrate between neighbouring sites within the glass structure. Several recent studies have confirmed that DC conductivity generally follows Arrhenius-type behaviour, where conductivity increases with temperature due to enhanced mobility of charge carriers (Rahman et al., 2024). The activation energy required for conduction depends on the rigidity of the glass network and the concentration of mobile ions.

In certain oxide glass systems, electrical conduction may involve both ionic and electronic charge carriers, leading to mixed ionic-electronic (MIE) conduction behaviour. Recent investigations have reported that the coexistence of mobile alkali ions and heavy metal or transition metal ions can produce competition between ionic transport and electronic hopping mechanisms (Kumar et al., 2024; El-Mallawany et al., 2023). In such systems, structural modifications influence both ionic mobility and the availability of electronic conduction pathways.

2.9.1 DC Conductivity of Borate Glass

Borate glasses have been extensively studied due to their flexible network structure and excellent glass-forming ability. The fundamental structural units of borate glasses consist of trigonal BO_3 and tetrahedral BO_4 groups, which form a network capable of accommodating various modifier oxides. The electrical conductivity behaviour of borate glasses is primarily governed by the presence of modifier cations and the formation of non-bridging oxygens within the network (Lakshminarayana et al., 2022).

Recent studies have reported that the addition of alkali oxides such as Li_2O, Na_2O, or K_2O significantly enhances the DC conductivity of borate glasses. This enhancement occurs because alkali ions act as mobile charge carriers that migrate through the glass network via thermally activated hopping between neighbouring sites (Singh et al., 2022). The introduction of modifier oxides breaks B–O–B linkages and generates NBOs, which increase the number of available pathways for ionic migration.

Several investigations conducted between 2020 and 2026 have demonstrated that the electrical conductivity of borate glasses is strongly influenced by the degree of network depolymerisation. As the concentration of modifier oxides increases, the glass network becomes more open and structurally flexible, which facilitates ion movement through the matrix (Rahman et al., 2024). However, excessive modifier content may also lead to structural clustering or reduced connectivity of conduction pathways, resulting in non-linear conductivity behaviour.

Structural transformations within borate glasses, such as the conversion of BO_3 units to BO_4 units, may also influence conductivity behaviour. These structural changes modify the distribution of NBOs and alter the connectivity of the glass network, which affects the migration pathways of mobile ions (Kumar et al., 2024). Consequently, the electrical conductivity of borate glasses is closely related to the structural configuration of the glass network.

2.9.2 DC Conductivity of Bismuth Borate Glass

Bismuth borate glasses have attracted considerable research attention due to their unique structural and electrical properties. The incorporation of bismuth oxide (Bi_2O_3) into borate glass systems introduces heavy metal ions that significantly modify

the glass network structure. Bismuth ions may act either as network modifiers or intermediate oxides depending on their concentration, leading to structural rearrangements within the borate network (El-Mallawany et al., 2023). These structural modifications can influence the distribution of borate units, including BO_3 and BO_4 groups, and alter the connectivity of the glass network.

Recent studies have shown that the incorporation of Bi_2O_3 can influence both ionic and electronic conduction mechanisms in borate glasses. The large ionic radius and high polarizability of Bi^{3+} ions modify the local bonding environment and may affect the migration pathways of alkali ions within the glass network (Lakshminarayana et al., 2022). In some cases, the presence of heavy metal ions may hinder the movement of alkali ions due to increased structural distortion and interaction with the surrounding oxygen atoms, resulting in reduced ionic conductivity.

Several investigations conducted between 2020 and 2026 have also reported that bismuth borate glasses may exhibit mixed ionic-electronic (MIE) conduction behaviour, where both ionic migration and electron hopping mechanisms contribute to the overall conductivity (Kumar et al., 2024; El-Mallawany et al., 2023). In such systems, ionic conduction typically occurs through the migration of alkali ions, while electronic conduction arises from electron transfer between localized states associated with heavy metal ions or structural defects within the glass network.

Structural modifications associated with Bi_2O_3 incorporation may also influence the formation of non-bridging oxygens (NBOs) and the distribution of borate structural units, which subsequently affect the rigidity of the glass network and the mobility of charge carriers (Rahman et al., 2024). The presence of NBOs generally increases the free volume within the glass network, providing pathways for ion migration and influencing electrical conductivity behaviour.

Although numerous studies have investigated the DC conductivity behaviour of borate and heavy-metal-modified glass systems, limited attention has been given to the combined influence of bismuth substitution and mixed ionic-electronic conduction in lithium borate glass systems containing silver nanoparticles. Most previous investigations have primarily focused on either structural modifications or electrical transport properties separately. Therefore, a more comprehensive study that simultaneously examines the relationship between structural evolution, elastic behaviour, and DC conductivity in bismuth-substituted lithium borate glass systems is still required. Understanding how Bi_2O_3 substitution affects charge transport

mechanisms and the glass network structure is essential for explaining conductivity anomalies and identifying compositional regions associated with mixed ionic–electronic behaviour.

2.10 Radiation Shielding Properties

Radiation shielding materials are widely used to reduce the harmful effects of ionizing radiation in medical, industrial, and nuclear applications. Ionizing radiation includes particles and electromagnetic waves such as alpha particles, beta particles, neutrons, gamma rays, and x-rays. Among these, gamma rays and X-rays are considered particularly hazardous because of their high penetration ability and strong ionizing power, which can damage biological tissues and cause serious health effects such as genetic mutations, skin damage, cataracts, and cancer (Naseer et al., 2021; Alzahrani et al., 2021).

Traditionally, materials such as lead and concrete have been widely used for radiation shielding due to their high density and strong attenuation capability. However, these conventional shielding materials present several limitations. Lead is toxic and environmentally hazardous, while concrete structures are bulky, opaque, and susceptible to cracking over time due to environmental conditions and radiation exposure. These drawbacks have encouraged researchers to explore alternative materials that are safer, lighter, and more versatile (Vadavathi et al., 2021; Lacomme et al., 2021).

In recent years, glass materials have gained considerable attention as promising radiation shielding materials. Glasses possess several advantages, including high transparency, chemical durability, good corrosion resistance, and the ability to incorporate heavy metal oxides (HMOs) into their structure. The incorporation of high atomic number elements such as bismuth (Bi), tungsten (W), and lead (Pb) significantly enhances the photon attenuation capability of glass materials (D'Souza et al., 2021; Cheewasukhanont et al., 2020). Due to these properties, glass-based shielding materials are increasingly being investigated for applications in medical imaging facilities, nuclear reactors, and radiation laboratories.

The shielding effectiveness of a material against gamma radiation is commonly evaluated using several parameters, including the mass attenuation coefficient (MAC), linear attenuation coefficient (LAC), half value layer (HVL), mean free path (MFP),

and effective atomic number (Z_{eff}). Among these parameters, the mass attenuation coefficient represents the probability of photon interaction with matter during radiation penetration and is considered one of the most fundamental indicators of shielding efficiency (Alzahrani et al., 2021). Materials with higher MAC values generally exhibit stronger radiation attenuation performance.

The half value layer and mean free path are also widely used to assess shielding effectiveness. HVL represents the thickness of material required to reduce the intensity of incoming radiation by half, while MFP indicates the average distance travelled by photons between successive interactions with atoms in the material. Lower HVL and MFP values correspond to better shielding performance (Lacomme et al., 2021). Recent studies have also utilized computational tools such as the Phy-X/PSD simulation program to evaluate radiation shielding parameters across wide photon energy ranges, allowing researchers to predict shielding performance efficiently without extensive experimental measurements (D'Souza et al., 2021).

2.10.1 Radiation Shielding Properties of Borate Glass

Borate-based glasses have been extensively studied due to their excellent glass-forming ability, structural flexibility, and ability to accommodate various modifier oxides. The borate glass network is mainly composed of trigonal BO_3 and tetrahedral BO_4 structural units, which provide a versatile framework for incorporating heavy metal oxides to enhance radiation shielding performance (Lakshminarayana et al., 2022).

Recent studies have demonstrated that borate glasses containing heavy metal oxides exhibit improved gamma-ray attenuation properties. The addition of high atomic number elements increases the probability of photon interaction through photoelectric absorption, Compton scattering, and pair production processes (Kumar et al., 2024). As a result, borate glasses modified with heavy metal oxides such as Bi_2O_3, PbO, and WO_3 have shown significantly higher mass attenuation coefficients compared with conventional glass compositions.

Several investigations conducted between 2020 and 2026 have reported that the radiation shielding capability of borate glasses depends strongly on glass composition, density, and photon energy. Increasing the concentration of heavy metal oxides generally increases glass density and effective atomic number, which enhances radiation attenuation performance (Rahman et al., 2024). In addition, structural

modifications such as the formation of non-bridging oxygens and changes in borate structural units may also influence the interaction of photons with the glass network.

Furthermore, the development of borate-based shielding glasses has been supported by computational tools such as the Phy-X/PSD simulation program, which allows the evaluation of radiation shielding parameters across a wide photon energy range. Several recent studies have reported good agreement between theoretical predictions obtained from Phy-X simulations and experimental measurements of attenuation coefficients (D'Souza et al., 2021). These findings highlight the potential of borate glasses as promising materials for radiation shielding applications.

2.10.2 Radiation Shielding Properties of Bismuth Borate Glass

Bismuth borate glasses have attracted considerable attention as potential radiation shielding materials due to the high atomic number and high density of bismuth oxide. The incorporation of Bi_2O_3 into borate glass systems enhances photon attenuation by increasing the probability of interaction between incident gamma rays and the glass matrix. The high atomic number of bismuth (Z = 83) significantly improves the photoelectric absorption process, particularly in the low-energy photon region, making bismuth-based glasses effective candidates for radiation shielding applications (Cheewasukhanont et al., 2020; D'Souza et al., 2021).

Recent studies have demonstrated that increasing the concentration of Bi_2O_3 in borate glasses generally improves radiation shielding performance. Higher Bi_2O_3 content increases both the density and effective atomic number of the glass system, which leads to higher mass attenuation coefficients and improved photon attenuation capability (Evangelin Teresa et al., 2021; Kumar et al., 2024). Consequently, glasses containing higher bismuth concentrations typically exhibit lower half value layer (HVL) and mean free path (MFP) values, indicating stronger radiation shielding efficiency.

In addition to improving radiation attenuation, bismuth borate glasses offer several advantages compared with conventional shielding materials. Unlike lead-based shielding materials, bismuth is considered less toxic and more environmentally friendly. Furthermore, bismuth-containing glasses maintain optical transparency, allowing them to be used in applications such as radiation shielding windows in medical imaging facilities and nuclear laboratories (D'Souza et al., 2021). The incorporation of Bi_2O_3 also modifies the glass network structure by influencing the distribution of BO_3 and BO_4

units and promoting the formation of BiO_6 polyhedral structures. These structural modifications can increase packing density and enhance the interaction probability between photons and the glass matrix (Lakshminarayana et al., 2022).

Recent literature also highlights the growing interest in combining heavy metal oxides with borate glass networks to develop multifunctional materials that simultaneously exhibit improved mechanical stability, electrical behaviour, and radiation shielding capability. However, despite the promising shielding performance reported for many heavy-metal-modified borate glasses, systematic investigations on bismuth-substituted lithium borate glass systems containing silver nanoparticles remain limited. Most previous studies have primarily focused on evaluating attenuation parameters without simultaneously examining the influence of structural modifications and charge transport behaviour on radiation shielding performance.

In particular, the combined effects of Bi_2O_3 substitution, mixed ionic–electronic (MIE) behaviour, and structural changes within the borate glass network have not been extensively explored in relation to photon attenuation characteristics. Structural changes such as the formation of non-bridging oxygens (NBOs), variations in borate structural units, and the presence of heavy metal polyhedral groups may influence not only the physical properties of the glass but also its radiation interaction mechanisms. Therefore, a comprehensive investigation is required to better understand how compositional variations influence radiation shielding efficiency in complex borate glass systems.

In this context, the present study evaluates the radiation shielding properties of $98[20Li_2O\text{-}xBi_2O_3\text{-}(80\text{-}x)B_2O_3]\text{-}2Ag$ glass samples using the Phy-X/PSD simulation program across a wide photon energy range of 15 keV to 15 MeV. This photon energy range covers the most relevant radiation energies encountered in practical applications such as medical imaging, nuclear medicine, industrial radiography, and nuclear reactor environments. The shielding performance of the investigated glass samples is assessed using key radiation attenuation parameters, including the mass attenuation coefficient (MAC), linear attenuation coefficient (LAC), half value layer (HVL), mean free path (MFP), and effective atomic number (Z_{eff}). By correlating these radiation shielding parameters with compositional variations in the glass system, this study aims to provide further insight into the potential of bismuth borate glasses as environmentally friendly alternatives to conventional lead-based radiation shielding materials.

2.11 Summary of Literature Reviews

Table 2.1
Summary of Literature Reviews

Author (Year)	Glass Composition/System	Method/Technique	Main Findings
Cheewasukhanont et al. (2020)	Bi_2O_3–B_2O_3 glass system	Radiation shielding simulation	Increasing Bi_2O_3 concentration improved gamma-ray attenuation due to higher density and atomic number of bismuth.
Alzahrani et al. (2021)	Heavy metal oxide borate glasses	Phy-X'PSD simulation	Mass attenuation coefficient (MAC) and effective atomic number increased with increasing heavy metal oxide content.
D'Souza et al. (2021)	$(60\text{-}x)B_2O_3$–$20SiO_2$–xBi_2O_3–ZnO–BaO glasses	Phy-X software analysis	Glasses with higher Bi_2O_3 content exhibited better radiation shielding performance, particularly at low photon energies.
Lakshminarayana et al. (2022)	Ag-doped borate glasses	FTIR, structural analysis	Silver incorporation modified BO_3/BO_4 distribution and increased non-bridging oxygen formation, affecting electrical and structural properties.
Singh et al. (2022)	Alkali borate glass systems	Electrical conductivity measurements	Mixed ionic–electronic conduction behaviour observed due to interaction between alkali ions and electronic carriers.
El-Mallawany et al. (2023)	Heavy metal oxide glasses	Elastic and electrical analysis	Structural modifications caused by heavy metal oxides significantly influenced elastic moduli and electrical conduction mechanisms.

Kumar et al. (2024)	Bismuth borate glass systems	Structural and radiation shielding analysis	Bi_2O_3 addition enhanced density, effective atomic number, and photon attenuation properties of glass materials.
Rahman et al. (2024)	Alkali borate glasses	Electrical and structural studies	Formation of non-bridging oxygens influenced ionic mobility and electrical conductivity behaviour in borate glasses.

2.12 Research Gap

Borate-based glass systems have been widely investigated due to their excellent glass-forming ability and structural flexibility. Previous studies have reported that the incorporation of heavy metal oxides such as Bi_2O_3 can significantly modify the structural, elastic, electrical, and radiation shielding properties of borate glasses. The presence of Bi_2O_3 increases the density and effective atomic number of the glass network, which enhances photon attenuation capability and improves radiation shielding performance (D'Souza et al., 2021; Kumar et al., 2024). In borate glasses, structural changes such as the transformation between BO_3 and BO_4 units and the formation of non-bridging oxygens (NBOs) can influence the rigidity and connectivity of the glass network, which subsequently affects elastic properties and electrical transport behaviour (Lakshminarayana et al., 2022).

Recent studies have also reported the presence of mixed ionic-electronic (MIE) conduction in certain oxide glass systems, where both ionic migration and electronic hopping mechanisms contribute to electrical conductivity (El-Mallawany et al., 2023; Singh et al., 2022). In such systems, compositional variations may lead to anomalies in elastic and electrical properties within specific compositional regions due to structural modifications in the glass network. However, most previous investigations have focused on individual properties such as structural characteristics, electrical conductivity, or radiation shielding performance separately.

Consequently, limited studies have examined the relationship between structural modification, elastic behaviour, electrical transport, and radiation shielding properties simultaneously in the same glass system. Understanding this relationship is important because the structural characteristics of glass strongly influence its mechanical stability, electrical conduction behaviour, and radiation attenuation efficiency. A comprehensive understanding of these combined properties can contribute to the development of multifunctional and cost-effective glass materials that may serve as transparent and environmentally friendly radiation shielding alternatives to conventional materials such as lead and concrete, particularly in applications including medical imaging facilities, nuclear laboratories, and industrial radiography.

Furthermore, research on bismuth-substituted lithium borate glasses containing silver nanoparticles remains limited. The incorporation of silver species may introduce additional electronic conduction pathways and influence the interaction between ionic

and electronic charge carriers, which may affect both DC conductivity behaviour and radiation attenuation characteristics. Therefore, a comprehensive investigation is required to understand how Bi_2O_3 substitution influences structural, elastic, DC conductivity, and radiation shielding properties simultaneously in borate glass systems.

In this study, the $98[20Li_2O\text{-}xBi_2O_3\text{-}(80\text{-}x)B_2O_3]\text{-}2Ag$ glass system with Bi_2O_3 concentrations of x = 3 to 11 mol% is investigated. Structural, elastic, and DC conductivity properties are analysed using XRD, FTIR spectroscopy, ultrasonic velocity measurements, and impedance spectroscopy, while radiation shielding performance is evaluated using the Phy-X/PSD simulation program over a photon energy range of 15 keV to 15 MeV, which represents a wide spectrum of photon energies commonly encountered in medical, industrial, and nuclear radiation applications. This study aims to provide a clearer understanding of the relationship between glass structure, elastic behaviour, charge transport mechanisms, and radiation shielding performance in mixed ionic-electronic bismuth borate glass systems.

CHAPTER 3
RESEARCH METHODOLOGY

3.1 Introduction

This section provides an overview of the materials employed, outlines the procedures for sample preparation, and offers comprehensive details on the characterizations conducted in the course of this research. The characterizations encompass X-Ray Diffraction Spectrometer (XRD) technique, Fourier Transmission Infrared Spectrometer (FTIR) measurement, Impedance Spectroscopy measurement, Ultrasonic Velocity Measurement and PHY-X /PSD Online software.

3.2 Materials

The starting material used for the preparation of the glass samples were of high purity to ensure minimal contamination and accurate compositional control. The chemicals used in this study include boron oxide (B_2O_3), lithium oxide (Li_2CO_3), bismuth oxide (Bi_2O_3) and silver oxide (Ag_2O). The purity of each chemical precursor used in the glass preparation is listed in Table 3.1. High purity chemicals were used to minimize the impurities that could influence the structural and electrical properties of the prepared glass samples.

Table 3.1
List of Oxide Powders, Chemical Formula and Molar Mass for Current Glass Samples.

Materials	Chemical Formula	Molecular Mass (g/mol)	Purity
Boron Oxide	B_2O_3	69.62	99.9%
Bismuth Oxide	Bi_2O_3	465.96	99.9%
Lithium Carbonate	Li_2CO_3	29.88	99.9%.
Silver Oxide	Ag_2O	231.74	99.9%.

3.3 Sample Preparation

The concentration of Bi_2O_3 in this study was limited to 3 to 11 mol% in order to maintain the glass-forming ability and structural stability of the prepared samples. The composition x = 0 mol% was not included because the objective of this study was to

investigate the effect of bismuth substitution on the properties of the lithium borate glass system. Therefore, a minimum concentration of x = 3 mol% Bi_2O_3 was selected to ensure that the influence of bismuth incorporation on the glass structure and physical properties could be clearly observed. Meanwhile, increasing the Bi_2O_3 content beyond x = 11 mol% may significantly alter the glass network and could lead to excessive structural depolymerisation or possible formation of metallic bismuth clusters, which may affect the transparency and stability of the glass samples. At very high concentrations of Bi_2O_3, the probability of crystallization or phase separation during the melt-quenching process increases, which may prevent the formation of a homogeneous amorphous glass structure. Previous studies have reported that moderate concentrations of heavy metal oxides are sufficient to modify the glass network and influence physical properties, such as density, elastic behaviour, electrical conductivity, and radiation shielding efficiency, without destabilizing the glass system. Thus, the selected compositional range of x = 3 to 11 mol% provides a suitable balance between structural modification and glass stability, allowing systematic investigation of the influence of Bi_2O_3 on the structural, elastic, DC conductivity, and radiation shielding properties of the glass system

Each glass samples were weighed in appropriate amount as required for each composition which were listed in Table 3.2.

Table 3.2
Compositions of Glass Samples at Increasing Bi_2O_3 Content (mol%)

Amount of Bi_2O_3 (mol%)	Glass Composition
3	$98[20Li_2O\text{-}3Bi_2O_3\text{-}77B_2O_3]\text{-}2Ag$
5	$98[20Li_2O\text{-}5Bi_2O_3\text{-}75B_2O_3]\text{-}2Ag$
7	$98[20Li_2O\text{-}7Bi_2O_3\text{-}73B_2O_3]\text{-}2Ag$
9	$98[20Li_2O\text{-}9Bi_2O_3\text{-}71B_2O_3]\text{-}2Ag$
11	$98[20Li_2O\text{-}11Bi_2O_3\text{-}69B_2O_3]\text{-}2Ag$

Table 3.3
Mass of Oxide Powders for Each Composition of 98[20Li_2O-xBi_2O_3-(80-x)B_2O_3]-2Ag glasses (x = 3 mol% to 11 mol%).

Amount of Bi_2O_3 (mol %)	B_2O_3 (g)	Bi_2O_3 (g)	Li_2CO_3 (g)	Ag_2O (g)
3	3.837	1.014	1.072	0.078
5	3.409	1.542	0.978	0.071
7	3.050	1.985	0.899	0.066
9	2.745	2.362	0.832	0.061
11	2.482	2.687	0.775	0.057

Glass specimens were prepared through the conventional melt-quenching technique, following a formulation of 98[20Li_2O-xBi_2O_3-(80-x)B_2O_3]-2Ag glasses with x varying from 3 mol% to 11 mol%. The method involved weighing and meticulously mixing analytical grade commercial powders of bismuth (III) oxide (Bi_2O_3), lithium carbonate (Li_2CO_3), boron oxide (B_2O_3), and silver oxide (Ag_2O) with a purity of at least 99.9%. This blend continuously grinding for 1 hour using an agate mortar and pestle to achieve a fine and homogeneous mixture. The resulting mixture was then placed in a porcelain crucible and melted in a box furnace at 1000 ℃ for 3 hours, ensuring complete melting of all polycomponent oxides based on their average melting temperature. The porcelain crucible was used in the melting-quenching process as it has high thermal stability and good chemical resistance at high temperatures. Porcelain crucibles are able to withstand temperature above 1000ºC which is required for melting oxide glass compositions. In addition, porcelain is chemically stable with oxide melts which is helpful in reducing contamination during glass preparation and allows uniform melting of the batch materials. The molten glass was rapidly quenched into a pre-heated stainless steel mold at 350 ℃ and annealed for 2 hours to alleviate mechanical stresses associated with the quenched sample, in accordance with the average glass transition temperature of the polycomponent oxides. A bulk sample from each composition was polished to create parallel opposite surfaces, approximately 4-5 mm thick, using coarse and fine sandpaper for subsequent density, ultrasonic velocity, and electrochemical impedance spectroscopy measurements. Additionally, extra samples for each composition were crushed and ground into a fine powder for XRD, FTIR, Impedence Spectroscopy and PHY-X /PSD Online software analyses. **Error! Reference source not found.** depicted the summary of process flow of current research methodology

employed for present project.

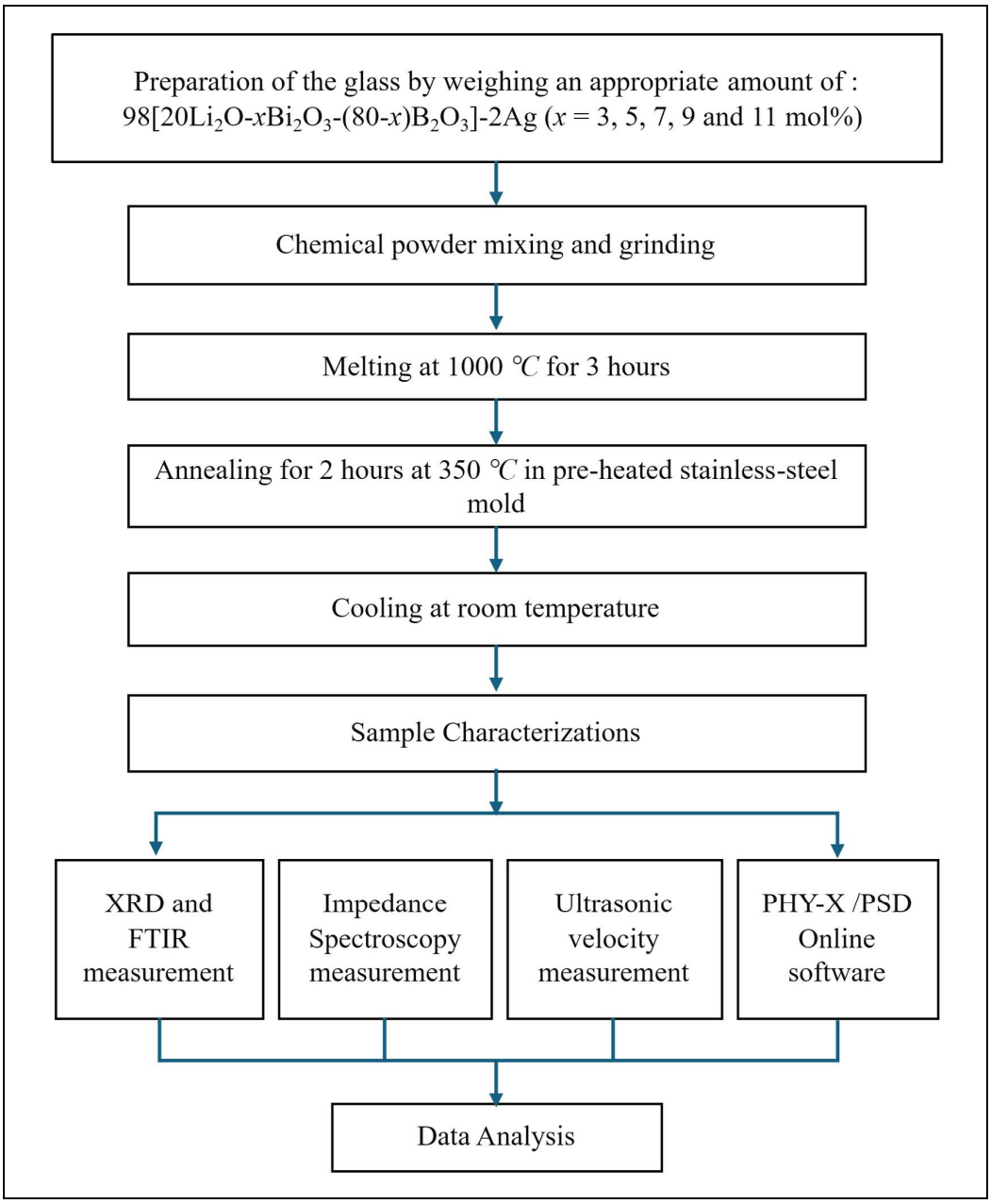

Figure 3.1 Process Flow for Sample Preparation of 98[20Li_2O-xBi_2O_3-(80-x)B_2O_3]-2Ag (x = 3, 5, 7, 9 and 11 mol%)

3.4 Sample Characterization

3.4.1 XRD Measurement

A non-destructive technique for distinguishing between amorphous and crystalline materials is X-ray diffraction (XRD). Since K_α is more intense than K_b, which would result in a low peak to noise ratio, it is employed in the majority of XRD measurements. The molecules in crystalline materials are arranged in their lattice location on a periodic basis. In the meanwhile, molecules were organized haphazardly in amorphous materials. When there is a periodic arrangement of atoms, high intensity sharp peaks, often referred to as constructive interference, are produced when X-rays strike the created lattice planes and are only scattered in specified directions. Instead of high intensity smaller peaks, X-rays that strike amorphous atoms would be scattered in various directions, resulting in a broad hump distributed in a large range (2θ).

X-ray tubes, divergence and soller slits, Goniometers, sample stages, receiving slits, monochromators, soller slits, and detectors are all part of the XRD setup. When incident X-rays strike a sample, constructive interference takes place and an intensity peak manifests itself as stated below;

$$2dsin\theta = n\lambda \tag{3.1}$$

where θ is the diffraction angle for lagging diffracted rays, d is the interplanar distance in crystalline materials, n is the order of the diffraction band, and λ is the wavelength of X radiation.

To ascertain the amorphicity, the sample powder for the current study was produced and put in a sample holder of a PAN Analytical X-Pert Pro X-Ray Diffractometer (XRD). At normal temperature, C_uK_α radiates (λ = 1.5406 Å) from the Copper anode over a broad Bragg angle range (2θ). These radiations are collimated, directed towards the sample powder's atoms, and diffracted. The sample will rotate facing in the direction of the detector after being positioned at a specific angle to the incident beam in the spectrometer's centre. The measured output, count rate, is obtained by converting the signal. A computer program and monitor then display the transformed signal as peaks for crystalline materials and broad hump for amorphous materials. The diagram of working principle of an X-ray diffractometer is shown as in Figure 3.2 and Figure 3.3.

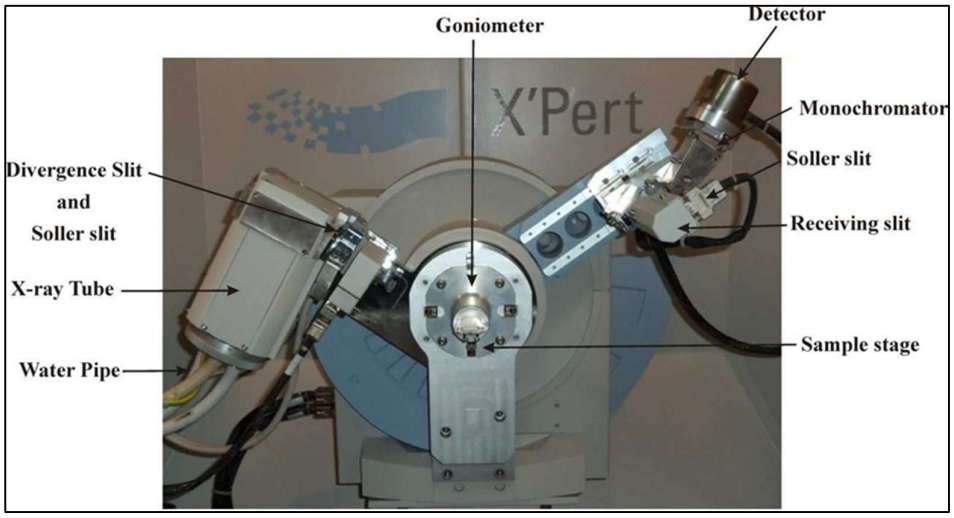

Figure 3.2 Instrumentation of PAN Analytical X-Pert Pro X-Ray Diffractometer

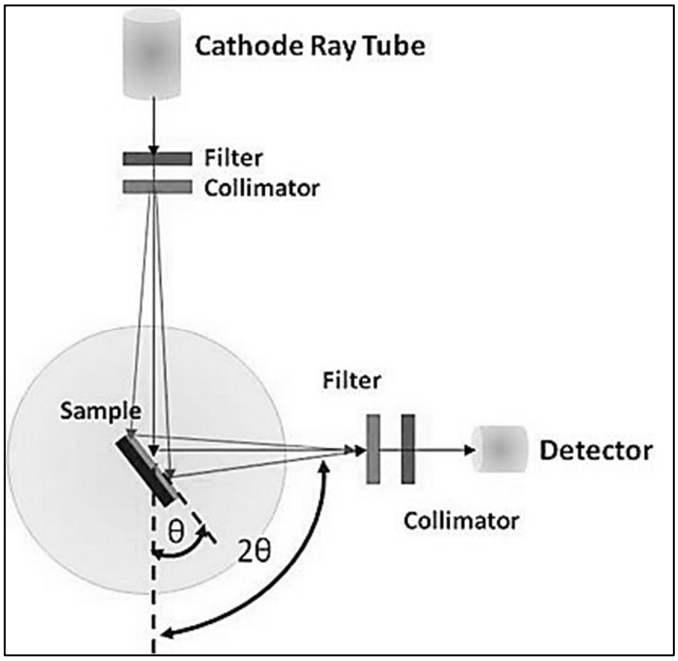

Figure 3.3 Working Principle of PAN Analytical X-Pert Pro X-Ray Diffractometer

3.4.2 Fourier Transforms Infrared (FTIR) Spectroscopy

The definition of infrared spectroscopy is the study of infrared light's interaction with materials. FTIR spectroscopy is employed to identify particular functional group types. Samples' molecules will absorb specific wavelengths of radiation when they are exposed to infrared radiation, changing the dipole moment of the sample molecules. As a result, the dipoles vibrate with energy comparable to the ground state to excited state transition in vibrational energy level. The vibrational energy gap can then be used to determine the frequency of the absorption peak. The possibility of an energy level transition and the variation in the dipole moment are linked to the intensity of absorption peaks. With the exception of a few homonuclear diatomic molecules like O_2, N_2, and Cl_2, which exhibit zero dipole change in their vibration and rotation, the majority of molecules are infrared active. The vibrational spectrum of the molecules in the samples is closely related to the infrared spectrum that is generated via FTIR measurement.

To obtain the reference spectrum, background scanning was done before the sample was exposed to infrared radiation. This is a crucial stage where the contributions of the environment (carbon dioxide and water vapor) and the instrument to the absorbance spectrum were eliminated. When calculating the ratio, just the sample spectrum remains to provide a satisfactory signal-to-noise ratio if the instrument and environment both contribute the same amount to the background and single beam spectra of the sample.

An infrared source (nichrome wire), an interferometer, a sample chamber, a detector, an amplifier, an A/D converter, and a computer make up an FTIR spectrometer. Infrared radiation from the source travels through the interferometer, which is made up of mirrors and a beam-splitter that combine to generate a single beam. The sample is then struck by the beam, with some of it being absorbed and the remainder passing through it. After that, the transmitted beam arrives at the detector. An interferogram is created when the signal is amplified and transformed into a digital signal using an analog-to-digital converter and amplifier, respectively. Ultimately, the interferogram undergoes a Fourier transform on a computer to convert it into the infrared spectrum.

Using the KBr pellet method and a Perkin Elmer model spectrum, infrared (IR) absorption was performed to detect the presence of functional groups in the current glass samples in wave number ranges from 400 to 2000 cm^{-1}. One FTIR

spectrophotometer that is not chilled. To prevent infrared beam scattering, which results in a sloping baseline, the powdered materials were broken down and combined with KBr at a fixed ratio of 1:80 until the particle size was less than 2 microns in diameter.

Lastly, the mixture is measured after being crushed with a hand press into a thin, clear sheet pellet. Since KBr is transparent and inert above 400 cm^{-1}, it is employed as an infrared transparent diluent. Following baseline correction and background spectrum measurement, absorbance data were acquired. The IR absorption spectrum was then displayed using Origin Pro 8 software. The Gaussian approach was used to deconvolute the obtained spectrums. An FTIR spectrometer's schematic diagram was displayed in Figure 3.4.

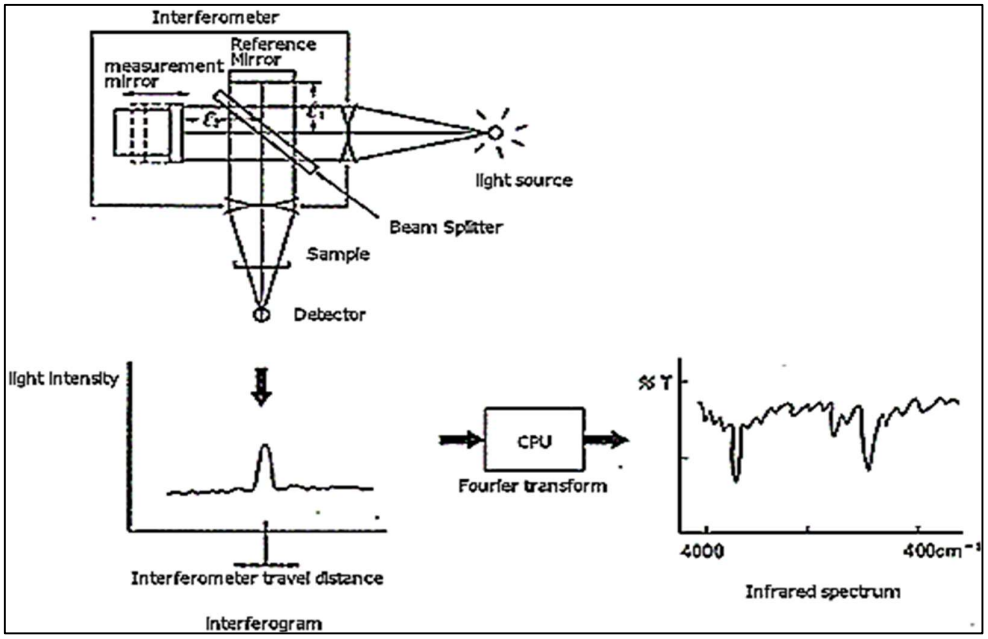

Figure 3.4 Process Flow of Fourier Transform Infrared (FTIR)

3.4.3 Calculation of Density

A great deal of a sample's physical characteristics is connected to its density; for example, the elastic moduli equations for glass samples specifically use the sample's density. Thus, for the current sample, the density (ρ) of bulk glass samples was evaluated using the Archimedes principle at room temperature using toluene as an immersion liquid and the following equation:

$$\rho = \left(\frac{W_a}{W_a - W_t}\right)\rho_t \tag{3.2}$$

where W_t is the sample weight in toluene, ρ_t is the toluene density (867 kgm^{-3}), and W_a is the sample weight in air. According to the Archimedes principle, any item submerged fully or partially in a fluid at rest experiences buoyant or upward force, the strength of which is equal to the weight of the fluid that the body has displaced. A body floating in a liquid experiences buoyant force, which is opposite in direction and equal in magnitude to the weight of the floating object; the object does not rise or fall. Diethyl phthalate (1120 kgm^{-3}), benzene (876 kgm^{-3}), and xylene (860.2 kgm^{-3}) are additional immersion liquids that can replace toluene. Water, however, cannot be utilized as an organic solvent for the current glass sample since it is made of borate, which is highly hygroscopic and might react with water to release ions from the glass bonds.

3.4.4 Ultrasonic Velocity Measurement

In ultrasonic testing, depending on the ultrasonic wave's intensity, both destructive and non-destructive methods are used. Low intensity ultrasonic waves are associated with non-destructive characterisation techniques, whereas high intensity ultrasonic waves are associated with destructive techniques. In order to better understand elastic moduli properties like Young's and bulk modulus, Poisson's ratio, shear modulus, hardness, and Debye temperature, this method is based on the propagation of ultrasonic waves that transmit energy through the material. This information is obtained by measuring the material's elastic constant. The current study focuses on low-intensity ultrasonic waves that have no effect on the sample being examined.

An example of an ultrasonic wave is a mechanical wave, often referred to as an acoustic wave, that travels above the range of human hearing, exceeding the 20 kHz audio frequency limit. The elastic characteristics and particle vibrations of the medium affect the ultrasonic wave's wavelength as it travels through it. Its speed varies along with the wavelength. The direction of vibration of the particle is dependent on the ultrasonic wave's propagation mode and direction. Ultrasonic waves propagate in four different ways: longitudinally, as a compression wave; transversely, as a shear wave; on the surface, as a Rayleigh wave; and on plates, as a lamb wave. Shear and

longitudinal waves are the most typical ways that ultrasonic waves propagate when measuring ultrasonic velocity.

The medium's particles vibrate in a direction parallel to the longitudinal wave's path when it travels through it. In the meantime, particles in a medium vibrate perpendicular to the direction of the wave as it propagates when shear waves pass through it. Shear and longitudinal wave propagation are shown in **Error! Reference source not found.**. Ultrasonic testing is used to find defects as well as the dimensions and properties of the material. The RITEC Advance Measurement System RAM-5000 is being used in this study to measure the ultrasonic velocity in glass samples using the pulse echo-overlap technique. Both the longitudinal and shear modes were measured at room temperature at 5 MHz. To ensure the best measurement accuracy, all cylindrical glass samples were then polished until two smooth parallel surfaces with a thickness of 4-5 mm were reached.

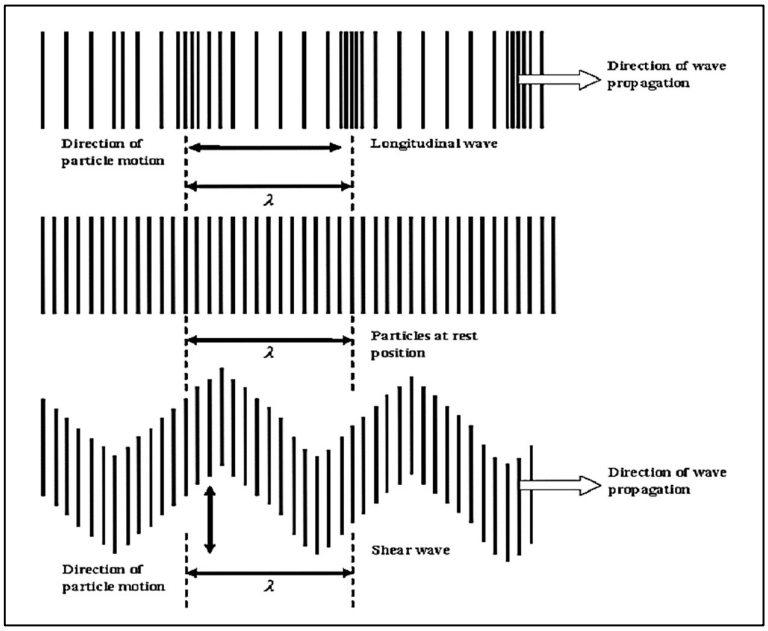

Figure 3.5 Illustration of Longitudinal and Shear Waves propagating in a medium

A piezoelectric transducer generates a brief ultrasonic pulse for use in the pulse echo technique. Subsequently, the transducer is coated with ultrasonic couplant shear gel to enable the transfer of ultrasonic waves into the glass sample. Because solid and air materials have different acoustic impedances, couplant must be used in this test. A useable ultrasonic signal can be obtained by dislodging the air and allowing additional sound energy to enter the glass thanks to the couplant. Furthermore, it is important to

always utilize a very thin layer of couplant to minimize phase inconsistencies and back-walled echoes caused by the couplant's tiny wavelength variations. Moreover, a rough sample surface will cause variations in the couplant layer thickness between the transducer and sample, which will distort the returning echo and cause the transducer to record slightly different sound trajectories, increasing the degree of uncertainty in the results. It is crucial to remember that the glass sample being measured needs to be devoid of discontinuities, such as cracks or defects, in order to prevent the transducer from picking up false echoes caused by cracks.

An ultrasonic wave is produced by the transducer, which transforms electrical energy into mechanical energy. The ultrasonic velocity measuring system's schematic set of instruments is shown in Figure 3.6. The transducer detects an echo when the longitudinal or shear ultrasonic pulses impact the back wall and return to the glass sample's front surface. The ultrasonic pulses propagate through the sample. After being detected, the signal is converted back into an electrical signal and shown on an oscilloscope and on computer software connected to the device. The following formula was used to determine the precise transit time required for the two types of signals which are longitudinal and shear waves to move between the glass sample's front and back surfaces

$$v = \frac{2d}{t} \tag{3.3}$$

where d is the glass sample's thickness, t is the transit time which is the amount of time it takes for ultrasonic waves to go back and forth across the sample's thickness and v is the ultrasonic velocity for both longitudinal and shear waves.

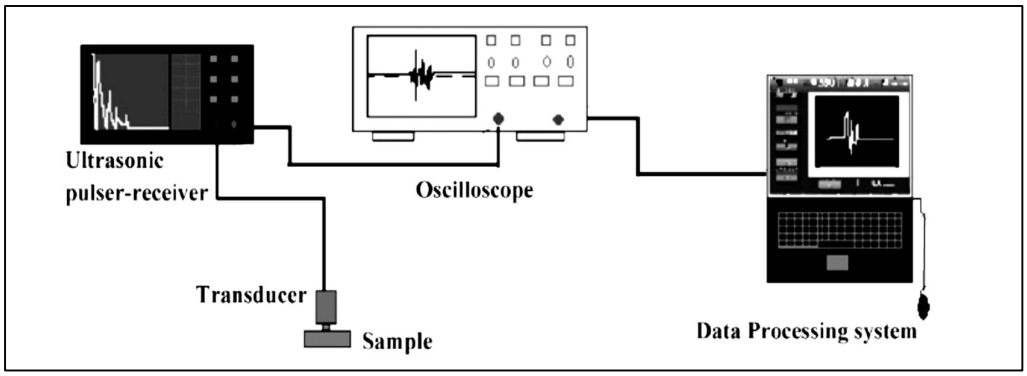

Figure 3.6 The Schematic Representation of Ultrasonic Testing (Pulse Echo-Overlap Technique)

The elastic moduli and other elastic parameters were calculated using the following equations;

Longitudinal modulus, $$C_L = \rho v_L^2 \quad (3.4)$$

Shear Modulus, $$\mu = v_S^2 \rho \quad (3.5)$$

Bulk modulus, $$K_e = C_L - \left(\frac{4}{3}\right)\mu \quad (3.6)$$

Young's Modulus, $$Y = \frac{9K\mu}{3K + \mu} \quad (3.7)$$

Debye temperature, $$\theta_D \left(\frac{h}{k_B}\right)\left(\frac{3PN_A}{4\pi V_a}\right)^{\frac{1}{3}} v_m \quad (3.8)$$

Poisson's ratio, $$\sigma = \frac{C_L - 2\mu}{2(C_L - \mu)} \quad (3.9)$$

Hardness, $$H = \frac{(1 - 2\sigma)E}{6(1 + \sigma)} \quad (3.10)$$

Mean sound velocity, $$v_m = \left[\frac{3v_L^3 v_S^3}{2v_L^3 + v_S^3}\right]^{\frac{1}{3}} \quad (3.11)$$

where V_L and V_S are longitudinal and shear velocity, respectively, $\hbar$ the Planck's constant, *kb* is the Boltzmann's constant, *NA* is the Avogadro's number, *P* is the number of atoms in the chemical formula and *Va* is the molar atomic volume obtained from following equation;

$$V_a = \frac{M_{glass}}{\rho_{glass}} \quad (3.12)$$

3.4.5 Impedance Spectroscopy Measurement

One of the appealing aspects of impedance spectroscopy is that it can be used to investigate the electrical and electrochemical properties of materials and systems. It is particularly useful when attempting to understand the behaviour of a real system by comparing it to an idealized model circuit made up of discrete electrical components. By determining the dielectric and conductivity of a material, impedance spectroscopy measurement has been used to assess its electric properties over a broad frequency and temperature range.

$$Z_s* = \frac{1}{Yp*} = \frac{i}{\omega Cp*} \tag{3.13}$$

The complex impedance $Z^*(\omega)$ of a capacitor consisting of two or more electrodes with the sample material positioned in between at a regulated temperature is measured by an impedance analyzer. The conductivity $\sigma^*(\omega)$ and complex permittivity $\varepsilon^*(\omega)$ spectra are evaluated evaluated from $Z^*(\omega)$. Complex parallel sample capacity is used to determine the sample impedance Z_s^* and the admittance Y_p^*. The complex dielectric constant ε^* correlates to both the empty cell capacity C_0 and the complex sample capacity C^*_p.

$$\varepsilon^* = \varepsilon' - i\varepsilon'' = \frac{C*_p}{C_0} \tag{3.14}$$

where ε' is real dielectric constant and ε'' is an imaginary dielectric constant. For a sample cell consisting of round parallel plates with diameter D and spacing d, C_o is calculated by

$$C_0 = \varepsilon_0 \frac{\pi(\frac{D}{2})^2 - Aspacer}{d} \tag{3.15}$$

where A_{spacer} is the average area of the spacer material inside the sample capacitor and ε_0 is the permittivity constant of empty space. Prior to attaching the sample material to the electrode for the interdigit electrode, the value of C_0 must be determined. In the interim, the definition of the complex dielectric modulus M^* is:

$$M^* = M^* + i\, M^* = 1 / \varepsilon^* \tag{3.16}$$

where M' is the real part of modulus formalism and M'' is the imaginary part of modulus formalism. The specific conductivity σ^* is related to the dielectric constant by:

$$\sigma^* = \sigma^* - i\sigma^* = i2\pi f \varepsilon_0(\varepsilon^* - 1) \tag{3.17}$$

Where σ', σ'' and f are real conductivity, imaginary conductivity and frequency respectively. Whereas, the loss factor tan δ is calculated by

$$\text{Tan } \delta = \frac{\varepsilon''}{\varepsilon'} = \frac{Z_S'}{Z_S''} \tag{3.18}$$

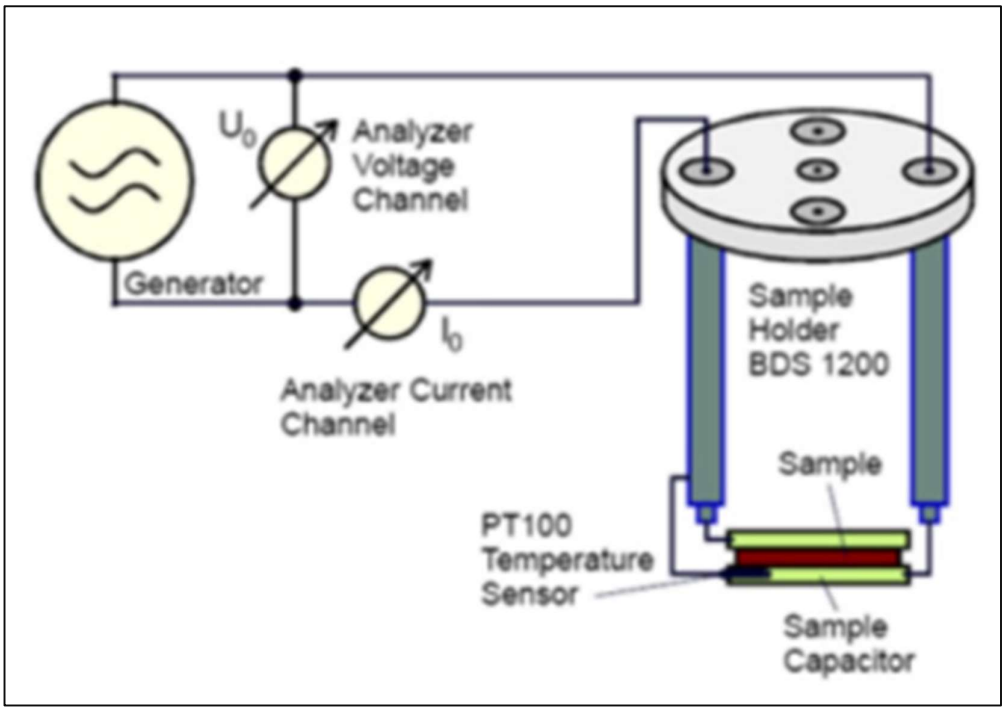

Figure 3.7 Schematic Diagram of Impedance Spectrocopy Measurement

A Novotherm controller unit controlled the temperature to within ± 0.1 K of the set-point using a PT100 platinum sensor as the temperature sensor. The WinDeta control software was used to set the sample's thickness and diameter. An auto-balance bridge circuit served as the impedance analyzer's primary measurement circuit. All measurements were computed and recorded automatically by the software packages WinDeta control.

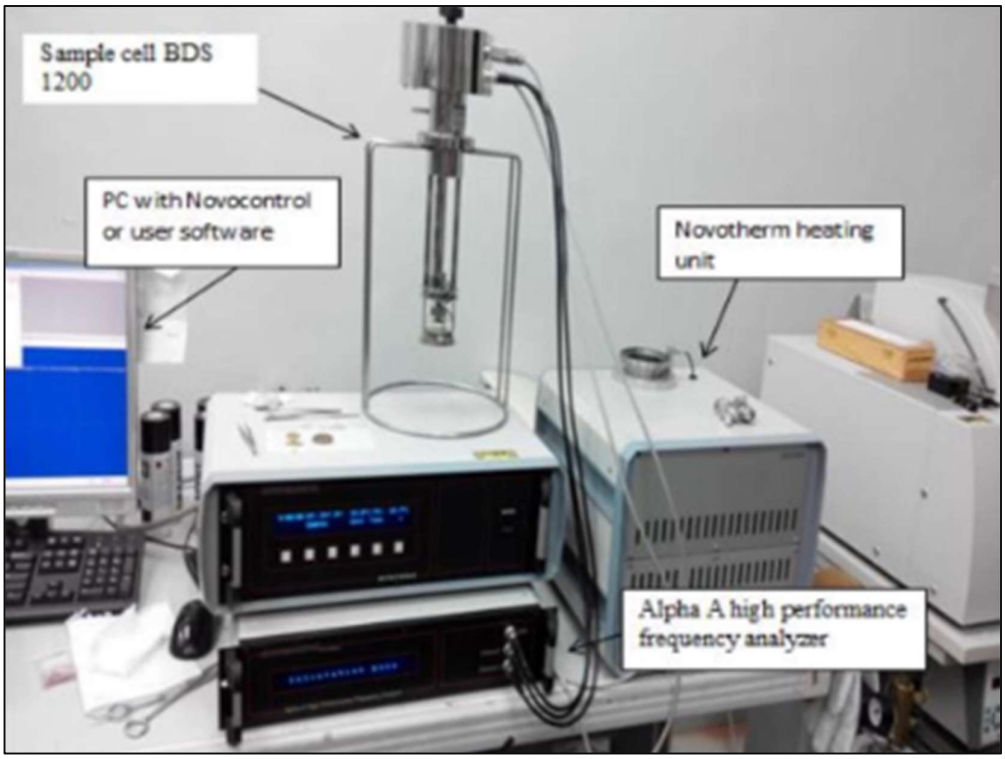

Figure 3.8 Novocontrol Alpha Analyszer of Conductivity Measurement

3.4.6 Phy-X/PSD Simulation Program

Phy-X/PSD simulation programme is used for calculating the important gamma radiation- shielding characteristics more accurately and swiftly over a wide range of gamma photon energies. Other related characteristics such as MFP, $Z_{eff,}$ and HVL are also significant to define the glass's potential in operating as gamma radiation shielding materials. These parameters was determined using the computer programs like the Phy-X/PSD platform or by using the μ/ρ values. In addition, MAC also were used for these characteristics of glass samples.

$$MAC = \mu_m = \frac{\mu}{\rho} = \sum_i W_i \left(\frac{\mu}{\rho}\right)_i \tag{3.19}$$

The MAC (μ/ρ) was used to describe the γ-ray penetration and interaction with the materials and theoretically can be calculated using the mixture rule where (μ/ρ)i is the mass attenuation coefficient of its constituent element and wi is the weight fraction of its constituent elements in the glass sample. Mean free path (MFP) is the average distance a moving particle, such as an atom, molecule, or photon, travels between

successive collisions, half value layer (HVL) represents gamma ray interaction of a material and relation of total atomic cross section and total electronic cross section are shown by $Z_{eff.}$

$$\mathrm{MFP} = \frac{1}{\mu} \tag{3.20}$$

$$\mathrm{HVL} = \frac{ln2}{\mu} \tag{3.21}$$

$$Z_{eff} = \frac{\sum f_i A_i (\frac{\mu}{\rho})_i}{\sum_{Z_i}^{A_i} (\frac{\mu}{\rho})_j} \tag{3.22}$$

CHAPTER 4
RESULTS AND DISCUSSION

4.1 Introduction

The structural, elastic, and radiation shielding characteristics of the 98[20Li_2O-xBi_2O_3-(80-x)B_2O_3]-2Ag (x = 3, 5, 7, 9 and 11 mol %) glass system are discussed in this chapter along with the results and analysis that were obtained from XRD, FTIR, ultrasonic velocity measurement, impedance spectroscopy measurement and PHY-X /PSD Online software. It was discussed how certain qualities behaved abnormally. Models for ring deformation and bulk compression were used to further examine how the addition of B_2O_3 affected the elastic characteristics.

4.2 Structural Properties

4.2.1 X-Ray Diffraction (XRD)

For all glass samples, the XRD results of 98[20Li_2O-xBi_2O_3-(80-x)B_2O_3]-2Ag for x = 3, 5, 7, 9 and 11 mol% as shown in **Error! Reference source not found.** revealed a broad hump peak at roughly 27° rather than acute Bragg's peaks (Samsudin et al., 2021). Considering there is no long-range order in the glass matrix, this broad hump peak indicates that the glass is amorphous.

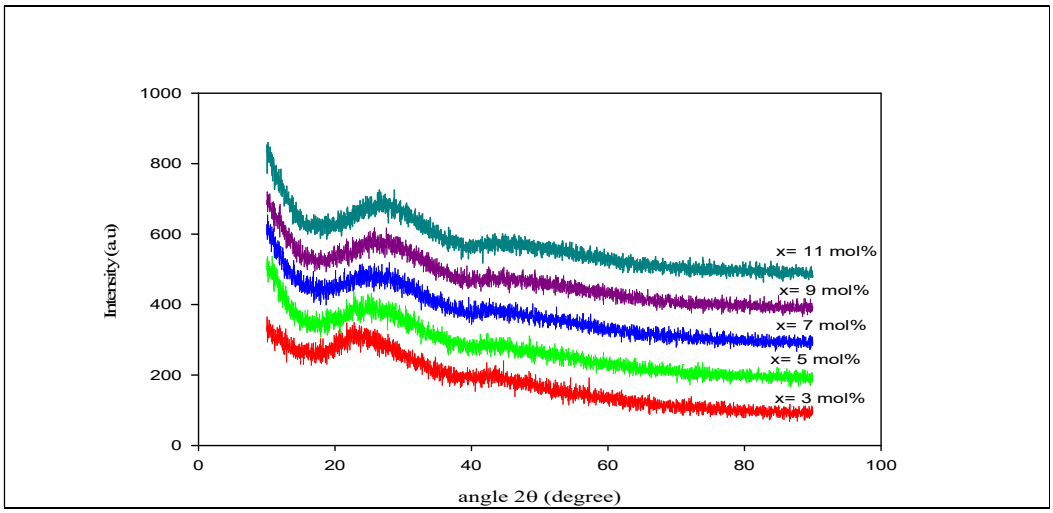

Figure 4.1 XRD spectra of 98[20Li2O-xBi2O3-(80-x)B2O3]-2Ag (x = 3 to 11 mol%) Glass Samples.

4.2.2 Infrared (IR) Absorption Spectra

Figure 4.2 shows the deconvoluted Fourier Transform Infrared (FTIR) spectra of the glass system 98[20Li_2O-$x$$Bi_2O_3$-(80-$x$)$B_2O_3$]-2Ag for compositions x = 3 to 11 mol%.

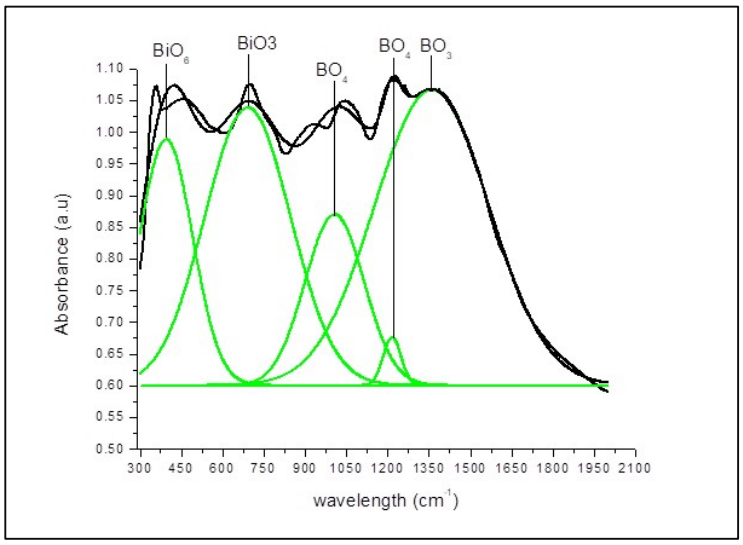

Figure 4.1 Deconvolution spectra of 98[20Li_2O-$x$$Bi_2O_3$-(80-$x$)$B_2O_3$]-2Ag ($x$ = 3 to 11 mol%) Glass Samples.

The FTIR spectra recorded at room temperature are presented in Figure 4.3.

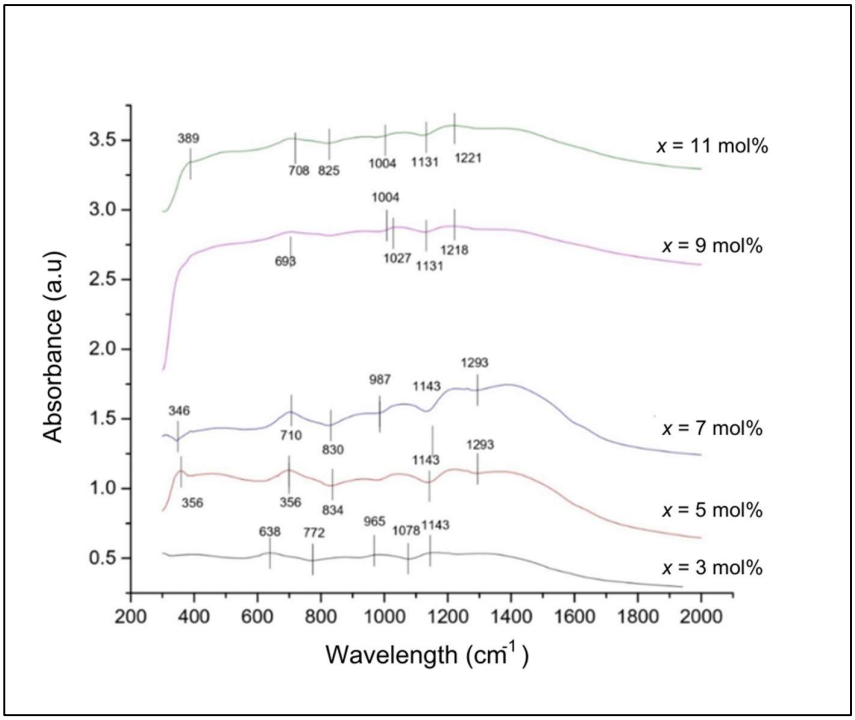

Figure 4.2 IR spectra of 98[20Li_2O-xBi_2O_3-(80-x)B_2O_3]-2Ag (x =3 to 11 mol%) Glass Samples.

The FTIR spectra of borate-based glasses generally exhibit characteristic absorption bands corresponding to the vibrational modes of various borate structural groups. These spectra can typically be divided into three main spectral regions (Lakshminarayana et al., 2022; Kumar et al., 2024). The first region, located between approximately 1200–1600 cm^{-1}, is attributed to the asymmetric stretching vibrations of B–O bonds in trigonal BO_3 units. The second region, observed within the range of 800–1200 cm^{-1}, corresponds to the stretching vibrations of B–O bonds in tetrahedral BO_4 units. The third region, appearing around 600–800 cm^{-1}, is associated with the bending vibrations of B–O–B linkages in the borate glass network (Singh et al., 2022).

The presence of absorption bands within these spectral regions confirms that both BO_3 and BO_4 structural units coexist in the investigated glass system. These units form the fundamental building blocks of the borate glass network. In pure B_2O_3 glasses, the network is typically dominated by trigonal BO_3 units arranged in boroxol ring

structures. However, the introduction of modifier oxides into the glass composition may lead to structural rearrangements within the network, resulting in the formation of other borate groups such as diborate, triborate and tetraborate units (Lakshminarayana et al., 2022).

The absorption band observed in the range of approximately 1290–1300 cm^{-1} is attributed to the asymmetric stretching vibration of B–O bonds in BO_3 units, while the band located around 1230–1240 cm^{-1} corresponds to B–O stretching vibrations associated with meta-borate and ortho-borate structural groups (Kumar et al., 2024). In addition, the band appearing near 1000–1050 cm^{-1} is related to the stretching vibration of BO_4 tetrahedral units, indicating the presence of four-coordinated boron atoms within the glass network (Singh et al., 2022).

The incorporation of Bi_2O_3 into the borate glass system introduces additional vibrational features associated with Bi–O bonds. The absorption band observed within the region of approximately 450–500 cm^{-1} can be attributed to the oscillation of Bi–O and Bi–O–B bonds related to BiO_6 octahedral structural units. This observation suggests that bismuth participates in modifying the borate glass network structure (Rahman et al., 2024). The formation of these structural units indicates that Bi_2O_3 acts as a network modifier that alters the connectivity and packing density of the glass matrix.

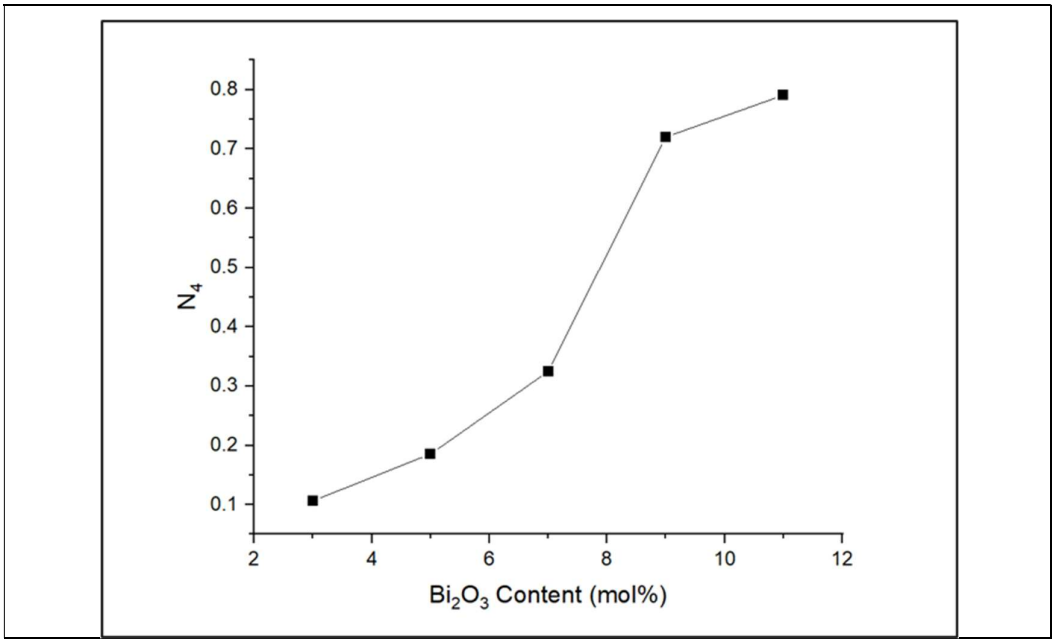

Figure 4.3 N_4 for 98[20Li_2O-$x$$Bi_2O_3$-(80-$x$)$B_2O_3$]-2Ag ($x$ =3 to 11 mol%) Glass Samples.

Furthermore, compositional variations observed in the FTIR spectra indicate changes in the relative proportions of BO_3 and BO_4 structural units with increasing Bi_2O_3 content. As shown in Figure 4.4, the fraction of four-coordinated boron atoms (N_4) increases gradually from x = 3 to 7 mol%, indicating a progressive conversion of trigonal BO_3 units into tetrahedral BO_4 units within the borate network. This conversion occurs because the introduction of modifier oxides increases the availability of oxygen ions, which promotes the formation of BO_4 units to maintain charge balance in the glass structure. A more pronounced increase in N_4 is observed within the composition range $7 < x \leq 9$ mol%, indicating that the rate of $BO_3 \rightarrow BO_4$ conversion becomes more significant in this region. This behaviour can be attributed to enhanced structural rearrangement within the borate network, where the increased oxygen availability accelerates the transformation of BO_3 units into BO_4 units. Consequently, the formation of BO_4 structural units becomes more dominant within this composition range. However, with further addition of Bi_2O_3, the structural role of bismuth becomes more significant.

The FTIR spectra show a shift of the Bi–O vibrational band toward higher wavenumbers, which indicates the formation of BiO_6 octahedral structural units (Figure 4.3). The incorporation of these heavy metal units introduces local structural distortion in the borate network due to the relatively large ionic radius and high polarizability of Bi^{3+} ions. As a result, the presence of Bi_2O_3 disrupts B–O–B linkages and promotes the formation of non-bridging oxygens (NBOs), which leads to partial depolymerization and weakening of the glass network. Additional evidence of these structural changes can be observed in the FTIR spectra where the absorption band associated with BO_4 units shifts slightly toward lower wavenumbers, while a new band appears near 1404 cm^{-1}, corresponding to the asymmetric stretching vibration of BO_3 units. These spectral features indicate redistribution of borate structural groups and variations in network connectivity within the glass matrix. Interestingly, the DC conductivity decreases at x = 9 mol%, despite the increase in BO_4 units observed from the FTIR analysis. This behaviour can be explained by the mixed ionic–electronic (MIE) effect, where the presence of relatively large Bi^{3+} ions from Bi_2O_3 obstructs the migration pathways of Li^+ ions within the glass network. The accumulation of these heavy ions therefore reduces the mobility of lithium ions, resulting in lower ionic conduction within the glass system. The FTIR analysis demonstrates that the incorporation of Bi_2O_3 significantly

modifies the structural organization of the borate glass network by altering the relative distribution of BO_3 and BO_4 units and introducing Bi–O structural groups. These structural modifications are expected to influence the physical properties of the glass system, including its elastic behaviour, electrical conductivity and radiation shielding performance.

The structural information obtained from FTIR analysis provides important insight into the relationship between glass network structure and the physical properties of the investigated system. In borate-based glasses, structural units such as BO_3 and BO_4 groups play a crucial role in determining network connectivity and rigidity. Variations in the relative proportion of these units can significantly affect the mechanical, electrical and radiation shielding properties of the material (Lakshminarayana et al., 2022; Singh et al., 2022).

These structural modifications influence the elastic behaviour of the glass system. The presence of NBOs weakens network connectivity and reduces structural rigidity, which may lead to a decrease in elastic moduli such as bulk modulus and Young's modulus. The anomalous elastic behaviour observed within the composition range 7–9 mol% Bi_2O_3 may therefore be associated with the competing effects of network strengthening through BO_4 formation and network depolymerisation caused by the generation of NBOs.

In addition to affecting the elastic properties, the structural changes observed in the FTIR spectra also influence the electrical conductivity behaviour of the glass system. The formation of non-bridging oxygens increases the availability of localized sites that facilitate the mobility of charge carriers within the glass matrix. However, excessive structural distortion or the formation of heavy metal polyhedral units may hinder ion migration pathways, resulting in variations in DC conductivity (Hisam et al., 2021).

Furthermore, these structural modifications play an important role in determining the radiation shielding performance of the glass system. The incorporation of Bi_2O_3 increases the density and effective atomic number of the glass, which enhances the interaction probability between incident photons and the glass matrix. At higher Bi_2O_3 concentrations, the presence of heavy metal structural units such as BiO_6 polyhedra contributes to improved photon attenuation properties, resulting in higher mass attenuation coefficients and lower half-value layer values (Rahman et al., 2024).

The deconvolution technique was used to determine parameters such as the band centre position (C_P) and relative area percentage (A_P). These parameters are associated with the vibrational modes of different structural units present in the glass network and provide useful information regarding their relative concentration. The corresponding band assignments and deconvolution parameters are summarized in Table 4.1.

By analysing the changes in CP (center position) and AP (area percentage) values at different Bi_2O_3 concentrations, the relative contributions of BO_3, BO_4, and Bi–O structural units within the glass network can be identified. For instance, the bands assigned to BO_4 units in the range of approximately 800–1100 cm^{-1} exhibit variations in relative area, indicating changes in the concentration of tetrahedral boron units as the Bi_2O_3 content increases. Likewise, the appearance of bands within the 400–500 cm^{-1} region, which are associated with Bi–O vibrations, confirms the formation of BiO_6 structural units in the glass matrix.

Therefore, Table 4.1 provides quantitative support for the FTIR spectral interpretation, as it shows the variation in band positions and relative intensities of the vibrational modes with changing composition. These changes reflect the structural evolution of the borate glass network with Bi_2O_3 substitution. Consequently, the information obtained from Table 4.1 helps to explain the structural modifications occurring in the glass system and provides a basis for correlating these structural changes with the observed variations in elastic properties, DC conductivity, and radiation shielding performance.

Table 4.1
IR spectra assignments with respects to their wavenumbers for 98[20Li_2O-xBi_2O_3-(80-x)B_2O_3]-2Ag glass samples

x = 3 mol%		x = 5 mol%		x = 7 mol%		x = 9 mol%		x = 11 mol%		ASSIGNMENTS
C_P	A_P	C_P	A_P	C_P	A_P	C_P	A_P	C_P	A_P	
-	-	356	0.4174	480	0.4131	465	5.30	476	0.6271	Oscillation of Bi–O and Bi–O–B bonds in octahedral BiO_6 structural units (Lakshminarayana et al., 2022; Kumar et al., 2024)
-	-	-	1.1254	929	0.1251	-	-	-	-	Symmetrical stretching vibration of Bi–O bonds in BiO_3 structural units (Rahman et al., 2024)
-	-	-	2.4000	688	1.8000	-	-	-	-	B–O–B bending vibrations in the borate glass network (Singh et al., 2022)
638	11.0000	-	-	-	-	736	13.5	731	15.1000	B–O–B bending vibrations associated with borate structural groups (Singh et al., 2022)
772	2..4000	834	21.2000	825	22.4000	901	11.40000	823	4.3000	B–O–B bending and stretching vibrations of BO_4 units in di-, tri-, tetra- and pentaborate groups (Lakshminarayana et al., 2022)
965	13.9000	1055	9.6000	1067	20.9000	1071	24.3000	1055	34.000	Stretching vibrations of BO_4 tetrahedral units in borate glasses (Kumar et al., 2024)
-	-	1217	6.2000	1226	8.8000	1232	6.9000	1235	4.0000	B–O stretching vibrations in BO_3 units from borate structural groups (Singh et al., 2022)
1143	5.60000	-	-	1394	32.3000	-	-	-	-	Asymmetric B–O stretching vibration of BO_3 units (Lakshminarayana et al., 2022)
-	-	1418	2.3000	-	-	1405	36.40000	1401	38.20000	B–O asymmetric stretching vibrations of BO_3 units in meta-, pyro- and orthoborate groups (Kumar et al., 2024)
-	-	-	-	1618	12.2	1630	7.40000	-	-	Vibrational band associated with OH or molecular water groups in glass network (Rahman et al., 2024)

4.2.3 Density and Molar Volume

Table 4.2
Values of Fraction of the Four Coordinated Boron Atoms (N_4), relative area of BO_4 and BO_3 units of $98[20Li_2O\text{-}xBi_2O_3\text{-}(80\text{-}x)B_2O_3]\text{-}2Ag$ (x =3 to 11 mol%) Glass Samples

x (mol%)	N_4	A_{BO4}	A_{BO3}
3	0.11	0.07	0.60
5	0.19	0.12	0.53
7	0.32	0.25	0.51
9	0.72	0.61	0.24
11	0.79	0.75	0.20

Table 4.3 displays the density (ρ), and molar volume (V_a) variations for the glass samples. The relationship between the molar volume and the glass density in the glass system is depicted in Figure 4.4. According to Table 4.3, the density exhibits an increase from 2522 kgm^{-3} for x = 3 mol% to 3597 kgm^{-3} for x = 11 mol% with a slight off-trend between x = 5 mol% to x = 9 mol%. This off-trend of density coincided with the minimum and maximum points of molar volume at x = 5 mol% and x = 9 mol% respectively. Meanwhile, the molecular volume showed a nonlinear trend where V_a experienced a minimum 3.069x10-5m^3 mol^{-1} at x = 5 mol% before increasing at x > 5 mol% to 3.263x10-5 m^3 mol^{-1} at x = 9 mol% then decreased to 3.108x10-5 m^3 mol^{-1} at x = 11 mol%. Briefly, V_a's nonlinear trend can be attributed for the rise in ρ. On the other hand, MIE might have been related to the shift in inclination for ρ at x = 5 mol% that correlated with the drop V_a at a comparable concentration. Given that the molecular volume of Bi_2O_3 (56.8 cm^3 mol^{-1}) was more than that of B_2O_3 (12.57 cm^3 mol^{-1}), a linear rise in the glass's volume was anticipated. On the other hand, contrary to expectations, the glass's molecular volume produced in this study increased nonlinearly, leading to a nonlinearity in the density. A sharp drop in molecular volume, V_a, at x = 5 mol% and a rise in total molecular mass, M due to the addition of Bi_2O_3 (465.96 g/mol) and the reduction of B_2O_3 (69.617 g/mol), could be the cause of the significant increase in density at x > 5 mol%. Density measurement provides a detailed understanding of structural changes in a glass network. Coordination number, cross-link density, glass's interstitial space dimension, structural softness or compactness, and

changes in geometric configuration have an impact on density. In the case of the current glass systems, the rise of ρ for $3 \leq x \leq 11$ mol% from 2522 to 3597 kgm^{-3}, respectively was greatly influenced by the substitution of heavier metal oxide, Bi_2O_3 with a larger increment in molecular mass of Bi_2O_3 (M = 465.46 g mol^{-1}) as compared to B_2O_3 (M = 69.62 gmol^{-1}). This led to a greater occupation of the glass's interstitial areas (Sabri et al., 2016b). It was anticipated that the glass's volume would rise linearly as Bi_2O_3's molecular volume (56.8 cm^{3}mol^{-1}) was greater than B_2O_3's (12.57 cm^{3}mol^{-1}). In addition, the bond strength of Bi-O (343 kJmol^{-1}) and B-O (373 kJmol^{-1}) also influenced the off-trend that occurred at x = 7 mol%. Ultrasonic wave mobility within the network became more flexible due to the addition of BI-O's reduced bond strength thus further weakening the structure of the glass.

As opposed to increasing linearly as predicted, the glass's molecular volume produced in this investigation increased nonlinearly, leading to nonlinearity in the density increase. Generally, ρ and M displayed proportional but contrasting behaviour to V_a. The changes in M and V_a mainly contributed to the rise in ρ in the system of glass as shown in Figure 4.4. Yet, the linear variation of structural changes in the glass system was distorted at $7 \leq x < 9$ mol%, indicating a possible correlation between the modifying role of Bi_2O_3 and the increased production of NBOs and interruption of B-O bonds.

Table 4.3
Values of density (ρ), molar volume (V_a) of the 98[20Li_2O-$x$$Bi_2O_3$-(80 x)B_2O_3]-2Ag

x (mol%)	ρ (± 1 kgm^{-3})	V_a (± 0.001 x 10^{-5} m^3 mol^{-1})
3	2522	3.202
5	2884	3.069
7	3019	3.188
9	3232	3.263
11	3597	3108

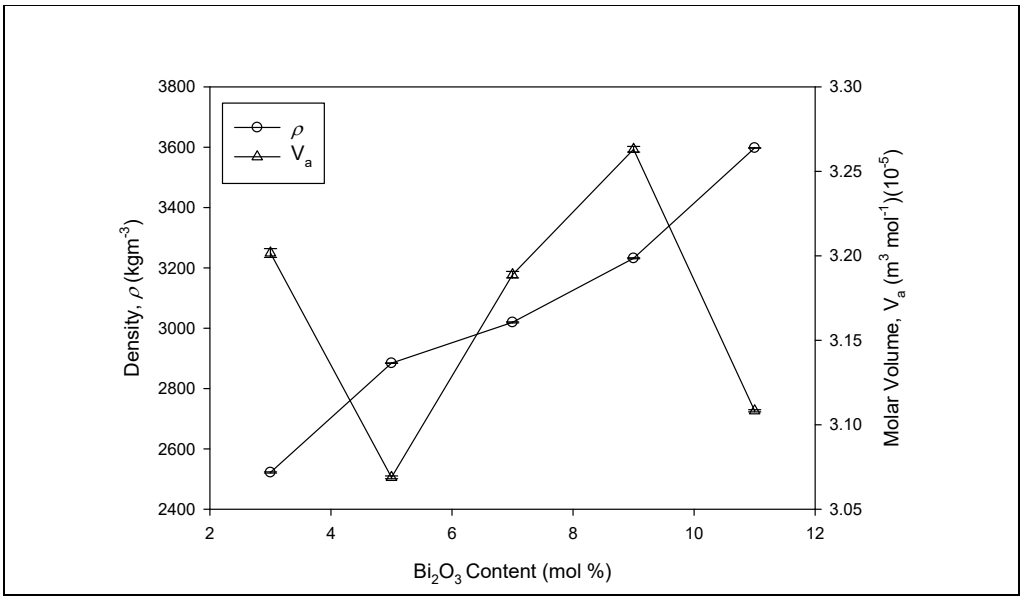

Figure 4.4 Density (ρ) and molar volume (V_a) upon addition of Bi_2O_3 for $98[20Li_2O\text{-}xBi_2O_3\text{-}(80\text{-}x)B_2O_3]\text{-}2Ag$ for x =3 to 11 mol% Glass Samples.

4.3 DC Conductivity

Table 4.4 depicts surge in DC conductivity for x < 7 mol% at -3.03668 Ω cm^{-1} to – 2.59768 Ω cm^{-1} before a steep decrease at – 0.70727 Ω cm^{-1} at x = 9 mol%. The DC conductivity, or σ_{DC}, of the glass samples generally increase when Bi_2O_3 is added, with the exception of a notable drop at x = 9 mol%, as seen in Figure 4.5 which is due to the result of MIE driven on by the massive Bi^{3+} ions in Bi_2O_3 hindering the migration of Li^+ ions, which will reduce ionic conduction in the glass system.

Table 4.4
Values of log DC conductivity (σ_{DC}) of the $98[20Li_2O\text{-}xBi_2O_3\text{-}(80\text{-}x)B_2O_3]\text{-}2Ag$ (x=3 to 11 mol%) Glass Samples.

x (mol%)	Log_{10} (σ_{DC}) (± 0.05 Ω cm^{-1})
3	-3.03668
5	-2.59768
7	-0.70727
9	-3.74723
11	-3.14185

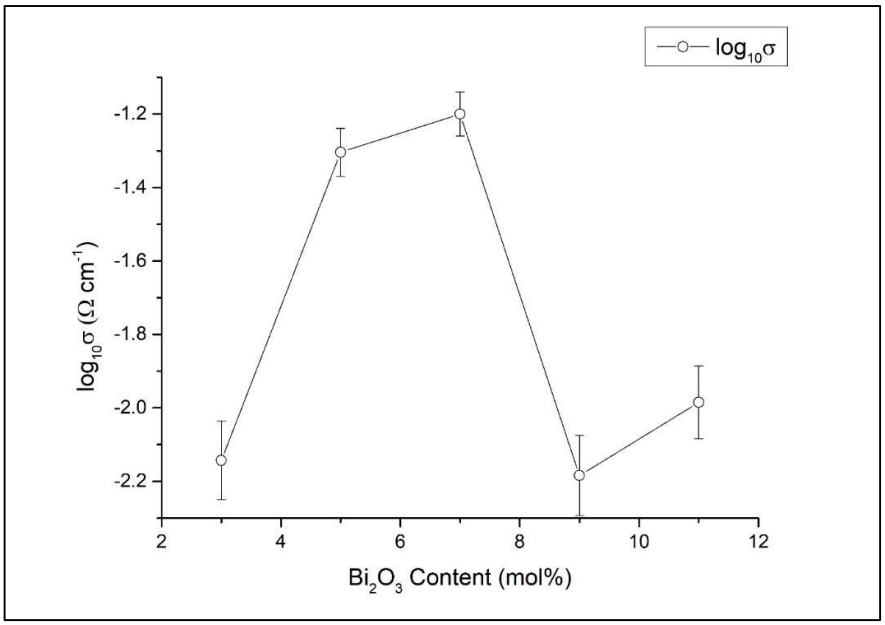

Figure 4.5 DC conductivity upon addition of Bi_2O_3 for 98[20Li_2O-$x$$Bi_2O_3$-(80-$x$)$B_2O_3$]-2Ag ($x$=3 to 11 mol%) Glass Samples.

4.4 Ultrasonic Velocities and Elastic Properties

Table 4.5 displays the variations of longitudinal modulus (C_L), shear modulus (μ), bulk modulus (K_e), Young's modulus (Y), hardness (H), Debye temperature (θ_D), and Poisson's ratio (σ) in 98[20Li_2O-$x$$Bi_2O_3$-(80-$x$)$B_2O_3$]-2Ag glass samples. The longitudinal velocity (V_L) and shear velocity (V_S) varies as the Bi_2O_3 content increases, as seen in Figure 4.6. As shown in Figure 8, the addition of Bi_2O_3 results in an initial rise in V_S from 2.923 kms^{-1} at x = 3 mol% to the highest value at 3.525 kms^{-1} at x = 7 mol%, subsequently a major drop at x > 7 mol%. Concurrently, a significant decline in V_L was noted at 3 < x ≤7 mol%, which was succeeded by a non-linear decline for x > 7 mol%.

Table 4.5
Values of Longitudinal Modulus (C_L), Shear Modulus (μ), Bulk Modulus (K_e), Young's Modulus (Y), Hardness (H), Debye Temperature (θ_D) and Poisson's Ratio (σ) for 98[20Li_2O-$x$$Bi_2O_3$-(80-$x$)$B_2O_3$]-2Ag ($x$ = 3 to 11 mol%) glass samples.

x (mol %)	V_L (± 0.01 kms^{-1})	V_S (± 0.01 kms^{-1})	V_m (± 0.02 kms^{-1})	C_L (± 0.3 GPa)	μ (± 0.1 GPa)	K_e (± 0.3 GPa)	Y (± 1 GPa)	H (± 0.2 GPa)	σ	θ_D (± 5 K)
3	5.607	2.923	3.271	79.3	21.5	50.6	56.6	2.68	0.31	424
5	5.375	3.039	3.381	83.3	26.7	47.8	67.4	4.17	0.26	444
7	5.066	3.525	3.831	77.5	37.5	27.5	77.4	11.73	0.03	497
9	5.173	2.867	3.194	86.5	26.6	51.1	67.9	3.93	0.28	411
11	5.054	2.833	3.154	91.9	28.89	53.4	73.4	4.41	0.27	413

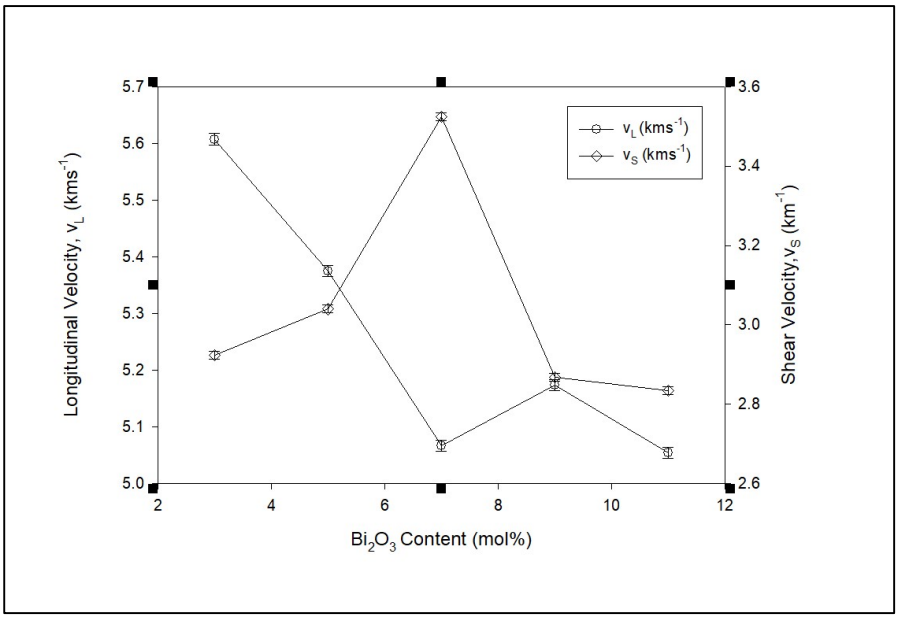

Figure 4.6 Longitudinal velocity (V_L) and shear velocity (V_S) upon addition of Bi_2O_3 for 98[20Li_2O-$x$$Bi_2O_3$-(80-$x$)$B_2O_3$]-2Ag ($x$ =3 to 11 mol%) Glass Samples.

Figure 4.7 indicates the variation of C_L and μ upon the addition of Bi_2O_3 for $98[20Li_2O\text{-}xBi_2O_3\text{-}(80\text{-}x)B_2O_3]\text{-}2Ag$ (x = 3 mol% to 11 mol%) glass samples. For $3 \leq x \leq 5$ mol% and $3 \leq x \leq 7$ mol%, respectively, a rising trend was seen in C_L and μ and at x = 7 mol%, both showed an opposing trend against one another. C_L exhibits a minimum value of 79.3 GPa whereas μ displays a maximum value of 37.52 GPa when x = 7 mol%.

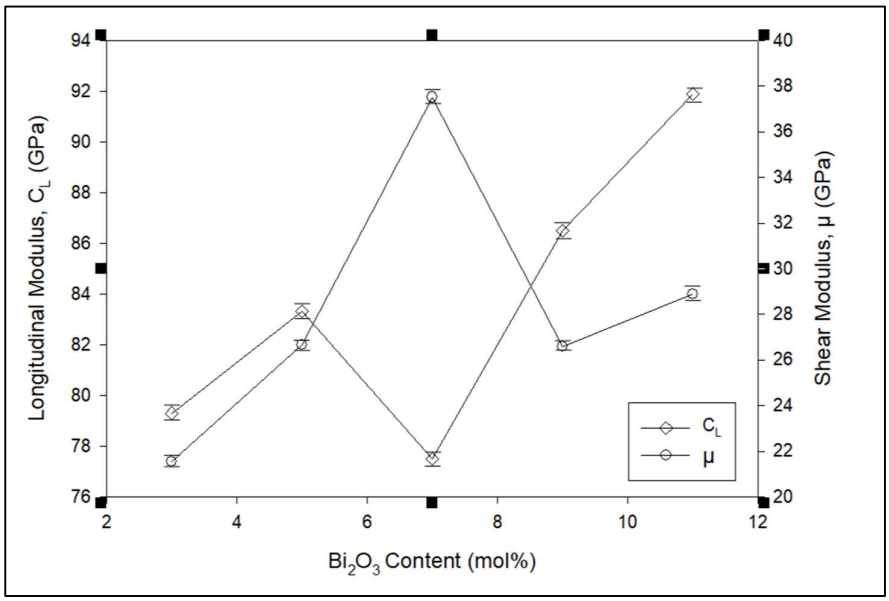

Figure 4.7 Longitudinal modulus (C_L) and shear modulus (μ) upon addition of Bi_2O_3 for $98[20Li_2O\text{-}xBi_2O_3\text{-}(80\text{-}x)B_2O_3]\text{-}2Ag$ (x =3 to 11 mol%)

Figure 4.8 exhibits the way K_e and Y change for each glass sample when Bi_2O_3 is added. Similar to C_L and μ, both moduli demonstrated a nonlinear pattern. K_e for example, had a sudden decrease from x = 5 mol% at 47.790 GPa to a minimum value of 27.479 GPa at x = 7 mol%, which came before a sharp rise at x > 7 mol%. Meanwhile, Y displayed a contrasting behaviour to K_e with a maximum value of 77.352 GPa at x = 7 mol%. This pattern coincided with the contrasting trend of C_L and μ at the same concentration of Bi_2O_3 (x = 7 mol%). Y indicated a similar pattern to μ, increasing steadily over $3 < x \leq 7$ mol% from 56.5 GPa to 77.4 GPa.

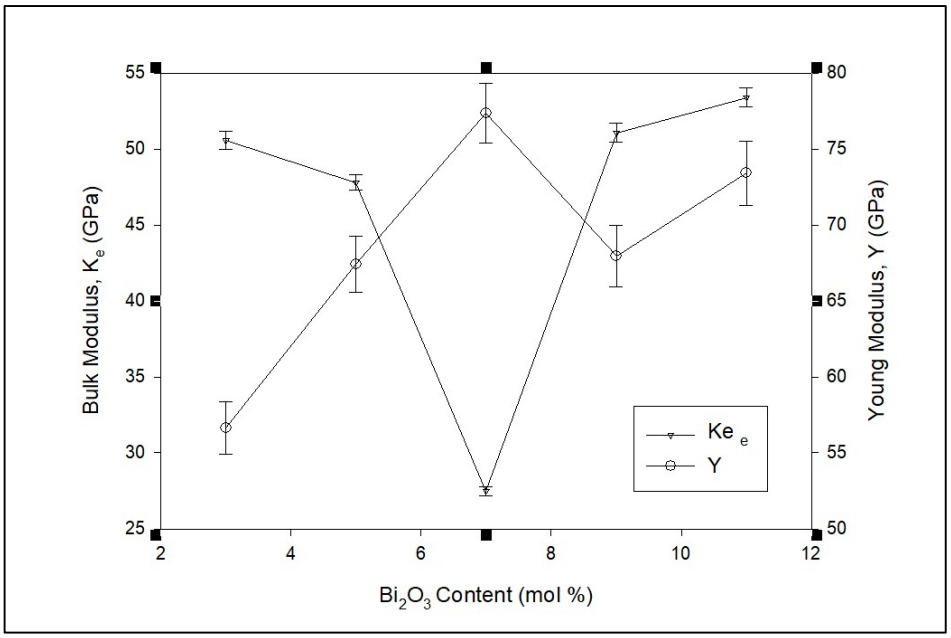

Figure 4.8 *Ke* and *Y* upon addition of Bi_2O_3 for 98[20Li_2O-*x*Bi_2O_3-(80-*x*)B_2O_3]-2Ag (*x* =3 to 11 mol%) Glass Samples.

Figure 4.9 illustrates how the addition of Bi_2O_3 content changes the Debye temperature, θ_D, and mean sound velocity, V_m, for the current glass system. The values of θ_D and V_m reached their peak at x = 7 mol%, after which the trend was disrupted by a great increase and then a large decrease. V_m showed a small reduction while a linear increase for x > 9 mol% was noticed for θ_D.

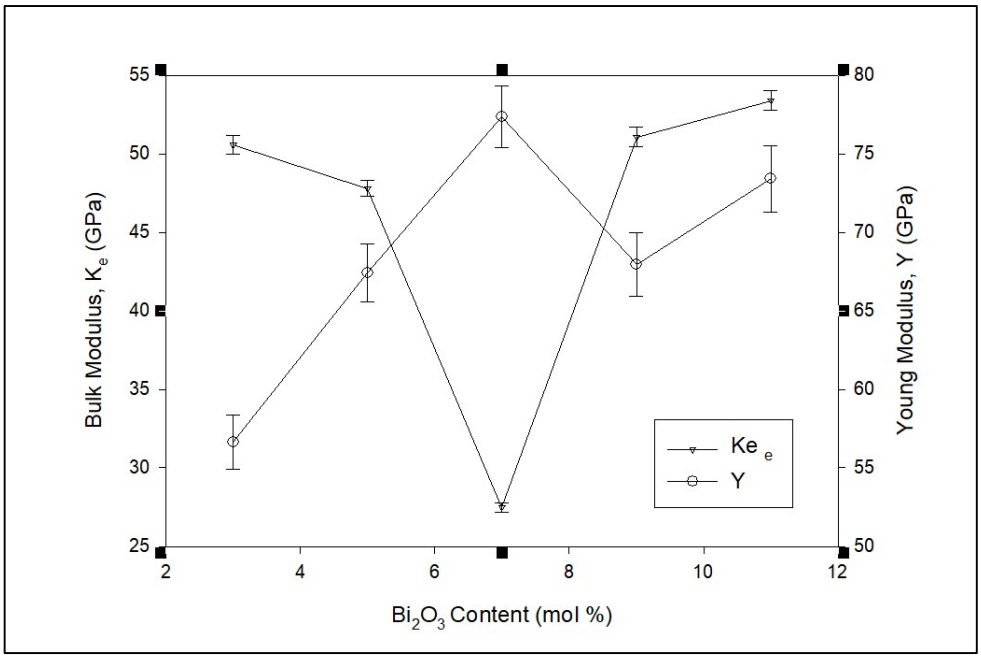

Figure 4.9 Debye temperature, θ_D and mean sound velocity, V_m upon addition of Bi_2O_3 for 98[20Li_2O-$x$$Bi_2O_3$-(80-$x$)$B_2O_3$]-2Ag for x =3 to 11 mol% Glass Samples.

A nonlinear change in hardness (H) and Poisson's ratio (σ) after the addition of Bi_2O_3 are shown in Figure 4.10. With a minimum value of 0.031 at x = 7 mol%, the plot of σ shows a linearly decreasing trend at 3 < x < 7 mol%, and a sharp rise for x > 7 mol%. Meanwhile, H exhibited almost linear increasing trend at 3 < x < 7 mol% with a maximum value of 11.735 GPa at x = 7 mol% before a rapid drop for x > 7 mol%.

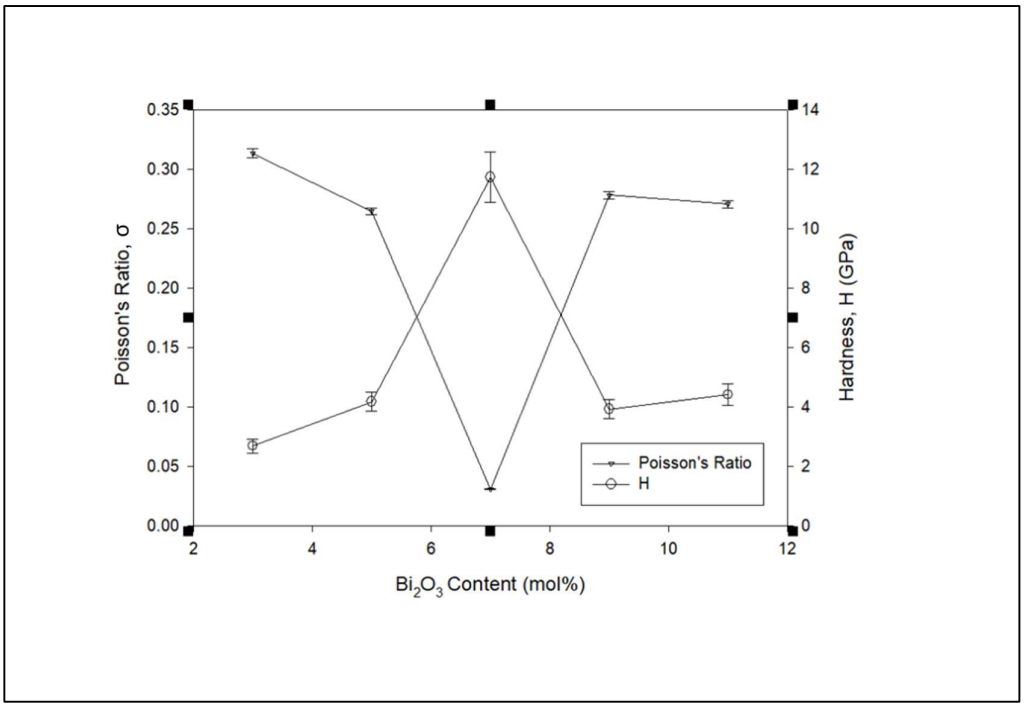

Figure 4.10 Poisson's ratio (σ) and hardness (H) upon addition of Bi_2O_3 for 98[20Li_2O-$x$$Bi_2O_3$-(80-$x$)B2O3]-2Ag ($x$ =3 to 11 mol%) Glass Samples.

The surge in *Vs,* μ and *Y* (Figure 4.6, Figure 4.7, Figure 4.8) with increasing Bi_2O_3 content of x < 7 mol% until reaching the highest value at x = 7 mol% was significantly affected by the rise in BO due to the formation of BO_4 units that increase the overall bonding and rigidity of the glass structure due to the existence of B-O bonds as in Figure 4.3. When x > 7 mol%, *Vs,* μ and *Y* portrayed rapid decrease, probably due to increase in the relative area and functional group of BiO_6 which linked to the rise in NBO, thus weakening the structure of the glass.

The deteriorating C_L and *Ke* as shown in Figure 4.7 and Figure 4.8 generally increased due to increase in BO as shown by the rise in N_4 which subsequently enhance the stiffness of the glass structure. However, a sudden drop at x = 7 mol% is because of high creation of NBO via BiO_6 contributes to the Bi_2O_3's function as a glass modifier. A surge in network bridging and interatomic force constants have been linked to variations in rigidity and stiffness in a wide range of oxide glass systems. The glass network's rigidity and stiffness increased with the early rise in *CL* and μ at x = 3 mol% as shown in Figure 4.7. The great decline in C_L at x = 7 mol% shows a greater decline in stiffness. This is further supported by FTIR results that showed peaks for x = 5 and 7

mol% shifted towards lower wavenumbers indicating the increased formation of Bi_2O_6 as NBOs which deteriorated the stiffness of the glasses.

K_e and Y rely on discrete moduli, C_L and μ. Given that K_e is linked to both C_L and μ, the nature of the bulk modulus (K_e) can be understood. The decline in C_L corresponds to the initial drop in Ke that was observed at $x < 7$ mol%. This similar behaviour between K_e and C_L indicates strong affect of C_L on K_e. Meanwhile, Y showed initial rise at $x < 7$ mol%, similar to the behaviour indicated by μ. This suggested that μ poised strong influence on Y.

This off-trend is believed as well to be due to the presence of the MIE impact in that region. These anomalies are further supported by the evidence of DC conductivity studies which showed steep decrease at region $7 \leq x \leq 9$ mol%. These occurrences indicated a decrease in the ionic region and a greater opening of the glass structure as NBO rose.

θ_D rose for $x < 7$ mol% and peaked at $x = 7$ mol%. This coincided with V_m. Increased θ_D indicates stronger stiffness and interatomic bonds of the glass network (Sabri et al., 2016b). A significant affect of V_m on elasticity of θ_D indicated by similar behaviours between these two parameters. A decrease in V_m and θ_D at $x > 7$ mol% is considered to be attributed to the accumulation of massive BiO_6 units and migration of smaller Li^+ ions across the network of glass, which correlated to the rise in the creation of NBO to open up the glass structure as shown in Figure 4.9. This corresponded to with the minimal value of DC conductivity at $x = 9$ mol%, suggesting that the glass is less stiff due to increased NBO production.

The Poisson's ratio (σ) is the ratio of transverse to longitudinal strain resulting from a tensile force and is contrarily impacted by the alteration in network's cross-link density of glass. The sharp drop in σ at $x = 7$ mol% contrasted with H, suggesting lower cross-linkage in the glass network. The large formation of BOs for $3 \leq x \leq 7$ mol% suggested a stronger network due to denser cross-linkage of the glass system. A conflicting behaviour between σ and H suggests that hardness is greatly affected by the change in the glass system's cross-linking through comprehension of σ.

4.4.1 Bulk Compression and Ring Deformation Models

Table 4.6 shows the values of cation-anion bond length (r), stretching force constant (F), coordination number (n_f), cross-link density per cation (n_c) whileTable 4.7 shows values of fraction of four coordinated boron atoms (N_4), average coordination number (n_{fave}), average cross-link density per cation (nc_{ave}), average B-O-B bond length (r_{B2O3}) and stretching force constant (F_{B2O3}) for of the glass samples.

Table 4.6
Values of cation-anion bond length (r), stretching force constant (F), coordination number (n_f), cross-link density per cation (n_c) for $98[20Li_2O\text{-}xBi_2O_3\text{-}(80\text{-}x)B_2O_3]\text{-}2Ag$ (x = 3 to 11 mol%) glass samples.

Oxide	r (nm)	F (Nm^{-1})	n_f	n_c
B_2O_3	0.138	660	3	1
	0.148	530	4	2
Bi_2O_3	0.240	192.24	6	4
Li_2O	0.159	243	6	4

The ring deformation and bulk compression model were utilized to further analyze the measured elastic properties of the $98[20Li_2O\text{-}xBi_2O_3\text{-}(80\text{-}x)B_2O_3]\text{-}2Ag$ glass systems. According to interatomic connection of oxides in glass such as stretching force constant, cation-anion bond length and coordination number, these mathematical models explained the compositional dependency of elastic moduli of glass samples. Based on the bulk compression model, the glass samples underwent compression that produced a magnitude which remained constant in terms of direction and interatomic bond length variations, all while maintaining the interatomic bind angles.

Table 4.7
Values of fraction of four coordinated boron atoms (N_4), average coordination number (n_{fave}), average cross-link density per cation (n_{cave}), average B-O-B bond length (r_{B2O3}) and stretching force constant (F_{B2O3}) for 98[20Li_2O-$x$$Bi_2O_3$-(80-$x$)$B_2O_3$]-2Ag ($x$ = 3 to 11 mol%) glass samples.

x (mol%)	N_4	n_{fave}	n_{cave}	r_{B2O3} (nm)	F_{B2O3} (Nm^{-1})
3	0.11	3.08	1.08	0.16	404
5	0.19	3.14	1.14	0.14	611
7	0.32	3.24	1.24	0.145	563
9	0.72	3.51	1.51	0.16	443
11	0.79	3.55	1.55	0.16	393

Table 4.8 lists the values of the glass samples' computed bulk modulus (K_{bc}), experimental bulk modulus (K_e), number of bonds per unit volume (n_b), average stretching force constant (F), and average cross link density (n_c).

Table 4.8
Values of theoretical bulk modulus (K_{bc}), experimental bulk modulus (K_e), ratio of K_{bc}/K_e , average ring size (l), average cross-link density (n_c), number of bond per unit volume (n_b) and average stretching force constant (F) for 98[20Li_2O-xBi_2O_3-(80-x)B_2O_3]-2Ag (x = 3 to 11 mol%) glass samples.

x (mol%)	K_{bc} (± 0.06 GPa)	K_e (GPa)	K_{bc}/K_e (± 0.02)	l (± 0.006 nm)	F (Nm^{-1})
3	80.5	50.6	1.59	0.50	342
5	94.5	47.8	1.98	0.58	559
7	92.3	27.5	3.36	0.65	503
9	91.5	51.1	1.79	0.52	395
11	95.6	53.4	1.79	0.50	348

Based on Figure 4.11, the ratio of K_{bc}/K_e exhibited a nonlinear increasing trend for $3 < x < 7$ mol% until a maximum value of 3.36 at x = 7 mol% was reached which preceded the sudden drop for $x > 7$ mol% and steady trend for $9 < x < 11$ mol%.

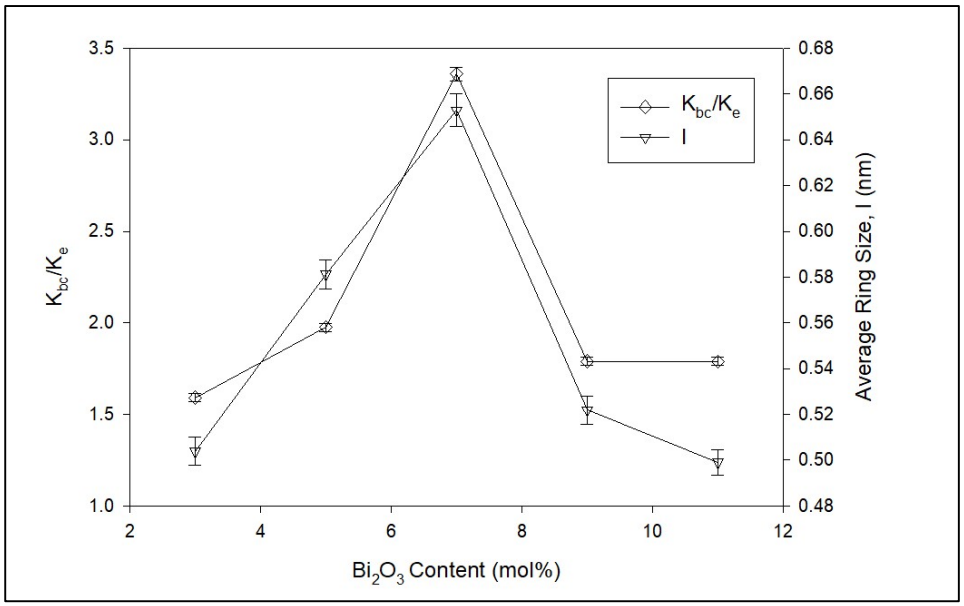

Figure 4.11 The ratio of K_{bc}/K_e and average ring size (l) upon addition of $Bi_2O_3$for $98[20Li_2O\text{-}xBi_2O_3\text{-}(80\text{-}x)B_2O_3]\text{-}2Ag$ for x =3 to 11 mol% Glass Samples.

Using ring deformation and bulk compression models, the elastic characteristics of $98[20Li_2O\text{-}xBi_2O_3\text{-}(80\text{-}x)B_2O_3]\text{-}2Ag$ for x = 3 to 11 mol% glass samples were quantitatively analyzed. Considering there is some bond bending involved, the anticipated K_{bc} value is greater than the experimental bulk modulus K_e, which is typically perceived. This suggests that the compression process requires significantly less energy than pure compression. It can be observed that the K_{bc}/K_e ratios are more than 1, suggesting the existence of ring deformation. For $x < 7$, the value of K_{bc} rose as the Bi_2O_3 content rose, possibly as a result of increased ring deformation. Since several rings may be distorted suggested to be because of bending under compression, the ratio of K_{bc}/K_e greater than 3 does not represent ideal isotropic conditions. Analyzing the variation in average ring size (l), which in consequently is affected by the concentration of BO and NBO provides insight into the dissimilarity in K_{bc}/K_e ratios. The highest value of l at x = 7 mol% indicates that the presence of high NBOs content by BiO_6 may have contributed to the ring parameter's enlargement by forming a lot of open rings that lower the network's resistance to deformation and increase ring deformation. The highest value of K_{bc}/K_e can also be clarified through this which correlated with the highest value of DC conductivity at the similar concentration as shown in Figure 4.5. The value of l dropped when $x > 7$ mol%, indicating that a larger concentration of BO resulted in an

increase in the network's resistance to deformation, which accounts for the declining K_{bc}/K_e value in the same area. The high value of N_4 at the same concentration provides more evidence for this as depicted in Figure 4.3.

4.5 Radiation Shielding Properties

4.5.1 Mass Attenuation Coefficient (MAC)

The evaluation of the mass attenuation coefficients of glass with varying concentrations of Bi_2O_3 at various gamma-ray energies were calculated using the intensity of incident and transmitted gamma rays at a given energy level (Alajerami et al., 2020). In this study, to identify the ability to attenuate radiation, the bismuth borate glass system was examined in the energy range of 0.015 – 15 MeV. The Phy-X/PSD online software was used to calculate the mass attenuation coefficient for the Li_2O-Bi_2O_3-B_2O_3-Ag glasses system, with varying bismuth contents. Since MAC defines the ability for a material to attenuate radiation, a greater value denotes a more effective shield (Lacomme et al., 2021). When all MAC (μ/ρ) values are examined, the MAC value decreases due to an increase in photon energy. In addition, the MAC increases also with increasing density of composition of glasses. Glasses with the lowest and highest MAC values are given as at x = 3 and 11 mol% of Bi_2O_3 content respectively. This is due to photoelectric absorption, Compton scattering, and pair formation processes altering the MAC value within this energy range (Kamislioglu, 2021). The variation in MAC values is therefore dependent on photon energy and atomic number. The maximum values for all the glasses can be observed at the lowest tested energy, 0.015 MeV and were equal to 21.383, 31.150, 39.192, 45.930 and 51.657 cm^2/g for the x = 3, 5, 7, 9 and 11 mol% glasses respectively. At this energy, it was seen that the MAC of the glasses dropped as the Bi_2O_3 concentration of the sample increased, possibly due to the increase in density that correlated with Bi_2O_3 concentration. Highest MAC value at x = 11 mol% indicated that the bismuth content changes with its atomic number and energy. Both density and atomic number was correlated positively with MAC, hence the x = 11 mol% glass sample has the greatest radiation shielding capability. As the incoming photon energy increases, the MAC of all glasses rapidly decreases and then slows down and becoming nearly constant. For instance, the MAC of the x = 11 mol% glass sample decreases as energy increased. Other samples such as at x = 3 mol% glass

sample followed a similar trend, with its MAC being equal to 21.383, 16.002, 6.141 and 2.976 cm^2/g at the same four energies respectively. As the intensity of the incoming radiation increases, more photons are able to travel through the sample, reducing its ability to absorb photons and MAC (Lacomme et al., 2021). As illustrated in the samples are most effective at lower energies, with x = 11 mol% was being the most effective, and that as energy increases, their shielding ability becomes less effective, to the point where the differences between the shields become negligible at high energies. It can be concluded that x = 11 mol% glass has greater attenuation capabilities than the other investigated samples.

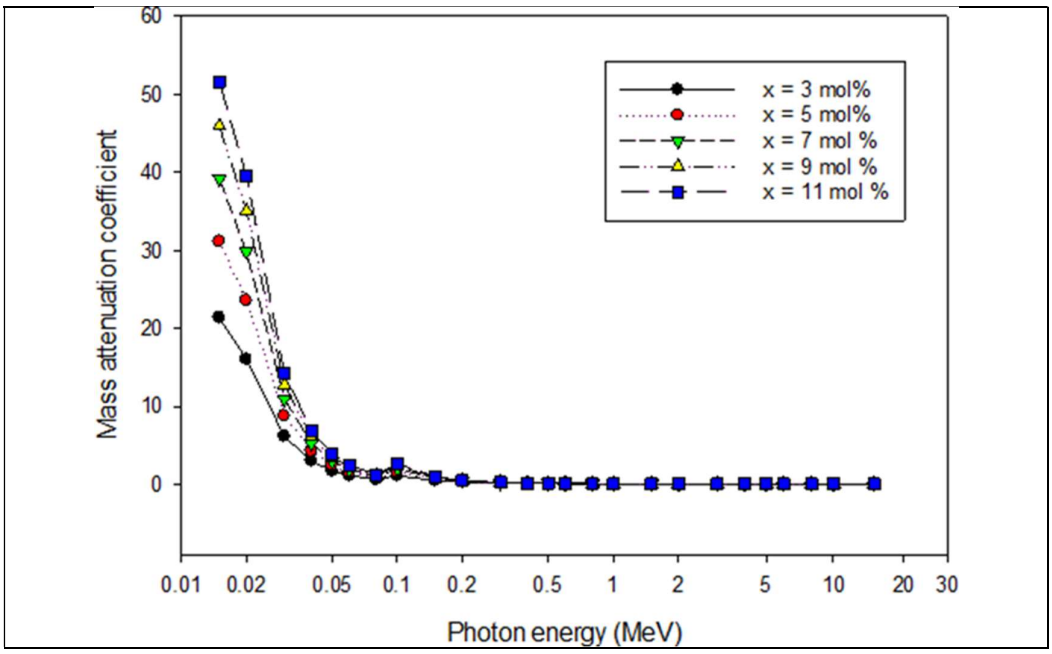

Figure 4.12 Variation of mass attenuation coefficients of the Li_2O-Bi_2O_3-B_2O_3-Ag glasses system.

4.5.2 Linear Attenuation Coefficient (LAC)

The LAC of the glasses against energy is shown in **Error! Reference source not found.Error! Reference source not found.**. LAC is quite similar to MAC, except that density was included in calculating the effectiveness of the samples. The same energies as in the previous figures were chosen. LAC trends are quite same as the MAC trends. **Error! Reference source not found.** shows the fluctuation of the linear coefficient (LAC) against incident of photon energy (MeV) for lithium bismuth borate silver glasses. The graph clearly indicated a significant reduction in energy from 0.015

MeV to 15 MeV, confirming the Compton scattering's supremacy (Lacomme et al., 2021). The greatest values for the glasses are observed at the lowest tested energy which was 0.015 MeV, and follow the trend at x = 11 mol% > 9 mol% > 7 mol% > 5 mol% > 3 mol% for all energies. For example, at 0.020 MeV, the LAC values are equal to 40.356, 68.034, 90.083, 113.359 and 142.166 cm-1, while at 15MeV, they are equal to 0.062, 0.080, 0.093, 0.107 and 0.126 cm-1 for x = 3, 5, 7, 9 and 11 mol% respectively. Then, these results demonstrated a correlation between the LAC values and the density and Bi_2O_3 content of the glasses, which caused the 11 mol% glass has the highest LAC. However, when energy increased, the LAC values dropped which were due to higher energy photons having greater penetrating power, reducing sample attenuation, and decreasing LAC (Almasoud, 2021). As, the Bi_2O_3 concentration and density of the glasses increased, so did their attenuation ability. It can be concluded that the x = 11 mol% glass as the most desirable radiation shielding properties. as the most desirable radiation shielding properties.

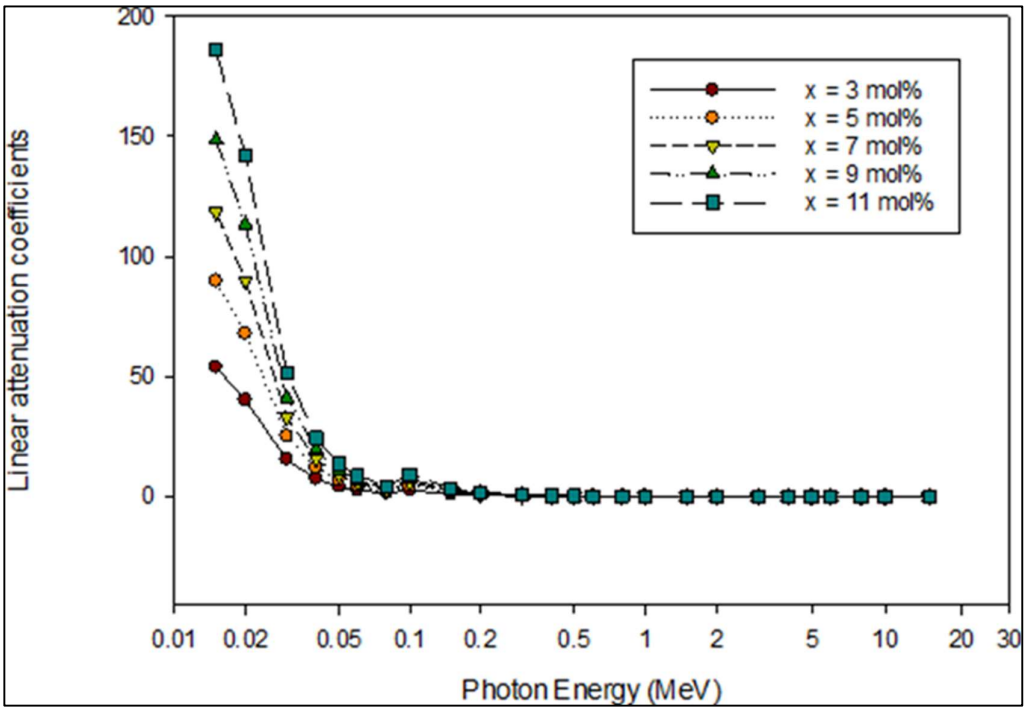

Figure 4.13 Variation of linear attenuation coefficients of the Li_2O-Bi_2O_3-B_2O_3-Ag glasses system against of the incident photon energy (MeV).

4.5.3 Half Value Layer

Because these characteristics are often used to estimate the radiation shielding properties of a material, the HVL values for the glass materials reported in this study have been determined. Figure 4.16 depicts the evolution of radiation flux glasses with respect to photon energy. The HVL graphs have been plotted based on data collected within the energy range of 0.015 to 15 MeV.

From the HVL values produced for the photon energy (E > 0.015 MeV) in the high energy region were almost constant. Between 0.2 MeV and 6 MeV, there is a considerable change in HVL and it has been observed that the maximum values increased in parallel with the increasing photon energy. HVL is the material thickness needed to cut the intensity of incoming radiation in half, hence a lower value of HVL indicated a better shield (Lacomme et al., 2021). At both energies, and at other energies as well, the 11 mol% glass has the lowest HVL, while 3 mol% has the greatest. These results indicated that for the same photon energy, 11 mol% required a much smaller thickness than 3 mol% to reduce the intensity of the radiation in half. Then, it appeared to increase gradually for energies more than 6 MeV, as photon energy was increased. As the results, high density glass (11mol%) demonstrated the most effective radiation protection property. As the radiation's intensity increases, more photons can travel through the glass, requiring a thicker layer of glass to reduce photons to safe levels. This trend implies that the glasses are more effective at lower energies, but their effectiveness decreases as the energy level increase

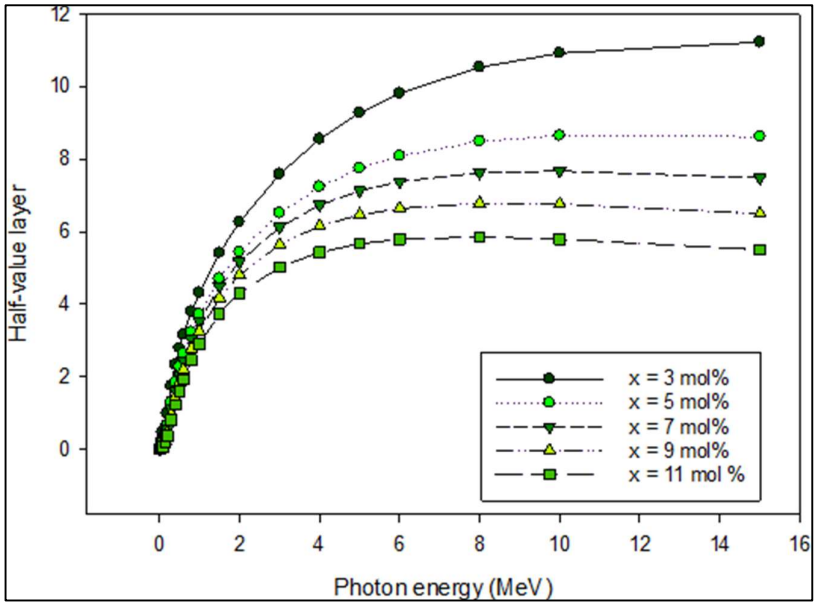

Figure 4.14 Variation of half value layer (HVL) of the Li2O-Bi2O3 B2O3-Ag glasses system.

4.5.4 Mean Free Path

The MFP was determined using the relationship MFP = 1/u. The mean free path is the distance between successive photon collisions with atoms inside a sample. A smaller MFP indicates a shorter distance between collisions, which increases the number of collisions and attenuation. Consequently, a smaller MFP is recommended. At various energies, the MFP of the samples against the molar volume of the different Bi_2O_3 content of the glasses was plotted. At any given energy, there is an inverse relationship between density and MFP. After reaching a maximum value, MFP tends to decline as photon energy increases. This variation is caused by different photon interaction processes with different energy regions in the absorber material. According shows that increasing the density of the glasses, as measured by the quantity of Bi_2O_3 content, can decreases the MFP and increases attenuation, that indicates that sample 11 mol% with the highest density, will absorbs the most radiation. Other hand, at all energies, the glass with the lowest density x = 3 mol% has the highest MFP that represented in the Figure 4.17. The MFP values also increase when the energy levels increase. As photon energy increases, the efficiency of the glasses decreases. This is related to the high penetrating power of photons with high energy, which necessitates the use of thick glass to absorb these photons (Almasoud, 2021).

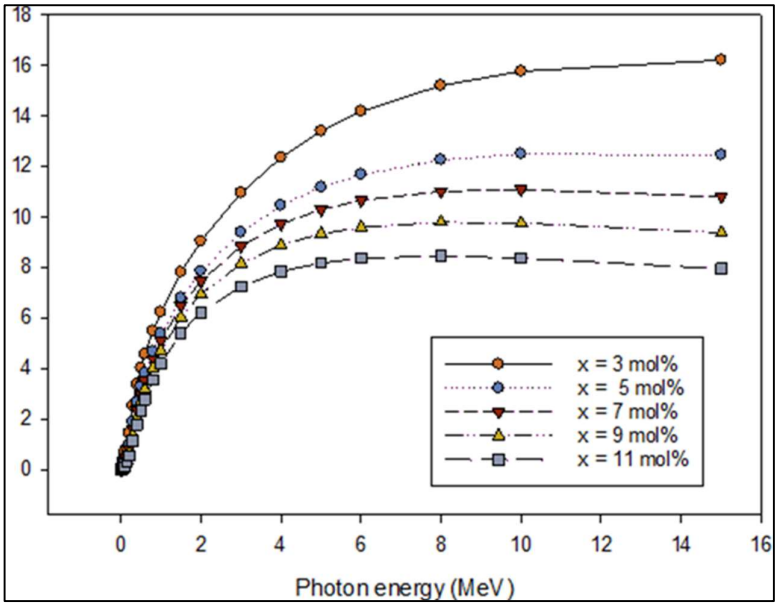

Figure 4.15 Variation of mean free path of the Li2O-Bi2O3-B2O3-Ag glasses system.

4.5.5 Effective Atomic Number

Effective atomic number (Z_{eff}) values are frequently employed to explore the energy-dependent changes of materials obtained during the production of alternative radiation shielding materials. Z_{eff} is the average atomic number of a chemical with a higher value indicates a more effective shield. In this study, Z_{eff} values were computed to determine the photon interactions of the Li_2O-Bi_2O_3-B_2O_3-Ag glasses materials. The radiation shielding feature is directly related to the Z_{eff} calculation results. The dependences of the Z_{eff} graph on photon energy for lithium bismuth borate silver glasses used for this investigation are shown in Figure 4.18.

As seen in Figure 4.18, compounds with a greater Z atomic number typically have a greater Z_{eff} value. At a specific energy, x = 3 mol% has the least Z_{eff}, while at x = 11 mol% has the greatest. For instance, at 0.050 MeV, the Z_{eff} values are equal to 38.96, 48.16, 54.26, 58.60 and 61.85 for 3 mol%, 5 mol%, 7 mol%, 9 mol% and 11 mol% respectively. The values follow the Bi_2O_3 content in the glasses because Bi_2O_3, has a much greater atomic number than B_2O_3. Additionally, the Z_{eff} of each glass sample decreases with increasing energy. Then, the values can be seen to rapidly decrease at lower energies and flattening out at higher energies. Since the photoelectric effect is largely dependent on atomic number, glasses containing Bi_2O_3 have a Z_{eff} value that decreases rapidly (Lacomme et al., 2021). Therefore, at x = 3 mol%, glass sample demonstrates the least radiation shielding potential out of the different molar volume of the Bi_2O_3 content of the glasses.

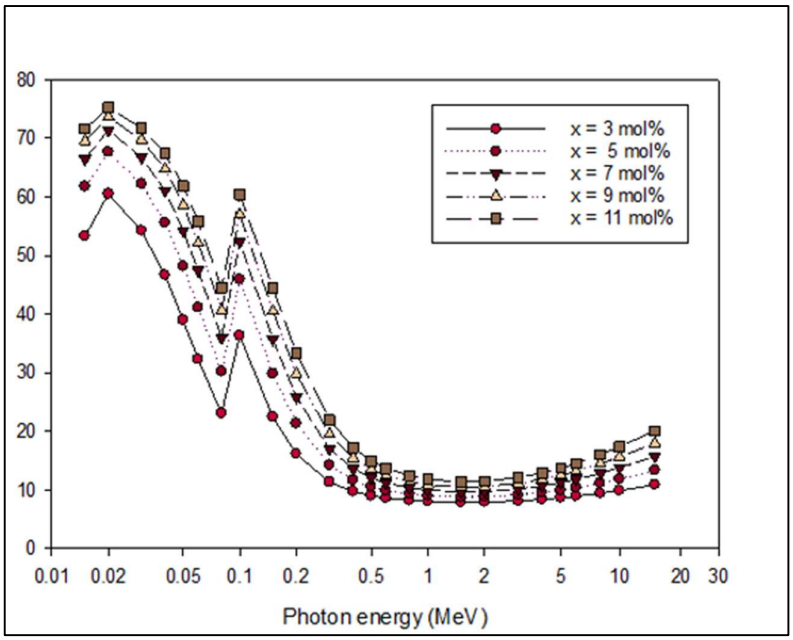

Figure 4.16 Variation of effective atomic number of the Li_2O-Bi_2O_3-B_2O_3-Ag glasses system.

CHAPTER 5
CONCLUSION AND RECOMMENDATION

5.1 Introduction

This chapter discussed about the conclusion and recommendation of this study. In this work, the structural, elastic, DC conductivity and radiation shielding properties of 98[20Li_2O-$x$$Bi_2O_3$-(80-$x$)$B_2O_3$]-2Ag glass were studied. The goals set out to investigate how Bi_2O_3 affects the characteristics of glass samples that were presented above were accomplished. Using the melt-quenching procedure, all of the glass samples were successfully created. They were then described using a variety of experimental approaches and examined through a variety of analytical techniques.

5.2 Conclusion

This study investigated the influence of bismuth oxide (Bi_2O_3) substitution on the structural, elastic, DC conductivity, and radiation shielding properties of the 98[20Li_2O–$x$$Bi_2O_3$–(80−$x$)$B_2O_3$]–2Ag glass system, where x = 3 to 11 mol%. The glass samples were successfully prepared using the melt-quenching technique and characterized using X-ray diffraction (XRD), Fourier transform infrared spectroscopy (FTIR), ultrasonic velocity measurements, impedance spectroscopy, and Phy-X/PSD simulation.

The XRD patterns confirmed that all prepared samples exhibited a broad diffraction hump, indicating the amorphous nature of the glass structure. FTIR analysis revealed the presence of BO_3, BO_4, and BiO_6 structural units, indicating that the incorporation of Bi_2O_3 modifies the borate glass network by introducing heavy metal structural units and promoting the formation of non-bridging oxygens (NBOs). These structural modifications influence the rigidity and connectivity of the glass network, which subsequently affects its physical properties.

The elastic properties of the glass samples showed non-linear compositional behaviour with increasing Bi_2O_3 concentration. An anomalous region was observed within $7 \leq x \leq 9$ mol%, where parameters such as bulk modulus, longitudinal modulus, and mean sound velocity exhibited unusual variations. This anomaly can be attributed

to structural rearrangements within the glass network caused by the incorporation of large Bi^{3+} ions, which alter the distribution of borate structural units and increase the formation of NBOs. These structural changes lead to temporary weakening of the glass network and affect its resistance to deformation.

The DC conductivity results showed that conductivity generally increased with increasing Bi_2O_3 concentration due to modifications in the glass structure that influence charge transport pathways. However, a distinct minimum in DC conductivity was observed at x = 9 mol%, indicating the presence of mixed ionic–electronic (MIE) behaviour. In this compositional region, the migration of Li^+ ions is partially hindered by the presence of large Bi^{3+} ions, which disrupt the migration pathways within the glass network and temporarily reduce ionic conduction.

The radiation shielding properties of the glass samples were evaluated using the Phy-X/PSD simulation program over a photon energy range of 15 keV to 15 MeV, which represents the typical photon energy spectrum encountered in medical, industrial, and nuclear radiation environments. The results demonstrated that radiation shielding efficiency increased with increasing Bi_2O_3 concentration. Among the investigated compositions, the glass sample containing 11 mol% Bi_2O_3 exhibited the highest mass attenuation coefficient (MAC) and the lowest half value layer (HVL) and mean free path (MFP) values. This improvement is attributed to the high atomic number and density of bismuth, which increase the probability of photon interaction with the glass matrix through photoelectric absorption and Compton scattering mechanisms.

A correlation between DC conductivity and radiation shielding behaviour was also observed. Structural modifications caused by Bi_2O_3 incorporation influence both charge transport and photon attenuation mechanisms. The formation of NBOs and heavy metal structural units modifies the glass network, which affects ionic mobility and increases photon interaction probability within the material.

Based on the obtained results, the glass sample containing 11 mol% of Bi_2O_3 demonstrated the best overall performance for radiation shielding applications. This composition exhibited enhanced photon attenuation due to its higher density and effective atomic number while maintaining stable glass structure and acceptable electrical behaviour. Therefore, the $98[20Li_2O–11Bi_2O_3–69B_2O_3]–2Ag$ glass system can be considered a promising candidate for transparent and environmentally friendly radiation shielding materials that may serve as alternatives to conventional lead-based shielding materials.

5.3 Recommendations

Based on the findings obtained in this study, several recommendations can be proposed for future research.

Further investigations may be conducted by extending the Bi_2O_3 concentration range beyond x = 11 mol% in order to examine how higher heavy metal oxide content influences the structural stability, elastic behaviour, and radiation shielding performance of the glass system. This may help determine the maximum concentration of Bi_2O_3 that can be incorporated while maintaining the amorphous nature of the glass.

The radiation shielding parameters evaluated in this study were obtained using the Phy-X/PSD simulation program. Therefore, future work may include experimental gamma-ray attenuation measurements using gamma spectroscopy techniques to validate the theoretical results obtained from the simulation and provide more comprehensive evaluation of the shielding performance.

Meanwhile, additional characterization techniques such as Scanning Electron Microscopy (SEM), Transmission Electron Microscopy (TEM), and Energy Dispersive X-ray Spectroscopy (EDS) may be employed to investigate the microstructure of the prepared glass samples and to confirm the presence and distribution of silver nanoparticles within the glass matrix.

Furthermore, the present study mainly focused on the structural, elastic, DC conductivity, and radiation shielding properties of the investigated glass system. However, the optical characteristics of the glass samples in the visible and near-infrared regions have not yet been investigated. Therefore, future studies may explore the photoluminescence properties of these glasses, particularly when doped with rare earth ions, using a fluorescence spectrophotometer. The optical parameters may also be evaluated using the Judd–Ofelt analysis, which can provide valuable information on the optical transition probabilities and emission characteristics of rare-earth-doped glass systems.

In addition, the incorporation of transition metal ions into the glass composition may introduce magnetic properties within the glass network. The magnetic behaviour of the present glass samples has not yet been examined. Therefore, future investigations may evaluate the magnetic properties of the glass system using magnetometers to determine parameters such as magnetic susceptibility and to study the interactions between magnetic ions across different compositions and temperature ranges.

Finally, further research may also investigate the optical, thermal, and mechanical properties of Ag-doped bismuth borate glasses in order to evaluate their suitability for practical applications such as transparent radiation shielding windows, optical devices, and protective materials in medical and nuclear environments.

REFERENCES

Al-Buriahi, M. S., Tonguc, B. T., & Sayyed, M. I. (2021). Investigation of gamma-ray shielding properties of heavy metal oxide glasses using the Phy-X simulation code. *Ceramics International*, 47(3), 3563–3571.

Al-Buriahi, M. S., Al-Hadeethi, Y., & Sayyed, M. I. (2022). Influence of heavy metal oxides on photon attenuation properties of glass systems. *Radiation Physics and Chemistry*, 196, 110121.

Al-Hadeethi, Y., & Sayyed, M. I. (2022). Radiation shielding properties of heavy metal oxide glasses: A review. *Radiation Physics and Chemistry*, 191, 109847.

Al-Hadeethi, Y., Sayyed, M. I., & Al-Buriahi, M. S. (2023). Elastic and radiation shielding behaviour of heavy metal oxide glasses. *Journal of Materials Science: Materials in Electronics*, 34, 1246–1259.

Al-Hadeethi, Y., Al-Buriahi, M. S., & Sayyed, M. I. (2024). Photon attenuation capability of bismuth-containing oxide glasses. *Ceramics International*, 50, 12458–12466.

Almuqrin, A. H., Gangareddy, J., Hivrekar, M. M., Pramod, A. G., Sayyed, M. I., Keshavamurthy, K., Fatima, N., & Jadhav, K. M. (2022). Nonlinear optical limiting and radiation shielding characteristics of Sm_2O_3-doped cadmium sodium lithium borate glasses. *Materials*, 15(6), 2124.

Alzahrani, J. S., Alrowaili, Z. A., Saleh, H. H., Hammoud, A., Alomairy, S., Sriwunkum, C., & Al-Buriahi, M. S. (2021). Structural and radiation shielding properties of Pb-Al alloys for nuclear shielding applications. *Progress in Nuclear Energy*, 142, 103992.

Bashter, I. I., & Al-Hadeethi, Y. (2023). Evaluation of radiation attenuation parameters of heavy metal oxide glasses. *Radiation Physics and Chemistry*, 203, 110547.

Cheewasukhanont, W., Kaewkhao, J., & Limsuwan, P. (2020). Gamma-ray shielding properties of bismuth borate glasses. *Radiation Physics and Chemistry*, 172, 108789.

D'Souza, J., Pawar, P., & Singh, V. P. (2021). Radiation shielding properties of borate-based glasses using Phy-X simulation. *Journal of Non-Crystalline Solids*, 561, 120743.

D'Souza, J., Pawar, P., & Singh, V. P. (2022). Evaluation of photon attenuation parameters of heavy metal oxide glasses. *Ceramics International*, 48, 20371–20379.

El-Mallawany, R. A. H., Al-Hadeethi, Y., & Sayyed, M. I. (2023). Structural and radiation shielding behaviour of heavy metal oxide glasses. *Radiation Physics and Chemistry*, 203, 110547.

Evangelin Teresa, A., Senthilkumar, K., & Arunkumar, A. (2021). Structural and radiation shielding properties of bismuth borate glasses. *Ceramics International*, 47, 14589–14598.

Hisam, R., Samsudin, N. M., & Yahya, A. K. (2021). Structural, elastic and electrical properties of mixed glass former systems. *Ionics*, 27, 619–634.

Hisam, R., Yahya, A. K., & Samsudin, N. M. (2022). Structural transition and electrical conduction behaviour in mixed ionic–electronic glasses. *Journal of Non-Crystalline Solids*, 584, 121511.

Jadhav, K. M., Gangareddy, J., & Hivrekar, M. M. (2023). Physical and shielding properties of rare-earth doped borate glasses. *Ceramics International*, 49, 14821–14829.

Kaur, P., Singh, K. J., & Kurudirek, M. (2020). Review of radiation shielding materials for gamma rays and neutrons. *Radiation Physics and Chemistry*, 176, 109018.

Kaur, P., Singh, K. J., & Singh, H. (2021). Structural and radiation shielding properties of heavy metal oxide glasses. *Ceramics International*, 47, 17420–17429.

Kumar, A., Singh, H., & Singh, K. J. (2024). Structural, elastic and radiation shielding properties of heavy metal oxide doped borate glasses. *Ceramics International*, 50, 10215–10225.

Kumar, A., Singh, H., & Singh, K. J. (2025). Elastic behaviour and structural modifications in heavy metal oxide borate glasses. *Journal of Materials Science*, 60, 3200–3212.

Lakshminarayana, G., Dong, G., & Qiu, J. (2022). Structural and spectroscopic properties of heavy metal oxide glasses. *Journal of Non-Crystalline Solids*, 585, 121515.

Lakshminarayana, G., Dong, G., & Qiu, J. (2023). Influence of modifier oxides on structural units and network rigidity of borate glasses. *Ceramics International*, 49, 18910–18920.

Lakshminarayana, G., Dong, G., & Qiu, J. (2024). Structural evolution and optical properties of heavy metal oxide glasses. *Optical Materials*, 136, 113534.

Rahman, S., Sayyed, M. I., & Al-Hadeethi, Y. (2024). Evaluation of photon attenuation in heavy metal oxide glasses using Phy-X software. *Radiation Physics and Chemistry*, 214, 111174.

Rahman, S., Al-Buriahi, M. S., & Sayyed, M. I. (2025). Gamma-ray shielding characteristics of heavy metal oxide glass systems. *Ceramics International*, 51, 14250–14261.

Sayyed, M. I., Al-Hadeethi, Y., & Al-Buriahi, M. S. (2022). Radiation shielding performance of heavy metal oxide glasses. *Journal of Materials Research and Technology*, 17, 2995–3004.

Sayyed, M. I., Al-Buriahi, M. S., & Lakshminarayana, G. (2023). Investigation of photon attenuation in heavy metal oxide glasses. *Radiation Physics and Chemistry*, 202, 110521.

Singh, H., Singh, K. J., & Kaur, P. (2022). Elastic properties and radiation shielding behaviour of borate glass systems. *Ceramics International*, 48, 15744–15753.

Singh, H., Singh, K. J., & Kaur, P. (2023). Structural and mechanical properties of heavy metal oxide glasses. *Journal of Non-Crystalline Solids*, 597, 121867.

Singh, H., Singh, K. J., & Kaur, P. (2024). Influence of heavy metal oxides on elastic properties of borate glasses. *Ceramics International*, 50, 19451–19460.

Vadavathi, A. M., Chinthakayala, S. K., Kollipara, V. S., Ramadurai, G., & Gadige, P. (2021). Physical and radiation shielding properties of bismuth borate glasses. *Ceramics International*, 47, 9791–9805.

Wang, F., Wang, Y., Zhang, D., Hao, Y., Liao, Q., Zhu, H., Zhou, J., & Zhu, Y. (2022). Effects of modifier oxides on the structural properties of borate-based glasses. *Journal of Nuclear Materials*, 560, 153500.

Yusof, N. N., Yahya, A. K., & Samsudin, N. M. (2023). Structural and electrical properties of alkali borate glasses. *Journal of Non-Crystalline Solids*, 601, 121930.

Zaid, M. H. M., Sidek, H. A. A., Matori, K. A., Mahmoud, K. A., Lacomme, E., & Sayyed, M. I. (2021). Mechanical and radiation shielding properties of heavy metal oxide glasses. *Journal of Materials Research and Technology*, 11, 1322–1330.

AUTHOR'S PROFILE

Nurul Atika Mohd Khalid obtained Bachelor of Science in Physics (Hons.) in 2019 from University Teknologi Malaysia (UTM) Skudai, Johor. Currently she is working on her master's research on mixed ionic-electronic glasses properties ranging from structural, elastic, DC conductivity and radiation shielding properties.

LIST OF PUBLICATION

Mohd Khalid, N. A., Mohd Rejab, M., Mansor, M. N., & Hisam, R. (2023). Investigation on the effect of bismuth concentration towards radiation shielding properties in Ag-embedded borobismuthate mixed ionic electronic glass system. *Scientific Research Journal, 20*(2), 115–129. https://doi.org/10.24191/srj.v20i2.22854